Mechanisms of STIM1-mediated endoplasmic reticulum-plasma membrane (ER-PM) contact formation

Dissertation

submitted to the

Combined Faculties for the Natural Sciences and for Mathematics

of the Ruperto-Carola University of Heidelberg, Germany

for the degree of

Doctor of Natural Sciences

presented by

M. Sc.-Biochemistry
Shan-Hua Chung

born in: Taoyuan, Taiwan

Dissertation

submitted to the

Combined Faculties for the Natural Sciences and for Mathematics of the Ruperto-Carola University of Heidelberg, Germany

for the degree of

Doctor of Natural Sciences

presented by

M. Sc.-Biochemistry Shan-Hua Chung

born in: Taoyuan, Taiwan

Oral-examination: 25th September 2014

Mechanisms of STIM1-mediated endoplasmic reticulum-plasma membrane (ER-PM) contact formation

Referees: PD Dr. Matthias Seedorf
Prof. Dr. Walter Nickel

Parts of the findings summarized in this thesis have been published as an article titled "Di-arginine signals and the K-rich domain retain the Ca^{2+} sensor STIM1 in the endoplasmic reticulum" in Traffic journal.

Ercan E, Chung SH, Bhardwaj R, Seedorf M (2012) Di-arginine signals and the K-rich domain retain the Ca^{2+} sensor STIM1 in the endoplasmic reticulum. Traffic, 13(7): 992-1003

Acknowledgements

I am very thankful to Dr. Matthias Seedorf (Centre of Molecular Biology, University of Heidelberg- ZMBH), my thesis supervisor, for his exemplary guidance, monitoring and constant encouragement during my stay in his laboratory. The help and guidance given by him time to time shall carry me a long way in the journey of life on which I am about to embark.

I would like to take this opportunity to thank to Prof Dr. Walter Nickel (Biochemistry Department, University of Heidelberg- BZH), my second supervisor, for his time, encouragement and discussion. I am also thankful to Prof Dr. Bernhard Dobberstein (ZMBH), Dr. Marius Lemberg (ZMBH) and Prof. Dr. Sabine Strahl (Centre for Organismal Studies, University of Heidelberg- COS) for brainstorming discussion and encouragement during and after my research seminars.

I will never forget the support from Dr. Holger Lorenz, Dr. Gonzalo Hernán Sendra and Christian Hoerth (Imaging facility, ZMBH). Without their intensive supports, I would never able to learn and perform all image analysis. I also thank Dr. Monika Langlotz (FACS, ZMBH) for her supports in flow cytometry experiments. I would also thank Prof. Dr. Frauke Melchior (ZMBH) and her colleagues for allowing me to use their gel filtration columns and for their technical help. I am also thankful to Prof. Dr. Oliver Gruss (ZMBH) and his colleagues for supporting me to perform in vitro microtubules cosedimentation assay. Prof. Dr. Gruss also provides me many suggestions and discussions especially regarding microtubule-binding experiments.

I must thank my wonderful colleagues and friends, especially Ebru, Fabio, Annett, Rajesh, Gerry, Petra, Silke and Wendelin. They were always ready to help me in technical problems and at times of other difficulties.

Words are not enough to describe the extraordinary atmosphere created by all my friends in Heidelberg, especially Ilaria, Steffi, Judith, Ana, Lucia, Andrius, Sarah, Diana, Conny and all my Taiwanese friends. I thank all of them to make me feel less homesick and feel like a second home far away from Taiwan. I especially would like to thank Mirela for constantly giving supports and encouragements during my PhD, thesis writing and for everything. I am very lucky and thankful to God to meet and have Mirela in my life. Without her support and company, I would not know how to accomplish all tasks encountered now and in the future.

I thank you mom, dad and my brother for always supporting me throughout my life. 我要在這邊感謝我的家人，特別是我的爸爸, 媽媽跟Andy，謝謝你們永遠支持我，作我永遠的後盾，讓我有勇氣追夢，即使離台灣,離家很遠，因為你們的愛與鼓勵，讓我能堅持下去並完成夢想。我要在此，與你們還有天上的外婆，一起分享這本博士論文以及博士學位的榮耀。

Summary

The coupling of endoplasmic reticulum (ER) and plasma membrane (PM) is crucial for calcium (Ca^{2+}) homeostasis. STIM1 and STIM2 are type I membrane proteins of the ER and function as Ca^{2+} sensors in a process known as store-operated calcium entry (SOCE). They sense a drop in luminal Ca^{2+} concentration and undergo conformational changes and oligomerization. The active oligomerized STIM proteins translocate to ER-PM contact sites, where they bind to phosphoinositides (PIPs) at the inner leaflet of the PM via their lysine (K)-rich domains and activate Orai1, a pore-forming Ca^{2+} release-activated Ca^{2+} (CRAC) channel subunit in the PM.

I found that STIM2, but not STIM1, contains a di-lysine ER-retention signal. This signal restricts the function of STIM2 as Ca^{2+} sensor to the ER while STIM1 can reach the PM via the classical secretary pathway. The intracellular distribution of STIM1 is regulated in a cell-cycle-dependent manner with cell surface expression of STIM1 during mitosis. Efficient retention of STIM1 in the ER during interphase depends on its K-rich domain and a di-arginine ER retention signal. SOCE enhances ER retention, suggesting that trafficking of STIM1 is regulated and this regulation contributes to STIM1's role as multifunctional component in Ca^{2+}-signaling.

In contrast to mitotic cells, interphase cells retain most of their STIM1 intracellularly. Under resting condition, the ER-resident STIMs are preferentially located in $PI(4,5)P_2$ containing preexisting ER-PM contact sites, which are expanded upon ER Ca^{2+} depletion. The lipid-binding, K-rich domains are required to localize STIM proteins in preexisting ER-PM contact sites. Moreover, STIM2 recruits ER more efficiently to the PM. This is consistent with the fact that STIM2 has higher lipid-binding affinity and lower activation threshold than STIM1 and that STIM2 functions as a regulator of basal Ca^{2+} homeostasis.

Finally, I studied the role of microtubules in ER-PM contact site formation. I observed that STIM1 aligns along microtubules. Alignment of STIM proteins with microtubules is a conserved process. In addition to accumulation of STIM1 at microtubule plus ends, STIM1 moves along microtubules in an EB-1-independent manner. I identified two EB-1-independent microtubule-binding sites located within the C-terminus of STIM1 and found that oligomerization increases the EB-1-independent microtubule-binding affinity of STIM1. However, the physiological function of this EB1-independent microtubule binding activity remains elusive.

Zusammenfassung

Die Kopplung von Endoplasmatischem Retikulum (ER) und Plasma Membran (PM) ist essentiell für die Regulierung des Calziumhaushaltes. STIM1 und STIM2 sind Typ I Membranproteine des ERs und funktionieren als Ca^{2+} Sensoren in einem Prozess, der Speicher-getriebene Calziumaufnahme (engl. store-operated calcium entry, SOCE) genannt wird. Diese Proteine erkennen ein Abfallen der luminalen Ca^{2+}-Konzentration und reagieren mit Konformationsänderungen und oligomerisieren. Die aktiven, oligomerisierten STIM Proteine verlagern sich in ER-PM Kontaktstellen, wo sie über ihre Lysin-(K)-reichen Domänen an Phosphoinositole (PIPs) in der inneren Lipidschicht der PM binden und Orai1 aktiveren. Orai1 ist eine porenbildende Ca^{2+}-Freisetzungs-aktivierte Ca^{2+} (CRAC) Kanaluntereinheiten in der PM.

Ich habe herausgefunden, dass STIM2 aber nicht STIM1 ein Di-Lysin ER-Retentionssignal enthält. Dieses Signal beschränkt die Funktion von STIM2 als Ca^{2+} Sensor auf das ER wohingegen STIM1 über den klassischen Sekretionsweg zur PM transportiert werden kann. Die intrazelluläre Verteilung von STIM1 wird abhängig vom Zellzyklus reguliert, wobei STIM1 während der Mitose auf der Zelloberfläche exponiert ist. Während der Interphase wird STIM1 über seine lysinreiche Domäne und ein Di-Arginin Motiv effizient im ER zurückgehalten. SOCE verstärkt das Zurückhalten im ER, was zu der Annahme führt, dass das Trafficking von STIM1 ein regulierter Prozess ist und, dass diese Regulation zur Rolle von STIM1 als multifunktionale Komponente des Ca^{2+}-Signalings beiträgt.

Im Gegensatz zu mitotischen Zellen wird in Interphasezellen der Großteil von STIM1 im Zellinneren zurückgehalten. Im Ruhezustand befinden sich im ER lokalisierte STIM-Proteine bevorzugt in bereits bestehenden ER-PM Kontaktstellen, die $PI(4,5)P_2$ enthalten und bei Entleerung des ERs von Ca^{2+} expandiert werden. Die lipidbindenden K-reichen Domänen sind erforderlich, um STIM-Proteine in bestehenden ER-PM Kontaktstellen zu verorten. Darüber hinaus rekrutiert STIM2 das ER effektiver an die PM. Dies ist im Einklang stehend mit der Tatsache, dass STIM2 sowohl mit einer höheren Affinität an Lipide bindet und einen niedrigeren Aktivierungsschwellenwert als STIM1 hat, als auch als ein Regulator der basalen Ca^{2+}-Homöostase wirkt.

Abschließend habe ich die Rolle von Microtubuli bei der Bildung von ER-PM Kontakten untersucht. Ich habe beobachtet, dass STIM1 entlang von Mikrotubuli lokalisiert ist. Die Anlagerung von STIM-Proteinen und Mikrotubuli ist ein konservierter Prozess. Zusätzlich zur Anreicherung von STIM1 an plus-Enden von

Mikrotubuli bewegt sich STIM1 auf eine von EB-1 unabhängige Weise an Mikrotubuli entlang. Ich habe zwei Regionen innerhalb des C-Terminus von STIM1 identifiziert, die unabhängig von EB-1 an Microtubuli binden können. Ich habe herausgefunden, dass Oligomerisierung die Affinität der EB-1 unabhängigen Bindung an Mikrotubuli von STIM1 steigert. Was die genaue physiologische Funktion dieser EB1-unabhängigen Bindung an Mikrotubuli ist bleibt jedoch unbekannt.

Table of Contents

1. Introduction

1.1 The structure and function of the ER

The endoplasmic reticulum (ER) plays a critical role in many cellular processes including protein synthesis, protein folding, protein modification, trafficking, lipid biosynthesis and calcium homeostasis (Chen et al, 2013).

The ER is a large continuous membrane-enclosed organelle. It contains three functionally and structurally distinct domains including nuclear envelope, ER cisternae (or membrane sheet) and peripheral tubular network (or ER tubules) (Fig 1-1A and B) (Friedman & Voeltz, 2011; Shibata et al, 2009; Voeltz et al, 2002). The nuclear envelope (NE) wraps the nucleus and functions as a selective barrier to control the transport of molecules in and out of the nucleus (Fig 1-1C) (Anderson & Hetzer, 2007; Zheng & Tsai, 2006). ER cisternae locate closely to NE and are often found studded with membrane-bound ribosomes. This suggests that ER sheets correspond to the rough ER and function as site of protein translation and modification of secretory and membrane proteins (Shibata et al, 2006). On the contrary, tubular ER spreads out predominately in the periphery. Tubular ER contains no membrane-bound ribosomes and corresponds to smooth ER, suggesting that this region specializes in lipid metabolism and/or Ca^{2+} homeostasis (Shibata et al, 2006).

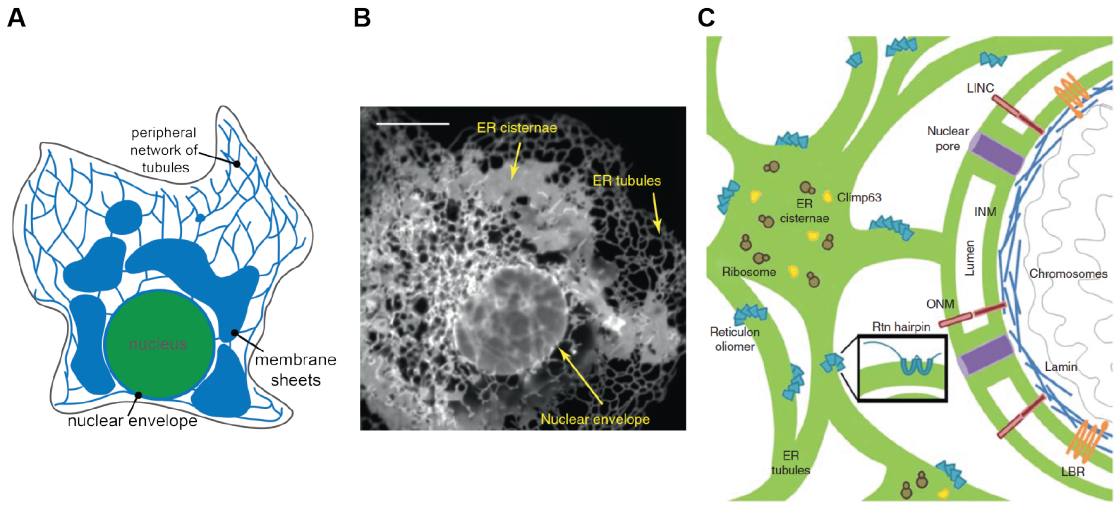

Figure 1-1. ER domains are stabilized by membrane-shaping proteins. (A). Cartoon depicts three structurally distinct domains of ER namely nuclear envelope (NE), membrane sheets (ER sheets or ER cisternae) and peripheral network of tubules (ER tubules). (B). COS-7 cells expressing ER membrane marker GFP-Sec61β. The ER network is comprised of NE, ER cisternae and ER tubules. (C). Model shows known ER domains (in green) and domain regulating proteins. The structure of NE

double membrane bilayer is regulated by the LINC complex (in red), nuclear pores (in purple) and lamin B-receptor (LBR) (in orange) interactions with lamin (in blue). The organization of the peripheral ER cisternae is regulated by Climp63 (in yellow) and large protein complexes such as polyribosomes (in brown). Reticulon proteins (in blue) oligomerize to control the tubular ER and curved edges of the cisternal ER. Adapted and modified from (English & Voeltz, 2013; Friedman & Voeltz, 2011; Shibata et al, 2010).

1.1.1 Factors that determine distinct ER structures in different ER domains

Both ER sheets and tubules are dynamic. They are constantly forming and collapsing. In previous studies, proteins shaping ER sheets and tubules have been identified. The tubular ER has high membrane curvature at its cross-sections. The morphology of ER tubule is determined and maintained by two families of curvature-stabilizing proteins, the reticulon (RTN) and DP1/Yop1p (Anderson & Hetzer, 2007; Voeltz et al, 2006; West et al, 2011). Depletion of RTN and DP1/Yop1p results in large reduction of tubular ER (Voeltz et al, 2006). RTN and DP1/Yop1p form immobile arc-shaped oligomers that increase the curvature of membranes resulting in membrane tubulation (Shibata et al, 2008; Voeltz et al, 2006). In fact, these proteins localize discriminately in tubular ER and edges of ER sheets (Shibata et al, 2010; Shibata et al, 2008; Voeltz et al, 2006) (Fig 1-1C), suggesting that RTN and DP1/Yop1p regulate the structure of multiple ER domains with high membrane curvature.

In ER sheet formation, RTN and DP1/Yop1p are required for stabilizing the high membrane curvature at sheet edges (Shibata et al, 2010). A coiled-coil, integral ER membrane protein, Climp63 is also essential for sheet-like ER formation. Overexpression of Climp63 leads to the proliferation of ER sheets. Depletion of Climp63 causes reduction of luminal width from 45-50 nm to 25-30 nm, suggesting that Climp63 serve as luminal spacer in ER sheets (Shibata et al, 2010).

1.1.2 ER-dynamics depends on microtubules

The ER is a highly dynamic organelle, undergoing constant reorganization and movement by interacting with the cytoskeleton. In animal cells, organization of ER tubular network highly depends on its ability to bind and move on microtubules (Terasaki et al, 1986). There are three mechanisms of the microtubule-dependent motility of tubular ER: microtubule movement mechanism, tip attach complex (TAC) mechanism and membrane sliding mechanism (Waterman-Storer & Salmon, 1998).

In the microtubule movement mechanism, tubular ER attaches to moving microtubules via direct or indirect interaction between ER resident proteins and microtubules. Climp63 (63 kDa cytoskeleton-linking protein) is a type II ER membrane protein containing a microtubule-binding domain and can link ER to microtubules. This interaction is important for stabilizing the extended ER network in the cell (Klopfenstein et al, 1998; Vedrenne & Hauri, 2006; Vedrenne et al, 2005).

Besides static interaction with microtubules, tubular ER can slide along acetylated microtubules, called ER sliding. This mechanism is the most common microtubule-dependent ER movement. About 70-95% of all ER movement events belong to this type (Friedman et al, 2010; Grigoriev et al, 2008; Waterman-Storer & Salmon, 1998). ER sliding is driven by microtubule motor proteins. Kinesin-1 and dynein drive ER moving towards plus-end and minus-end of microtubules, respectively (Wozniak et al, 2009).

In the tip attachment complex (TAC) dynamics, ER tubules elongate via associating with the growing end (plus-end) of microtubules. One example for TAC movement is achieved by the interaction between the ER integral membrane protein STIM1 and the microtubule plus-end binding protein, EB-1 (end-binding protein-1) (Grigoriev et al, 2008). Compared to sliding events, the TAC dynamics is less frequent and slower in mammalian cells (Friedman et al, 2010).

1.1.3 ER during mitosis

During mitosis (M-phase), NE and peripheral ER undergo dramatic structural and functional changes. The NE breaks down and the fragments of NE membrane and membrane proteins are absorbed into peripheral ER (Anderson & Hetzer, 2008; Kutay & Hetzer, 2008; Puhka et al, 2007; Yang et al, 1997). Peripheral ER remains continuous during the transition between interphase and mitosis. Mitotic ER consists of a highly reticulated tubular ER but no ER sheets (Puhka et al, 2007). This dramatic structural change of ER in M-phase causes its functional change, including reduction of ER exit sites and ribosome density (Prescott et al, 2001; Puhka et al, 2007), suggesting that the ER-dependent translation and transport in M-phase are reduced. Besides changes in structure and function, mitotic ER also changes its localization. During M-phase, ER locates near the plasma membrane (PM) and away from the mitotic spindle.

1.2 Interaction of ER with other organelles.

The ER network spreads throughout the cell and has contacts with most other membrane-bound organelles, including mitochondria, Golgi, endosomes, peroxisomes and PM (Fig 1-2) (English et al, 2009; Levine & Loewen, 2006). These contacts allow nonvesicular transport of ER synthesized lipids and sterols (Lebiedzinska et al, 2009; Toulmay & Prinz, 2011). Besides exchanging small molecules with other organelles, these contact sites also allow the ER to communicate with other organelles, such as in case of Ca^{2+} signaling (Lebiedzinska et al, 2009; Toulmay & Prinz, 2011).

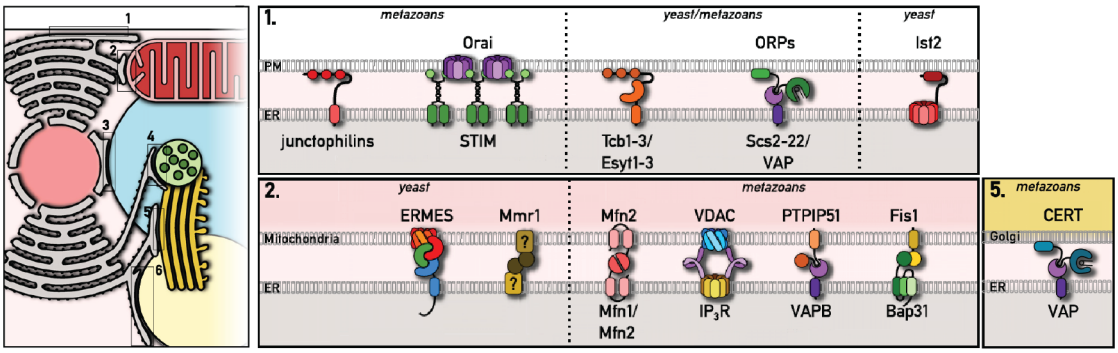

Figure 1-2. Established and potential tethers at various membrane contact sites (MCSs). Potential tethers between the (1). ER and PM in metazoan, yeast or both, (2). ER and mitochondria and (5). ER and Golgi. Adapted and modified from (Helle et al, 2013).

1.2.1 Interaction of ER with mitochondria

In HeLa cells, 5-20% of mitochondria surface is in contact with ER (Rizzuto et al, 1998). The average distance between ER and mitochondria is 30 nm as determined by electron microscopy (EM) (Csordas et al, 2010; West et al, 2011). The contact sites between ER and mitochondria are associated with several cellular functions, including Ca^{2+} signaling, lipid transfer and mitochondria division (Friedman & Voeltz, 2011; Rizzuto et al, 1998; Vance, 1990). The ER and mitochondria are tethered by several tethering complexes, including ERMES, VDAC- IP3R, Mitofusin-2, VAPB-PTPIP51 and the Bap31-Fis1 complex (Fig 1-2.2) (Helle et al, 2013).

In yeast, the ER-mitochondria encounter structure (ERMES) complex tethers ER to mitochondria and is comprised of MMM1 (an integral ER membrane protein), MDM12 (a cytosolic protein), MDM10 and MDM34 (integral outer mitochondrial membrane proteins) (Fig 1-3) (Kornmann et al, 2009). It has been proposed that ERMES function is required for Ca^{2+} exchange and mitochondrial protein import (Kornmann & Walter, 2010; Meisinger et al,

2007). In addition, this complex has a role in regulation of transfer of lipids from ER to mitochondria (Osman et al, 2009). A tailed-anchored mitochondrial protein, Gem1 (Miro – mitochondrial Rho GTPase in metazoans) regulates mitochondrial motility and morphology via binding to a kinesin motor protein in Ca^{2+} dependent manner (Fig 1-3A) (Wang & Schwarz, 2009). While the local Ca^{2+} concentration reaches high levels at the ERMES-mediated ER-mitochondria contact sites, Gem1 binds Ca^{2+} via its EF-hand domains. Binding of Ca^{2+} leads to association of Gem1 with kinesin resulting in dissociation of kinesin and microtubules (Fig 1-3A) (Kornmann & Walter, 2010).

The ERMES complex is also involved in the regulation of mitochondrial protein import. In addition to its function in ERMES, Mdm10 regulates the assembly of outer mitochondrial membrane β-barrel proteins such as Tom40 (translocase of outer mitochondrial membrane) via interacting with the sorting and assembly machinery (SAM) complex (Meisinger et al, 2007), suggesting a crosstalk between ER-mitochondria junctions and mitochondrial protein import (Fig 1-3B). Furthermore, ERMES-mediated ER-mitochondria contacts facilitate the targeting of soluble lipid carrier proteins such as oxysterol-binding protein (OSBP) and ceramide-transfer protein (CERT) (D'Angelo et al, 2008; Kornmann & Walter, 2010) and allow nonvesicular transfer of lipids between ER and mitochondria (Fig 1-3C).

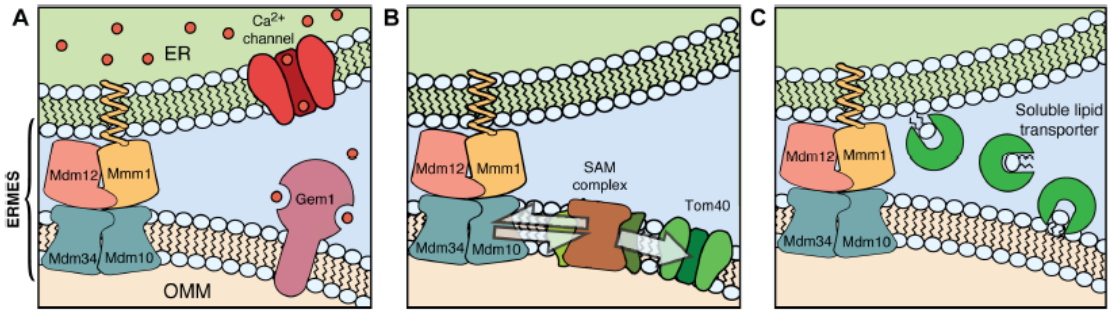

Figure 1-3. Proposed role of ERMES in Ca^{2+} exchange, mitochondrial protein import and phospholipids exchange. Schematic representation of ERMES-mediated ER-mitochondria contact sites playing role in (A). facilitating Ca^{2+}-saturation of Gem1 which plays a role in regulation of mitochondrial morphology and motility (B). the assembly of the translocase of outer mitochondrial membrane, Tom40 via interaction of Mdm10 with SAM complex (C). facilitating the targeting and shuttling of soluble lipid-transfer proteins between ER and mitochondria. Adapted and modified from (Kornmann & Walter, 2010).

In mammalian cells, Mitofusin2 (MFN2) has been shown to tether ER and mitochondria (de Brito & Scorrano, 2008). ER-localized MFN2 forms homo or hetero-complexes with MFN2 or MFN1 on the outer membrane of mitochondria forming ER-

mitochondria contact sites (de Brito & Scorrano, 2008). The MFN2-mediated ER-mitochondria contacts have crucial function in Ca^{2+} signaling (Pizzo & Pozzan, 2007). Another tethering complex, the VDAC-GRP75-IP_3R complex also plays an important role in Ca^{2+} homeostasis. Both ER-located inositol 1,4,5 receptor (IP_3R) and mitochondria-located voltage dependent anion channel 1 (VDAC) associate with a cytosolic chaperone – glucose –regulated protein 75 (GRP75) forming a complex, which tethers ER with mitochondria. (Szabadkai et al, 2006). The VDAC-GRP75-IP_3R complex-mediated ER-mitochondria contacts allow Ca^{2+} transferring mouth-to-mouth from the ER-located inositol 1,4,5 receptor (IP_3R) to the mitochondria-located voltage dependent anion channel 1 (VDAC). Knockdown of GRP75 decreases ER-mitochondria Ca^{2+} exchange (Szabadkai et al, 2006).

Apart from these two complexes, another ER-mitochondria tethering complex – VAPB-PTPIP51B is also important in Ca^{2+} homeostasis (De Vos et al, 2012). VAPB – the vesicle-associated membrane protein (VAMP)-associated protein (VAP), which is an integral ER membrane protein, interacts with the outer mitochondrial membrane protein, protein tyrosine phosphatase-interacting protein 51 (PTPIP51). Another potential ER-mitochondria tethering protein complex is Bap31-Fis1 (Helle et al, 2013). B-cell receptor-associated protein 31 (Bap31), which is an integral ER membrane protein, associates with the outer mitochondrial membrane protein, fission 1 homologue (Fis1). The Bap31-Fis1 tethering complex has been suggested to play a role in apoptosis regulation (Iwasawa et al, 2011).

1.2.2 Interaction of ER with Golgi

The ER-Golgi contacts regulate the transfer of secreted proteins and lipids (Glick & Nakano, 2009). The trafficking between ER and PM involves anterograde (COPII mediated), retrograde (COPI mediated) and direct nonvesicular transport (Barlowe et al, 1994; Hanada, 2010; Ladinsky et al, 1999; Malhotra et al, 1989).

The integral ER membrane proteins VAP-A and VAP-B interact with oxysterol-binding protein (OSBP) and ceramide-transfer protein (CERT) forming ER-Golgi contacts, which are important in biosynthesis of phosphoinositides and sphingolipids (Kawano et al, 2006; Peretti et al, 2008). In yeast, ORP Osh4 has an overlapping phophatidylinositol 4-phosphate (PI4P) and sterol-binding site. It has been proposed that Osh4 acquires PI4P from the Golgi membrane and exchanges it for a sterol at the ER (de Saint-Jean et al, 2011; Lev, 2012). These ER-Golgi contact sites are crucial for nonvesicular lipid transfer between two organelles.

Furthermore, a cytosolic protein, CERT associates with VAP, ceramide and phosphoinositide 4-phosphate (PI4P) on the Golgi membrane, forming ER-Golgi contact sites (Fig 1-4). Ceramide, the precursor of sphingomyelin is transported from the ER to the trans-Golgi by CERT at these ER-Golgi contact sites in a nonvesicular manner (Hanada, 2010; Hanada et al, 2009). The FFAT domain of CERT binds to the integral ER membrane protein, VAP and the pleckstrin homology (PH) domain of CERT binds to PI4P on the Golgi membrane resulting in stable ER-Golgi contact sites (Fig 1-4) (Hanada et al, 2009). The steroidogenic acute regulatory protein (StAR)-related lipid-transfer (START) domain of CERT transports ceramide from ER to Golgi (Fig 1-4). Transport of ceramide to the Golgi is important for the synthesis of sphingolipids (English et al, 2009). High concentration of sphingolipids and glycosphingolipids promote the phosphorylation of CERT leading to its inactivation and reduction in ceramide transport (Fig 1-4) (Breslow & Weissman, 2010). Furthermore, phosphatidylinositol (PI) synthesized in the ER can be transported to the Golgi by phosphatidylinositol transfer proteins (PITPs) at ER-Golgi contact sites (Peretti et al, 2008). PITPs transfer phosphatidylinositol (PI) and phosphatidylcholine (PC) between membranes, exchanging PI for PC and vice versa (Wiedemann & Cockcroft, 1998).

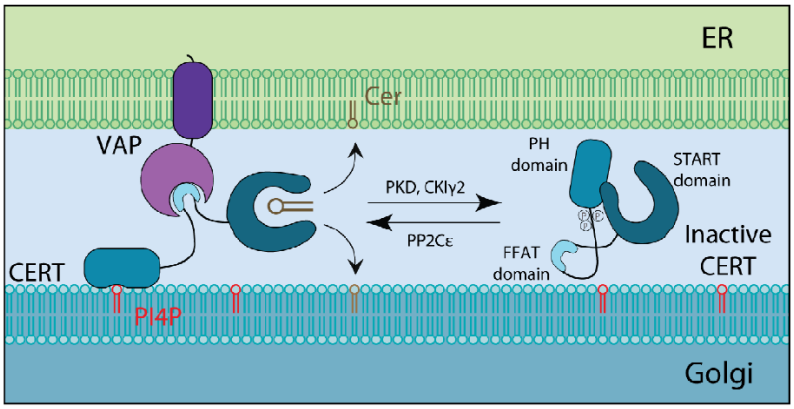

Figure 1-4. Nonvesicular transport of ceramide lipid at ER-Golgi contact sites. CERT couples the membranes of ER and Golgi by binding to PI4P lipid (red) on the Golgi membrane via its PH domain and to the integral ER membrane protein, VAP by its FFAT domain. CERT transports ceramide (brown) from ER to Golgi by its START domain. Inactivation and activation of CERT is regulated by protein kinase D (PKD) and casein kinase I (CKIγ2)-dependent phosphorylation and protein phosphatase 2C (PP2Cε)-dependent dephosphorylation, respectively. Adapted and modified from (Hanada et al, 2009; Helle et al, 2013).

1.3 Interaction of ER with the plasma membrane

The ER network has many positions where it is closely apposed to the PM in yeast and mammalian cells (< 50 nm) (Pichler et al, 2001; West et al, 2011). EM analysis has revealed that around 20-50% of PM is covered by tubular ER, called cortical ER in yeast (Wei et al, 2012; West et al, 2011; Wolf et al, 2012). The average distance between cortical ER and PM is around 30 nm in yeast (West et al, 2011; Wolf et al, 2012). The close distance between ER and PM leads to exclusion of ribosomes from PM-adjacent face of the ER and creates a ribosome-free membrane microcompartment (West et al, 2011; Wolf et al, 2012). In mammalian cells, the ER-PM contacts are not so abundant at resting state (Giordano et al, 2013; Orci et al, 2009). Upon contact formation, the distance between ER and PM is within 10 nm where ribosomes are excluded (Orci et al, 2009). Previous studies have identified the ER-PM contacts as sites of PI metabolism, nonvesicular transfer of sterols and Ca^{2+} level regulation (Baumann et al, 2005; Carrasco & Meyer, 2011; Li & Prinz, 2004; Stefan et al, 2011). Additionally, ER-PM contacts also play important roles in the control of organelle shape and morphology, inter-organelle communication, cell stress response and signaling networks (Stefan et al, 2013).

1.3.1 ER-PM contact sites mediate lipid-transport

The ER-PM contacts have been involved in nonvesicular transport of sterol lipids (Lev, 2010; Toulmay & Prinz, 2011). A conserved family of oxysterol-binding protein (OSBP)-related proteins (ORPs) localize to ER-PM contact sites in both yeast and mammalian cells (Lehto et al, 2005; Schulz et al, 2009). Several ORPs contain a pleckstrin homology (PH) domain that binds to PIP lipids in the PM (Roy & Levine, 2004). In addition, ORPs carry a motif containing two phenylalanine residues in an acidic tract (FFAT), which binds to integral ER membrane proteins named VAPs (Fig 1-5A) (Loewen & Levine, 2005). These protein-protein and protein-lipid interactions lead to tethering of ER and PM and serve as a platform for the sterol-binding motif of ORPs. ORPs drive the directional transport of newly synthesized sterol from the ER, where PI4P levels are relatively low, to the PM (Fig 1-5A) (Stefan et al, 2013). After delivery, PIP4 may prevent the re-extraction of sterol from the PM (Fig 1-5A) (de Saint-Jean et al, 2011). In addition, ORPs are also suggested to function as sterol-sensing signal transduction proteins (Beh et al, 2012).

1.3.2 ER-PM contact sites mediate regulation of cell signaling networks

PIP4-signaling is an essential mechanism in the control of cell growth and polarity, hormone and Ca^{2+} signaling, and regulated secretion and endocytosis (Hammond et al, 2012; Minogue & Waugh, 2012). An ER-localized PIP phosphatase, Sac1, regulates PI4P levels at the ER-PM contact sites formed by ER-localized VAP proteins and ORP family members (Fig 1-5B) (Manford et al, 2012; Stefan et al, 2011). ORP serve as sensors of PI4P in the PM, and control PI4P levels by activating the Sac1. PI4P turnover by Sac1 relieves PI4P inhibition of sterol extraction from the PM and may drive ORP-stimulated PM to ER sterol lipid transfer (Jansen et al, 2011). In addition, it has been demonstrated that OSBP of the ORP family attenuates mitogen-activated protein kinase (MAPK) signaling upon binding cholesterol and downstream protein phosphatases (Wang et al, 2005).

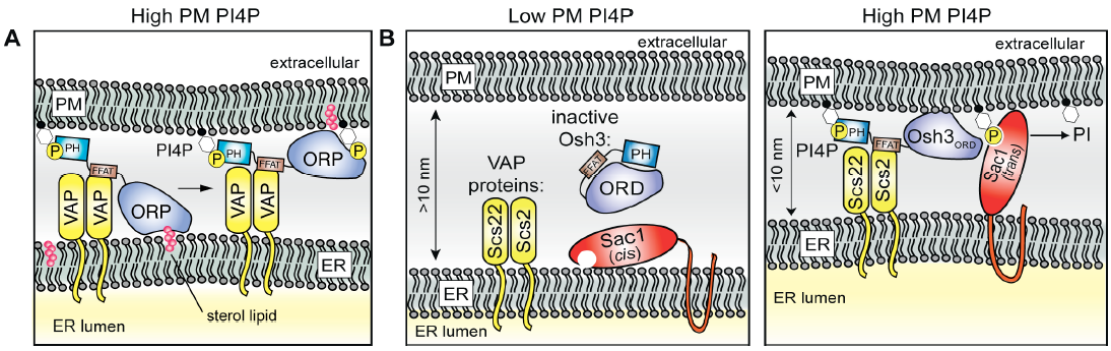

Figure 1-5. ER-PM contact sites mediate sterol lipid transfer and phosphoinositide metabolism. (A) Coupling of ER and PM facilitates nonvesicular transfer of sterol lipid from ER to PM. ORPs are recruited to ER-PM membrane contact sites via protein-protein and protein-lipid interactions (Schulz et al, 2009). The FFAT motif of ORPs binds integral ER membrane proteins called VAPs and the PH domain of ORPs binds PI4P in the PM (Loewen & Levine, 2005; Roy & Levine, 2004). The conserved sterol-binding domain of ORPs extracts newly synthesized sterol lipids (magenta) from the ER where PI4P levels are relatively low and delivers to the PM in a regulated manner (de Saint-Jean et al, 2011). Interactions between the sterol-binding domain of ORP and PI4P may inhibit extraction of sterol delivered to the PM (de Saint-Jean et al, 2011). (B) High levels of PI4P at the PM recruit and activate Osh3 (OSBP homolog in yeast) at ER-PM contact sites. Osh3 binds to VAP proteins, Scs2/Sc22 at the ER membrane via its FFAT domain and binds to PI4P at the PM through its PH domain. These interactions bring PM and ER membranes in close apposition having less than 10 nm distance. The integral ER membrane protein, Sac1 is recruited at these contact sites and is activated by Osh3 where its PIP phosphatase activity results in PI4P turnover at the PM. Adapted and modified from (Stefan et al, 2011; Stefan et al, 2013).

The ER-anchored protein tyrosine phosphatase PTP1B directly dephosphorylates PM-localized receptor tyrosine kinases (RTKs) at ER-PM contact sites (Fig 1-6), indicating a function of PTP1B at ER-PM junctions (Haj et al, 2012). PTP1B also interacts with and regulates the nonreceptor tyrosine kinase Src at ER-PM contact sites. PTP1B-Src interaction recruits Src to cell adhesion complex (Monteleone et al, 2012) where PTP1B dephosphorylates Eph receptors associated with cell-cell contacts (Haj et al, 2012). These findings suggest that inter-organelle signaling at ER-PM contacts control cell-cell communication during normal cell development and disease states, such as tumor cell progression (Stefan et al, 2013).

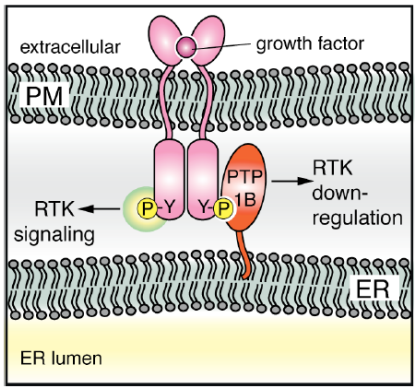

Figure 1-6. Growth factor receptor signaling is regulated at ER–PM membrane contact sites. The ER-anchored protein tyrosine phosphatase isoform PTP1B interacts with ligand-bound (RTK) and dephosphorylates it at ER-PM junctions. Adapted and modified from (Stefan et al, 2013).

1.3.3 Role of ER-PM contact sites in organization of ER and stress responses

In yeast, three conserved protein families have been identified as ER-PM tethers, which are VAP proteins Scs2/22, Ist2 (anoctamin family), and the tricalbin proteins Tcb1/2/3 (orthologs of synaptotagmin-like proteins E-Syt1/2/3) (Fig 1-7) (Loewen et al, 2007; Manford et al, 2012; Min et al, 2007; Tian et al, 2012; Toulmay & Prinz, 2012; Wolf et al, 2012). The ER-PM tethering proteins are anchored in the ER and interact with the PM via cytoplasmic lipid-binding and protein-binding domains (Fig 1-7). Loss of all six ER-PM tethers leads to a massive reduction of cortical ER from ~ 40% to ~ 5% (Manford et al, 2012) resulting in changes in ER morphology, accumulation of high levels of PI4P on the PM and constitutive activation of unfolded protein response (UPR) (Manford et al, 2012). These observations suggest a role for ER-PM contacts in ER function and stress signaling pathways (Stefan et al, 2013).

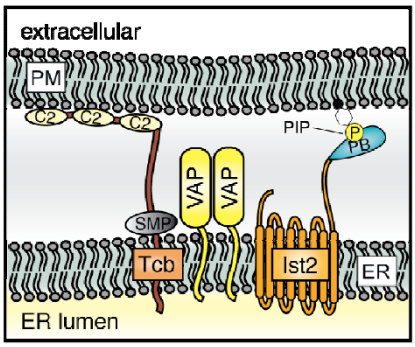

Figure 1-7. ER-PM contact sites in yeast. Three families of integral ER proteins tether the cortical ER to the PM: the VAP proteins Scs2/22, Ist2, and the tricalbins. Adapted and modified from (Stefan et al, 2013).

1.3.4 ER-PM contact sites mediate calcium transport

Ca^{2+} signaling plays an essential role in a wide range of physiological events including muscle contraction, neurotransmission, fertilization, gene transcription, cell proliferation and division, secretion, apoptosis and several others (Berridge et al, 2003; Berridge et al, 2000; Clapham, 2007; Lewis, 2001). Ca^{2+} signaling involves the concerted action of Ca^{2+} release channels in Ca^{2+} storage organelles and Ca^{2+} entry channels in the PM (Soboloff et al, 2012). The ER represents the major intracellular store of Ca^{2+} in metazoans (Koch, 1990). Moreover, ER-PM contacts are required for activation of several Ca^{2+}-channels in the ER and PM (Carrasco & Meyer, 2011; Elbaz & Schuldiner, 2011). Thus, release of Ca^{2+} into the cytosol activates several downstream signaling pathways. One example for this is the sarcomere contraction in muscle cells. Endo/sarcoplasmic reticulum (ER/SR)-PM junctions are important for this process. (ER/SR)-PM junctions were first discovered in muscle cells by EM (Porter & Palade, 1957). The formation of SR-PM contacts is mediated by the junctophilins (JPH).

JPH 2 is consistently expressed in excitable cells and serves as a bridge to maintain the ~ 12 nm close apposition of SR and PM required for efficient interaction between ion channels (Garbino et al, 2009; Takeshima et al, 2000). The cytoplasmic membrane occupation and recognition nexus (MORN) motifs of JPH2 bind $PI(4,5)P_2$ at the PM leading to SR-PM contact formation in muscle cells (Fig 1-8) (Garbino et al, 2009; Garbino & Wehrens, 2010; Takeshima et al, 2000).

During excitation-contraction coupling, voltage-gated Ca^{2+} channels (VGCCs) in PM invaginations (named T-tubules) activate the closely opposed ryanodine receptors 2 (RyR2) in the ER leading to Ca^{2+} release from SR lumen to cytosol, thereby induce contraction of

the sarcomere (Fig 1-8) (Endo, 2009; Garbino & Wehrens, 2010). Ca^{2+} is pumped back into SR lumen by the sarco/endoplasmic reticulum Ca^{2+} ATPase (SERCA) or removed by the Na^{+}/Ca^{2+} exchanger (NCX) resulting in myocyte relaxation (Garbino & Wehrens, 2010). Many mutations in JPH2 have been identified in patients with hypertrophic cardiomyopathy (Landstrom et al, 2007).

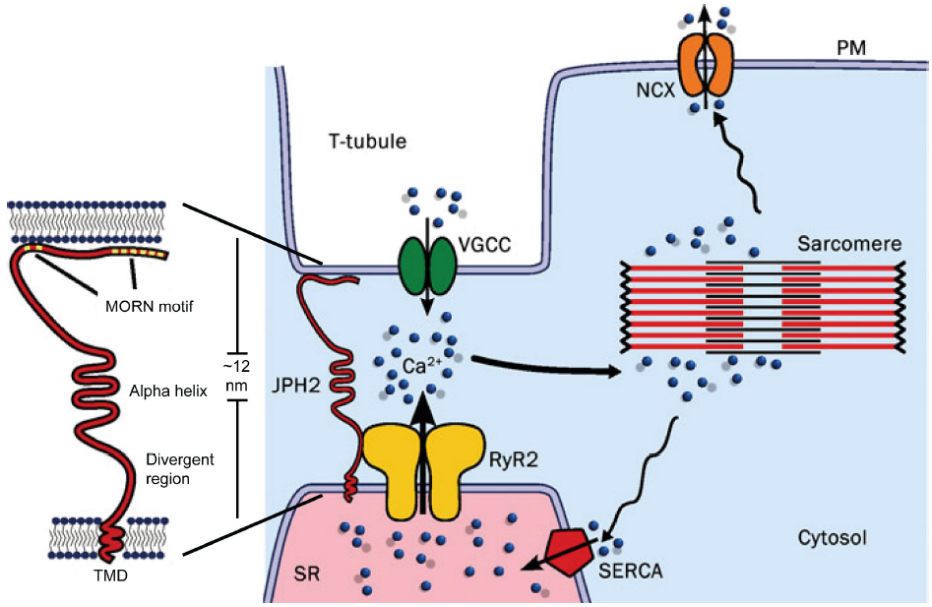

Figure 1-8. Molecular components responsible for excitation-contraction coupling in muscles. The depolarization-triggered opening of VGCCs results in Ca^{2+}-induced Ca^{2+} release from SR resident RyR. Junctophilin (JPH2), an integral SR membrane protein mediates this crosstalk by establishing SR-PM contacts via interaction of MORN motifs with PM lipids (Takeshima et al, 2000). The Ca^{2+} released into the cytosol leads to sarcomere contraction and myocyte relaxation is achieved by the action of NCX exchanger or SERCA. Adapted and modified from (Garbino & Wehrens, 2010).

1.4 Store-operated calcium entry

ER-PM junctions are also platforms for store-operated Ca^{2+} entry (SOCE) (Carrasco & Meyer, 2011; Liou et al, 2005). SOCE is a conserved process in all metazoans, which maintains physiological ER Ca^{2+} concentration. Besides refilling depleted ER Ca^{2+} stores, SOCE generates long-term Ca^{2+} signals that control many cellular functions, including gene expression, cell differentiation, secretion, contraction and Ca^{2+} homeostasis in most non-excitable and many excitable cell types (Hogan et al, 2010; Parekh & Putney, 2005; Soboloff et al, 2012). Two main players have been identified in the SOCE pathway: stromal interacting molecule (STIM) and Ca^{2+} release-activated Ca^{2+} channel protein 1 (Orai1) (Liou et al, 2005; Prakriya et al, 2006; Roos et al, 2005). STIM has two main functions in SOCE.

Firstly, sensing ER Ca^{2+}-depletion and secondly, coupling the store Ca^{2+}-level to the activation and deactivation of the Ca^{2+} release-activated Ca^{2+} channel (CRAC) in the PM (Muik et al, 2008; Park et al, 2009; Srikanth et al, 2010; Yuan et al, 2009). This is achieved by direct contact of STIM with lipids and Orai1 in the PM at ER-PM junctions (Bhardwaj et al, 2013; Ercan et al, 2009; Park et al, 2009; Walsh et al, 2010; Xu et al, 2006).

1.4.1 Domain architecture and function of STIMs

Specialized domains in STIM1 and STIM2 play different roles in SOCE, including Ca^{2+}-sensing, translocation and formation of ER-PM contacts and channel-activation. The molecular domains of STIM1 and STIM2 are conserved in vertebrates (Cai, 2008) and shown in Fig 1-9. The N-terminal EF-hand domains in STIM1 and STIM2 are located in the ER lumen and sense the luminal Ca^{2+} concentration. Both STIM proteins have two EF-hand domains, namely canonical EF-hand (cEF) and hidden EF-hand (hEF). The two EF-hand domains of STIM proteins operate together in a tightly associated complex with the sterile alpha motif (SAM) domain to finely sense luminal Ca^{2+} (Stathopulos et al, 2006; Stathopulos et al, 2009; Stathopulos et al, 2008; Zheng et al, 2008; Zheng et al, 2011). At resting luminal Ca^{2+} level (~ 400 μM), Ca^{2+}-bound cEF forms a tight and stable EF-hand-SAM configuration. Upon Ca^{2+} level decrease, Ca^{2+} dissociates from the cEF-hand domain. This Ca^{2+} dissociation leads to unfolding and destabilization of ER-hand-SAM complex and triggers activation and oligomerization of STIM proteins (Covington et al, 2010; Li et al, 2007; Park et al, 2009; Williams et al, 2002; Wu, 2006). Consistently, the expression of STIM1 and STIM2 with mutations in the EF-hands led to constitutive coupling of ER and PM and constitutive store-independent Ca^{2+} entry (Brandman et al, 2007; Ercan et al, 2009; Liou et al, 2005; Soboloff et al, 2006b; Stathopulos et al, 2008; Zhang et al, 2005). The dissociation constant (K_d) of STIM2 for Ca^{2+} is ~ 400 μM, whereas STIM1 has K_d of 200 μM (Zheng et al, 2008). This difference in K_d indicates that STIM2 is more sensitive to small changes in luminal Ca^{2+} level than STIM1 (Brandman et al, 2007). Thus, STIM2 may function as a feedback regulator that stabilizes basal cytosolic and ER Ca^{2+} levels (Brandman et al, 2007).

STIM1 and STIM2 have three coiled-coil domains (CC1-3) (Fig 1-9), which play a role in their self-oligomerization (Soboloff et al, 2012). It has been suggested that STIM1 forms homo-complexes (dimer) via the coiled-coil domain at resting state (Fig 1-10) (Baba et al, 2006; Covington et al, 2010; Muik et al, 2008; Penna et al, 2008; Williams et al, 2002). Two individual studies identified the minimal domain of STIM1 required for Orai1 channel activation: as cytosolic Ca^{2+} release activated Ca^{2+} (CRAC) channel activation domain

(CAD) (residues 342-448) (Park et al, 2009) and STIM1-Orai activating region (SOAR) (344-442) (Yuan et al, 2009), hereafter called SOAR. Purified CAD was reported to form tetramer *in vitro* (Park et al, 2009), whereas SOAR was reported to form dimers (Yuan et al, 2009) and a recently published crystal structure (Yang et al, 2012) of STIM1 SOAR supports this observation.

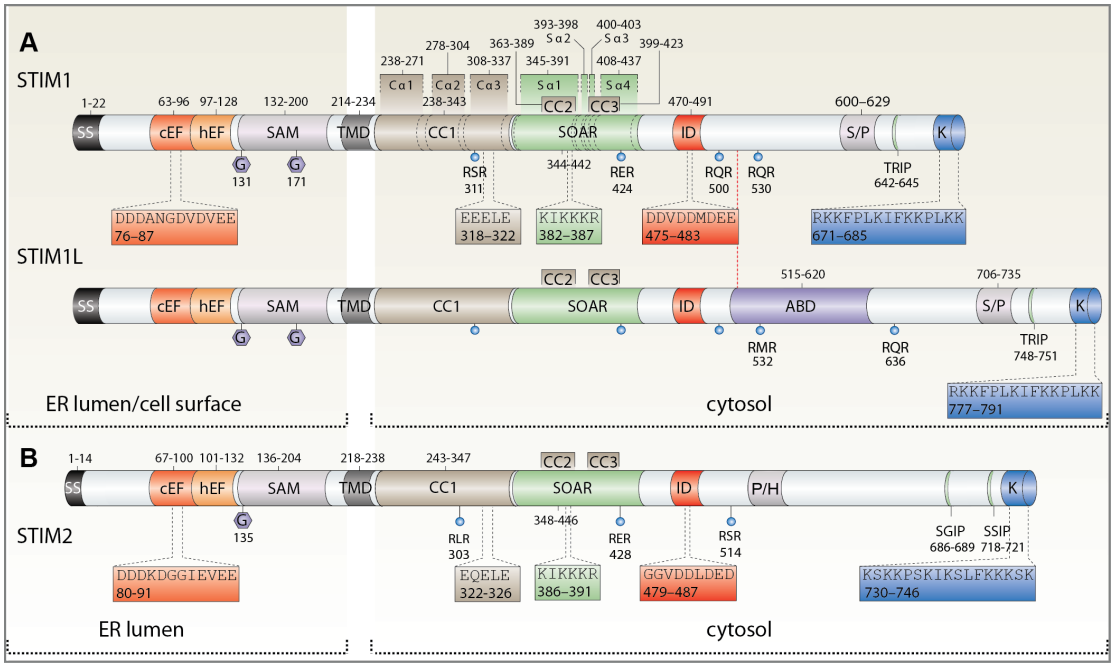

Figure 1-9. The molecular domains of human STIM1, STIM1L-isoform and STIM2. (A) Human STIM1 and STIM1L isoform comprising of 685 and 791 amino acid residues, respectively **(B)** STIM2 comprising of 746 amino acids residues are shown. Signal sequence (SS), canonical EF-hand domain (cEF) with amino acid sequence of Ca^{2+}-binding loop, hidden EF-hand domain (hEF), sterile alpha motif (SAM), transmembrane domain (TMD), coiled-coil domains 1-3 (CC), three predicted α-helices of CC1 (Cα1-3), (Soboloff et al, 2012) STIM-Orai activating region (SOAR), four α-helices of SOAR (Sα1-4), inactivation domain (ID), actin-binding domain (ABD) in STIM1L, serine/proline-rich region (S/P), proline/histidine-rich region (P/H), microtubule plus end tracking protein EB1 binding motif TRIP motif in STIM1 and SGIP/SSIP motifs in STIM2 (Ser/Thr-x-Ile-Pro), the K-rich domains with their amino acid sequences (all with residue numbers) and the orientations of N- and C-termini are shown. Asn-linked glycosylation sites are shown as hexagons. Arginine retention signals (RXR) are depicted as blue circles with residue numbers. Adapted and modified from (Darbellay et al, 2011; Graham et al, 2011; Rajesh, 2013; Soboloff et al, 2012).

Upon ER Ca^{2+} store depletion, STIM1 translocates to ER-PM contacts (space less than 10 nm) where Orai1 is recruited and activated (Orci et al, 2009). A short polybasic

region within the SOAR domain (residues 382-387; KIKKKR) (Fig 1-9) interacts electrostatically with a cluster of acidic residues in the cytosolic C-terminus of Orai1 (Calloway et al, 2010; Korzeniowski et al, 2010; Yang et al, 2012). Mutation of the basic residues (KIKKKR) implicated in the electrostatic interaction with Orai1 prevented STIM1-Orai1 interaction and channel activation (Calloway et al, 2010; Korzeniowski et al, 2010; Yang et al, 2012). At resting state, CC1 interacts with SOAR via an inhibitory α-helix (residues 310-337), thereby inhibits the function of SOAR (Covington et al, 2010; Yang et al, 2012; Zhou et al, 2013). Consistently, deletion of the inhibitory helix activates SOCE constitutively. Mutation of acidic residues (residues 318-322; EEELE) within the helix releases SOAR and results in constitutive activation of STIM1 (Kim & Muallem, 2011; Korzeniowski et al, 2010). This inhibitory interaction keeps STIM1 as dimer at resting state (Covington et al, 2010; Yang et al, 2012).

An acidic inhibitory domain (ID), which locates downstream of SOAR, mediates fast Ca^{2+}-dependent inactivation of Orai1 (Derler et al, 2009; Lee et al, 2009) (Fig 1-9). Downstream of ID is a Pro-rich domain, namely Ser/Pro-rich domain in STIM1 and Pro/His-rich domain in STIM2 (Soboloff et al, 2012). The function of this Pro-rich domain is not clear except that it may provide flexibility to the C-terminal tails (Soboloff et al, 2012).

STIM1 has an EB-1 binding motif (S/TxIP: Ser/Thr-x-Ile-Pro) in its C-terminal domain. EB-1 is a microtubule-plus-end-tracking protein, which binds to growing (plus) ends of microtubules (Akhmanova & Steinmetz, 2008; Kumar & Wittmann, 2012). STIM1 associates with EB-1 via its EB-1 binding motif (S/TxIP) resulting in comet-like movement towards the cell periphery (Grigoriev et al, 2008; Honnappa et al, 2009). STIM2 also has two such S/TxIP motifs (Fig 1-9).

STIM1 and STIM2 both have lysine-rich (K-rich) domains at their extreme C-termini with eight and nine basic residues, respectively (Fig 1-9). The initial recruitment of activated STIM1 oligomers to ER-PM contacts is mediated by the interaction of the K-rich domain and the phosphatidylinositol phosphate (PIP) lipids at the inner leaflet of the PM (Ercan et al, 2009; Liou et al, 2007; Walsh et al, 2010) (Fig 1-11). Tetramerization of the STIM1 K-rich domain via cytosolic coiled-coil domains is required for efficient binding to $PI(4,5)P_2$-containing PM-like liposomes, which is consistent with an oligomerization-driven STIM1 activation (Bhardwaj et al, 2013). In contrast, dimerization of the STIM2 K-rich domain is sufficient for binding PM phosphoinositides efficiently (Bhardwaj et al, 2013). Furthermore, unlike STIM1, the K-rich domain of STIM2 forms an amphipathic α-helix, which contributes to its higher affinities towards lipids and Ca^{2+}/Calmodulin (CaM) (Bhardwaj et al, 2013; Ercan

et al, 2009). Preincubation of purified STIM2 K-rich domain with CaM inhibited its binding to $PI(4,5)P_2$-containing liposomes, suggesting that elevated cytosolic Ca^{2+} levels may down-regulate STIM2-mediated ER-PM contacts via binding of CaM to its K-rich domain (Bhardwaj et al, 2013).

The isoforms of STIM called STIM1L is shown in Fig 1-9A. STIM1L splice variant is present in skeletal muscle and is as strongly expressed as STIM1 (Darbellay et al, 2011). STIM1L binds to cortical actin via its actin-binding domain and Orai1 forming permanent clusters. Forming STIM1L-cortical actin-Orai1 cluster allows the immediate and repetitive activation of SOCE in excitable cells (Darbellay et al, 2011).

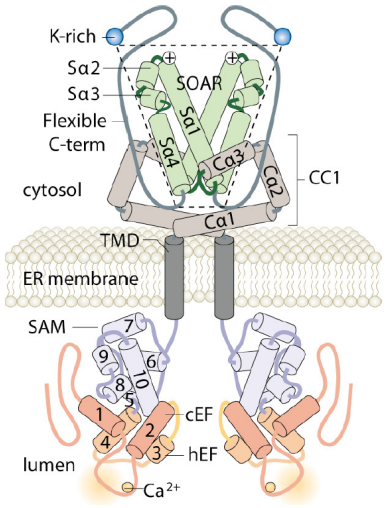

Figure 1-10. Proposed structure of resting STIM1 dimer. The luminal EF-hand domain is bound with Ca^{2+} in the resting STIM1. Structure of dimeric STIM1 contains a number of α-helices (shown as cylinders) in cEF, hEF and SAM domains (Zheng et al, 2011). The predicted α-helices in CC1 (Cα1-3; refer Fig 1-9A) are shown in a folded configuration. SOAR dimer with each unit comprising four α-helices (Sα1-4; refer Fig 1-9A) is also shown as locked in closed conformation by electrostatic interactions between of Sα1 of SOAR with Cα3 of CC1 (refer Fig 1-9A for residues involved in this inhibitory interaction) (Covington et al, 2010; Korzeniowski et al, 2010; Muik et al, 2008; Yang et al, 2012). The polybasic region of SOAR is depicted as (+). The C-terminal flexible region and the K-rich domain are shown as grey line and blue circle, respectively. Flexible regions of the protein are shown as lines. Adapted and modified from (Rajesh, 2013; Soboloff et al, 2012; Stathopulos et al, 2008).

1.4.2 The molecular mechanism of SOCE

The concerted action of described domains control SOCE in a step-wise manner, which is shown in Fig 1-11. STIM1, STIM2 and Orai1 are activated during SOCE in several steps in the following order (Soboloff et al, 2012) (Fig 1-11).

1. At resting state, both STIM1 and Orai1 form homo-dimers (Baba et al, 2006; Covington et al, 2010; Demuro et al, 2011; Muik et al, 2008; Penna et al, 2008). STIM1 and Orai1 localize diffusely in the ER and PM, respectively (Feske et al, 2006; Wu, 2006). STIM1 forms a dimer via CC1 and SOAR as described before (Fig 1-10 and 1-11). However, whether STIM2 also assembles as dimer at resting state is not known.
2. Ligand binding to G-protein coupled receptors or tyrosine kinase receptors, activates phospholipase Cβ or phospholipase Cγ2 (PLC), respectively, resulting in hydrolysis of phosphatidylinositol 4,5-bisphosphate PI(4,5)P_2 at the inner leaflet of PM and generates inositol 1,4,5-trisphosphate (IP_3).
3. IP_3 diffuses rapidly within the cytosol and binds to the ER-located IP_3 receptor (IP_3R) resulting in release of ER Ca^{2+} through the IP_3R.
4. (a). Upon Ca^{2+} concentration drop in the ER, Ca^{2+} dissociates from STIM1 and STIM2 EF-hand domains.

   (b). Aggregation and interaction of EF-SAM induces an extended conformation of the coiled-coil domains resulting in dissociation of the Cα3 inhibitory helix and SOAR (Fig 1-10) and exposure of SOAR.
5. (a). Activated STIM1 dimer further undergoes oligomerization via coiled-coil domains and translocates to ER-PM contact sites.

   (b). Higher-order STIM1 oligomer binds PI(4,5)P_2 at the inner leaflet of the PM avidly via their K-rich domains leading to extension and stabilization of ER-PM contact sites.
6. Orai1 is recruited to STIM1-mediated ER-PM contact sites.
7. Contemporaneously, binding of SOAR domains of STIM proteins to the C-terminus of Orai1 opens the CRAC channels, generating a Ca^{2+} influx across the PM into the cytosol (Muik et al, 2008; Park et al, 2009; Yuan et al, 2009). Orai1 in its active state is tetrameric (Demuro et al, 2011; Penna et al, 2008). Current stochiometric model of STIM1-Orai1 interaction suggests that eight STIM1 molecules form an active complex with one tetrameric Orai1 (Li et al, 2011; Soboloff et al, 2012).
8. ER store is refilled with Ca^{2+} by SERCA, which is corecruited at these ER-PM contact sites (Krapivinsky et al, 2011).

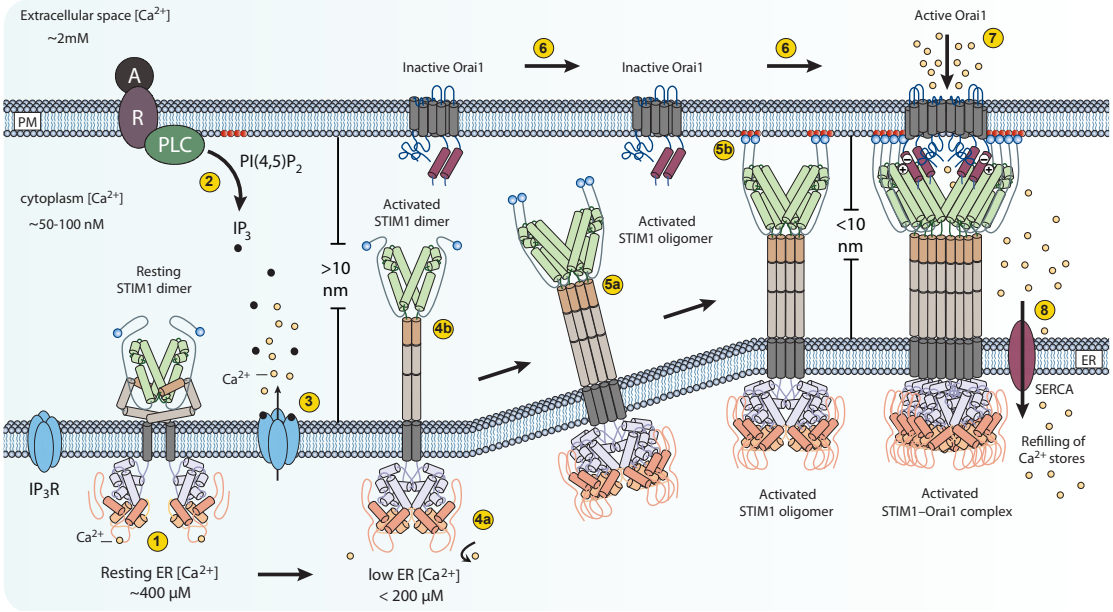

Figure 1-11. Cartoon presents the current model of SOCE. Release of IP_3 in response to a stimulus triggers release of Ca^{2+} from IP_3R resulting in depletion of ER Ca^{2+} stores. Consequently, STIM1 undergoes conformational changes upon loss of Ca^{2+} from its luminal EF-hand domain and accumulates at ER-PM junctions. This is facilitated by interaction of its K-rich cytosolic domain with $PI(4,5)P_2$ at the PM. Orai1 also accumulates at ER-PM contact sites where interaction of STIM1 with Orai1 establishes the functional CRAC channel resulting in Ca^{2+} influx into the cytosol. SERCA refills the stores by pumping the cytosolic Ca^{2+} into the ER. Adapted and modified from (Rajesh, 2013; Soboloff et al, 2012).

1.4.3 Localization of STIM1 on the cell surface and within subdomains of the tubular ER

STIM2 is exclusively localized in the ER whereas ~ 5-10% of STIM1 is located in the PM (Saitoh et al, 2011; Soboloff et al, 2006a; Soboloff et al, 2006b). Although role of STIM1 is mostly defined in the ER, STIM1 was initially found on the surface of stromal cells (Manji et al, 2000; Oritani & Kincade, 1996; Soboloff et al, 2012; Williams et al, 2001). Consistently, overexpressed $His_{(6)}$-STIM1 reaches the surface of HEK293 cells (Hauser & Tsien, 2007).

The mouse homologue of STIM1 traffics to the cell surface, where it interacts with pre-B cells via its N-terminal region leading to increased proliferation (Oritani & Kincade, 1996). Also, in bone marrow stromal cells, surface STIM1 binds to mature B-lymphocytes and other lympho-haematopoietic cell lineages (Kincade et al, 1998). These studies suggest the surface STIM1 mediates cell-cell interactions and functions in growth regulation (Saitoh et al,

2011). Also, surface STIM1 has been reported to regulate Ca^{2+} entry via store-independent arachidonate-regulated heteromeric Orai1/Orai3 Ca^{2+} influx (ARC) channels (Mignen et al, 2007).

Although 5-10% of STIM1 localizes on the cell surface, the majority of STIM1 is retained in the ER. So far, the distribution of STIM1 within subdomains of the ER is still under debate. One model suggests that STIM1 dimer distributes evenly throughout the ER membrane at resting state (Liou et al, 2007; Luik et al, 2006). The other model suggests that STIM1 localizes within specific subdomain of tubular ER (Orci et al, 2009; Wu, 2006). Orci et al. defined three structurally distinct subdomains in tubular ER namely precortical (pre-cER), cortical and thin cortical ER using EM. Properties of these three ER subcompartments are summarized in Table 1.1 (Orci et al, 2009). Pre-cER consists of thin ER subdomains enriched in STIM1 but depleted of ER proteins containing a KDEL motif such as BiP (binding immunoglobulin protein and GFP-KDEL (Baba et al, 2006; Orci et al, 2009; Shen et al, 2011). These thin ER subdomains of pre-cER are often observed extending along microtubules (Orci et al, 2009). Pre-cER is about 500 nm away from the PM and devoid of contacts with PM (Table 1.1). Upon activation of SOCE the pre-cER is transformed to cortical and thin cortical ER and both appose the PM. The cortical ER has average length of 200-400 μm and is frequently found along microtubules, with ribosomes absent from the side facing the PM ((Orci et al, 2009; Shen et al, 2011); Table 1.1). Approximately half of the cortical ER exhibits a distinct morphology and forms thinner cortical ER (thickness: 24 ± 0.4 nm), called thin cortical ER ((Orci et al, 2009; Shen et al, 2011); Table 1.1). EM studies revealed that the thin cortical ER is depleted of BiP and is highly enriched in STIM1 ((Lur et al, 2009; Orci et al, 2009; Shen et al, 2011); Table 1.1), suggesting that thin cortical ER is a specialized region dedicated to calcium regulation and not engaged in protein translocation and folding (Shen et al, 2011).

Table 1.1. Properties of ER subcompartments (Orci et al, 2009; Shen et al, 2011).

Properties	Pre-cER	cER	Thin cER
Average length		200–400 µm	
Distance from PM	>500 nm	11.3±2.9 nm (cryosections), 8.3±0.3 nm (Epon sections)	1.3–14.7 nm (Epon sections)
Thickness		73±3 nm	24±0.4 nm
Appearance	Thin ER subdomains devoid of contacts with the PM and apposed to microtubules	Flattened ER sheets deprived of ribosomes on their PM side and physically connected to conventional ER cisternae, often aligned along microtubules	Thinner cER subdomains continuous with the thick cER, deprived of ribosomes also on their cytosolic side
Proportion		0.23% of PM (resting cells), 1.24% (thapsigargin), 5.44% (thapsigargin+STIM1)	50% of the cER
STIM1	Enriched	Weak	Enriched
BiP	Excluded	Present	Excluded

2. Hypothesis and aim of the thesis

In order to function in SOCE, STIM proteins require ER localization. Unlike STIM1, STIM2 localizes exclusively in the ER. 5-10% of STIM1 localize on the cell surface, but the majority of STIM1 remains intracellular. Therefore, the first aim of this study was to investigate which mechanisms and signals retain STIM1 and STIM2 in the ER and allow trafficking of STIM1 to the cell surface

Although the basic molecular mechanism of SOCE is understood, the molecular bases of the translocation process in SOCE remains elusive. In order to decipher the translocation process of STIM proteins in SOCE, the second aim of my thesis was to study whether STIM1 localizes in specific ER subdomains at resting state, namely preexisting ER-PM contact sites. According to a previous EM study, STIM1 accumulates in the cortical ER and associates with the cortical microtubules. In addition, purified GFP-STIM1C binds $PI(4,5)P_2$-containing liposomes via its K-rich domain *in vitro*. Based on these two previous studies, I hypothesized that STIM1 localizes in the preexisting ER-PM contact sites. Upon Ca^{2+} store depletion, STIM1 accumulates at these preexisting ER-PM contact sites leading to expansion of ER-PM contact sites, where Orai1 is recruited and activated. Moreover, I aimed to identify which signals in STIM1 are involved in accumulation of STIM1 in preexisting ER-PM contact sites.

Finally I analyzed the role of microtubules in STIM1 localization and STIM1-mediated ER-PM contacts formation. It has been reported that STIM1 associates with the microtubule plus end protein EB-1, which links STIM1 to microtubule plus ends. To investigate whether STIM1 associates with microtubules in an EB-1-independent manner, I performed colocalization assays of STIM1 mutants with microtubules *in vivo* and *in vitro* microtubule cosedimentation assay.

3. Materials and Methods

3.1 Molecular Biology Methods

3.1.1 Polymerase Chain Reaction (PCR)

Materials and equipment

Taq DNA Polymerase (New England Biolabs-NEB)

10X Standard *Taq* Reaction Buffer (NEB)

Phusion® High-Fidelity DNA Polymerase (NEB)

Pfu Turbo DNA Polymerase (Agilent Technologies)

10X *Pfu* Polymerase Buffer (Agilent Technologies)

dNTPs (NEB)

Primers (Eurofins MWG Operon, Sigma-Aldrich Fluka)

PCR tubes (G. Kisker GbR)

T3 Thermocycler (Biometra®)

3.1.1.1 Standard PCR

Forward and reverse primers were designed with desired restriction sites and contain four extra flanking bases at the 5' end. The DNA fragments were amplified by PCR from plasmid DNA with different set of primers. The PCR reaction mixture was prepared as described in Table 3.1 below.

Table 3.1 Reaction mixture of standard PCR

Template DNA	200 ng
10X Standard *Taq* Reaction Buffer	1X
dNTPs mix	250 µM
Forward primer	0.5 µM
Reverse primer	0.5 µM
DMSO	3%
Phusion Polymerase	2 units (1 µl)
Taq DNA Polymerase	2.5 units (0.5 µl)
dH_2O	to 50 µl
Total	50 µl

All the standard PCR reactions were performed using the condition in Table 3.2. The elongation time was calculated as 15-30 sec/kb of fragment to be amplified.

Table 3.2 Standard PCR conditions

Step no.	Step	Temperature	Time	Cycles
1	Initial denaturation	98°C	30 sec	1
2	Denaturation	98°C	30 sec	Steps 2-4 (25 cycles)
3	Annealing	55-60°C	30 sec	
4	Elongation	72°C	15-30 sec/kb	
5	Final extension	72°C	5 min	1
6	Pause	4°C	∞	

3.1.1.2 Site-directed mutagenesis

Site-directed mutagenesis (SDM) was used to create point mutations. The primers were designed with mutation sites in the center flanked by 15 bases on both ends. The PCR mixture for SDM was prepared as described in Table 3.3. All the SDM reactions were performed using condition as mentioned in Table 3.4.

Table 3.3 Reaction mixture for site-directed mutagenesis

Template DNA	25 ng
10X *Pfu* Buffer	1X
dNTP mix	250 µM
Forward primer	0.2 µM
Reverse primer	0.2 µM
Pfu polymerase	1.25 Units (0.5 µl)
dH_2O	To 25 µl
Total	25 µl

Table 3.4 PCR conditions for site-directed mutagenesis

Step no.	Step	Temperature	Time	Cycles
1	Initial denaturation	95°C	30 sec	1
2	Denaturation	95°C	30 sec	Steps 2-4 (18 cycles)
3	Annealing	52°C	60 sec	
4	Elongation	68°C	2 min/kb	
5	Pause	4°C	∞	

3.1.1.3 Deletion mutagenesis

In order to create truncated mutants of a gene, forward and reverse primers with phosphate modification at 5'-end were used. Forward and reverse primers were designed by selecting about 20 bases downstream and upstream of the site to be deleted, respectively. The PCR reaction for deletion mutagenesis was prepared as described in Table 3.5.

Table 3.5 PCR conditions for deletion mutagenesis

Template DNA	50 ng
10X Standard *Taq* Reaction Buffer	1X
dNTPs mix	400 µM
Forward primer	0.5 µM
Reverse primer	0.5 µM
DMSO	3%
Phusion Polymerase	2 units (1 µl)
dH_2O	to 50 µl
Total	50 µl

All the PCR reactions were performed using conditions as mentioned in Table 3.6. The elongation time was calculated as 15-30 sec/kb of fragment to be amplified.

Table 3.6 PCR conditions for deletion mutagenesis

Step no.	Step	Temperature	Time	Cycles
1	Initial denaturation	98°C	30 sec	1
2	Denaturation	98°C	30 sec	Steps 2-4 (30 cycles)
3	Annealing	55-60°C	30 sec	
4	Elongation	72°C	15-30 sec/kb	
5	Final extension	72°C	5 min	1
6	Pause	4°C	∞	

3.1.2 Cloning

Materials and Methods

Restriction Enzymes (NEB)

10X Restriction Enzyme Buffer (NEB)

100X BSA (NEB, B9001S)

T4 DNA Ligase (NEB, M0202S)

T4 DNA Ligase Buffer (NEB, B0202S)

Mini-DNA isolation kit (Qiagen)

NucleoSpin® plasmid (Macherey-Nagel)

Nucleobond Midi-prep kit PC100 (Macherey-Nagel)

QIAquick PCR purification Kit (Qiagen)

NuceloSpin® Gel and PCR Clean-up (Macherey-Nagel)

Medium and Plates

Luria Broth (LB) medium: Tryptone (10 g), Yeast extract (5 g) and NaCl (10 g) in 1L

LB plates: LB medium containing 1.5% agar (Gerhardt et al, 1994; Sambrook, 2001)

3.1.2.1 Restriction enzyme digestion

Vector (4 µg) and insert (50 µl), generated from standard PCR, were digested by restriction enzymes (NEB), followed by purification and ligation. Digestion reactions were performed according to the protocols provided by NEB.

3.1.2.2 DpnI digestion

After PCR for site-directed or deletion mutagenesis, template DNA (whole PCR reaction) was digested by 20 units DpnI (NEB) at 37°C for at least 2 hours, followed by purification. Amplified fragments were purified either by PCR purification kit (Qiagen) or NuceloSpin® Gel and PCR Clean-up kit.

3.1.2.3 Ligation

Ligations were performed at 22°C for 1 hour. Ligation reactions were prepared as mentioned in Table 3.7.

Table 3.7 Ligation reaction mixture

Standard cloning				Truncation mutagenesis			
		Ligation	Control			Ligation	Control
Vector (plasmid DNA)	100 ng	✔	✔	DNA1 (generated from forward primer)	50 ng	✔	✔
Insert (PCR product)	1:5 (molar ratio)	✔	0	DNA2 (generated from Reverse primer)	1:1	✔	✔
10X ligation Buffer	1X	✔	✔	10X ligation Buffer	1X	✔	✔
T4 Ligase	0.5 µl (200 units)	✔	✔	T4 Ligase	0.5 µl (200 units)	✔	0
dH_2O	to 10 µl	✔	✔	dH_20	to 10 µl	✔	✔
Total	10 µl			Total	10 µl		

3.1.3 Transformation

The ligation products were further transformed into competent *E.coli* DH5α strain ($CaCl_2$ treatment, (Inoue et al, 1990)). Therefore, 10 µl ligation reaction was incubated with 100 µl competent cells on ice for 20 minutes. The cells then were treated with a heat shock (42°C for 45 seconds), followed by recovery for 3 minutes on ice. After addition of 1 ml LB

medium, cells were incubated at 37°C for 1 hour. The cells were plated on LB plates containing either ampicillin (100 µg/ml) or kanamycin (30 µg/ml) antibiotics.

3.1.4 Plasmid DNA Isolation

In order to isolate plasmid DNA, either Qiagen plasmid MINI-DNA isolation kit or NuceloSpin® Plasmid kit were used. For isolating bigger amount of plasmid DNA, Nucleobond Midi-prep kit PC100 was used.

Table 3.8 Plasmids used in this study

Plasmid	Description	Resistance in *E. coli*	Source/ Reference
pMF40	expression, $His_{(6)}$-GFP	Amp	M. Fisher
pEE10	eGFP	Kan	(Ercan et al, 2012)
pEE15	Kir6.2-HA-GFP	Amp	(Ercan et al, 2012)
pEE41	Sur1	Amp	B. Schwappach
pEE47	expression, $His_{(6)}$-GFP-STIM1C	Amp	(Ercan et al, 2012)
pEE71	HA-STIM1	Kan	(Ercan et al, 2012)
pEE72	HA-STIM2	Kan	(Ercan et al, 2012)
pEE83	CD3δ-GFP	Kan	H. Lorenz
pEE84	ss-RFP-KDEL	Kan	H. Lorenz
pEE92	HA-STIM1 ΔK	Kan	(Ercan et al, 2012)
pEE96	HA-STIM1 ΔK-K_{STIM2}	Kan	(Ercan et al, 2012)
pEE112	HA-STIM1 S668D	Kan	E. Ercan
pEE113	HA-STIM1 S486D	Kan	E. Ercan
pEE114	HA-STIM1 S486 and S668D	Kan	E. Ercan
pEE127	HA-STIM1 R500A (500RQR to AQA)	Kan	(Ercan et al, 2012)
pEE128	HA-STIM1 R500, 530A (500RQR and 530RQR to AQA)	Kan	(Ercan et al, 2012)
pEE130	HA-STIM1 R311, 500 530A (311RSR to ASA, 500RQR and 530RQR to AQA)	Kan	(Ercan et al, 2012)
pEE137	HA-STIM1 R530A (530RQR to AQA)	Kan	(Ercan et al, 2012)
pEE138	HA-STIM1 ΔK, R500A	Kan	(Ercan et al, 2012)
pEE139	GFP-Orai1	Kan	E. Ercan
pEE140	mCherry-Orai1	Kan	E. Ercan
pEE164	HA-STIM1 R311A (311RQR to AQA)	Kan	(Ercan et al, 2012)

pEE177	GFP-Orai1 E106A	Kan	(Ercan et al, 2012)
pMS580	expression, $His_{(6)}$-GFP-*M.brevicollis* STIMC	Amp	R. Bhardwaj
pMS617	HA-STIM1N-TMD-Monosiga-STIMC	Kan	R. Bhardwaj
pMS628	HA-STIM1-GFP	Kan	R. Bhardwaj
pMS629	HA-STIM1-mCherry	Kan	R. Bhardwaj
pMS632	HA-STIM2-GFP	Kan	R. Bhardwaj
pMS633	HA-STIM2-mCherry	Kan	R. Bhardwaj
pMS664	expression, $His_{(6)}$-STIM1N	Amp	This study
pMS676	expression, $His_{(6)}$-GFP-STIM1 (233-322)	Amp	R. Bhardwaj
pMS678	expression, $His_{(6)}$-GFP-Lucine Zipper (GCN4)	Amp	(Bhardwaj et al, 2013)
pMS692	HA-STIM1ΔK-K_{STIM2}-GFP	Kan	R. Bhardwaj
pMS693	HA-STIM1ΔK-K_{STIM2}-mCherry	Kan	R. Bhardwaj
pMS694	HA-STIM2ΔK-K_{STIM1}-GFP	Kan	R. Bhardwaj
pMS695	HA-STIM2ΔK-K_{STIM1}-mCherry	Kan	R. Bhardwaj
pMS706	HA-STIM1ΔK-GFP	Kan	This study
pMS707	HA-STIM1ΔK-mCherry	Kan	This study
pMS708	HA-STIM2ΔK-GFP	Kan	R. Bhardwaj
pMS709	HA-STIM2ΔK-mCherry	Kan	R. Bhardwaj
pMS740	HA-STIM1N-TMD-Monosiga-STIMC-K_{STIM2}	Kan	This study
pMS770	mCherry-$Gly_{(5)}$-FLAG-PH (PLC-δ1)	Kan	This study
pMS771	expression, $His_{(6)}$-GFP-STIM1 ΔEB-1 (642TRIP to ARNP)	Amp	This study
pMS782	expression, $His_{(6)}$-GFP-STIM1 (451-670), ΔEB-1 (642TRIP to ARNP)	Amp	This study
pMS787	expression, $His_{(6)}$-GFP-STIM1 (233-390)	Amp	This study
pMS788	expression, $His_{(6)}$-GFP-STIM1 (233-455)	Amp	This study
pMS789	expression, $His_{(6)}$-GFP-STIM1 (233-554)	Amp	This study
pMS796	HA-STIM1(1-390)-GFP	Kan	This study
pMS797	HA-STIM1 ΔEB-1(642TRIP to ARNP)-GFP	Kan	This study
pMS799	HA-STIM1(1-390)-mCherry	Kan	This study
pMS800	HA-STIM1 ΔEB-1(642TRIP to ARNP)-mCherry	Kan	This study
pMS810	expression, $His_{(6)}$-GFP-Lucine Zipper (GCN4)-STIM1(233-322)	Amp	This study
pMS811	expression, $His_{(6)}$-GFP-Lucine Zipper (GCN4)-STIM1(233-390)	Amp	This study
pMS813	HA-STIM1ΔK,ΔEB-1(642TRIP to ARNP)-	Kan	This study

	mCherry		

3.2 Mammalian Cell Culture Methods

Materials, Media and Chemicals

10 cm dishes (TPP)
DMEM Glutamax (Gibco, 61965)
DMEM/F12 (Gibco, 21331)
Opi-MEM (Gibco, 31985)
Fetal Bovine Serum (FBS) (Gibco, 10270-106)
Polyethylenimine (PEI) Max (Polysciences)
Glutamine (Gibco, 25030)
0.05% Trypsin-EDTA (Gibco, 25300)
Fugene HD (Roche)

3.2.1 Cell lines

Table 3.9 cell lines used in this study

Cell line	Description
HEK293T	HEK293T cells are derived from human embryonic kidney cells and transformed with large T antigen of the SV40 virus.
HeLa	HeLa cells are derived from human cervix carcinoma.
RPE-1	RPE-1 cells are derived from human retinal-pigmented epithelial cells and telomerase reverse transcriptase immortalized.
U2OS	U2OS cells are derived from human osteosarcoma cells.
COS7	COS7 cells are derived from *Cercopithecus aethiops* kidney cells. COS7 cells are transformed with large T antigen of the SV40 virus.

3.2.2 Maintaining cells in culture

All cells were maintained at 37°C, 5% CO_2 in a cell chamber. The cells were passaged when they reach about 90-95% confluence.

Table 3.10 Condition for culturing cell lines

Cell line	Description
HEK293T	DMEM/F12, 10% FBS, 2 mM Glutamine
HeLa	DMEM Glutamax, 10% FBS, 2 mM Glutamine
RPE-1	DMEM/F12, 10% FBS, 2 mM Glutamine
U2OS	DMEM Glutamax, 10% FBS, 2 mM Glutamine

COS7	DMEM Glutamax, 10% FBS, 2 mM Glutamine

3.2.3 Transfection of cells

In order to introduce plasmid DNA into mammalian cells, Fugene or PEI Max reagents were used. The cells were transfected when they reach about 60-70% confluence. The reaction mixture was prepared as mentioned in table 3.11.

Table 3.11 mixture for transfection

Transfection 1		Transfection 2	
DNA	1 µg	DNA	0.5 µg
Fugene HD	3 µl	PEI Max	5 µl
Opi-MEM	100 µl	Medium, 2mM Glutamine, no FBS	200 µl

For transfection 1, the mixture was mixed well and kept at room temperature for 20 minutes. Next, the mixture was added onto the pre-seeded cells for 16-20 hours.

For transfection 2, the mixture was mixed well and kept at room temperature for 10 minutes. After incubation, 800 µl medium (2 mM Glutamine, 5% FBS) was added to the mixture. Next, transfection mixture was added onto the pre-seeded cells for 4 hours. The medium was aspirated and 10 ml medium (2 mM Glutamine, 10% FBS) was added. Cells were further kept in incubator for 12-16 hours.

3.3 Flow Cytometry

Materials, Buffers and Equipments

6-well dishes (TPP)

FACS tubes (NeoLab)

FACSFlow buffer (Becton Dickinson, 342003)

Propidium iodide (Invitrogen, P3566)

Brefeldin A (BFA) (Sigma, B7651)

FACSCanto II (Becton Dickinson)

Table 3.12 Antibodies used in flow cytometry experiments

Antibody	Species	Dilution	Source
anti-HA.11	mouse	1:200	BAbCO, clone:16B12
anti-mouse PE-conjugated AffiniPure F (ab')2 fragment	goat	1:150	Invitrogen (P852)

3.3.1 Flow Cytometry

HEK293T cells were seeded in 6 well plates. Next day, cells were cotransfected with 0.5 µg/µl GFP and 0.5 µg/µl STIM1 constructs. 16-20 hours later, cells were collected by resuspension in 1 ml medium and transferred to 1.5 ml pre-cold Eppendorf tubes. Cells were spun down at 4°C, 370 x *g* for 2 min. Cells were washed with ice-cold FACSFlow buffer, followed by incubation with the anti HA antibody for 30 min on ice. Next, cells were washed with ice-cold FACSFlow buffer once and incubated with secondary antibody for another 30 min on ice. After the incubation, cells were washed with ice-cold FACSFlow buffer and stained with 1 µg Propidium iodide on ice. 30,000 intact HEK293T cells were analyzed in a FACSCanto II machine. The percentage of cells with HA signals on the surface was calculated according to the ratio of PE-positive cells to GFP and PE double positive cells. All cytometry experiments results are the averages of at least three independent experiments and were plotted in Microsoft Excel.

3.4 Microscopy Techniques

Materials and Chemicals

12-well dishes (TPP)

µ-slide, 8 well (ibidi GmbH)

Lab-Tek Chambered Coverglass, 8 well (Thermo Fisher Scientific, 734-2062)

Round coverslips (12 mm diameter, Peske)

Formaldehyde (FA) (methanol free) (Polysciences, 04018)

Thapsigargin (Tg, Calbiochem, 586005)

Hoechst (Invitrogen, 33342)

Equipments

Olympus xcellence PointFRAP microscopy (IX81 inverted)

Olympus xcellence 3D PALM/STORM/TIRF/ScannerFRAP microscopy

Zeiss LSM780 confocal microscopy

Table 3.13 Antibodies used in immunoflorescence experiments

Antibody	Species	Dilution	Source/Reference
anti-HA.11 Clone:16B12	mouse	1:1000	BAbCO
anti-Calreticulin	rabbit	1:300	Affinity Bioreagents
anti-STIM1N	guinea pig	1:250	This study, (Ercan et al, 2012)
anti-α-tubulin (WA3)	mouse	1:100	E. Schiebel
anti-α-tubulin Clone:DM1A	mouse	1:1000	Sigma-Aldrich Fluka
anti-mouse Alexa Fluor® 488	goat	1:600	Invitrogen
anti-mouse Alexa Fluor® 568	goat	1:600	Invitrogen
anti-mouse Alexa Fluor® 647	goat	1:600	Invitrogen
anti-rabbit Alexa Fluor® 488	goat	1:600	Invitrogen
anti-rabbit Alexa Fluor® 568	goat	1:600	Invitrogen
anti-guinea pig Alexa Fluor® 546	goat	1:500	Invitrogen

3.4.1 Immunofluorescence

For immunofluorescence experiments, cells were seeded either onto overslips in 12-well dish, into µ-slide or Lab-Tek chambered coverglass. Next day, cells were transfected with 0.1-0.5 µg/µl of desired plasmid DNA for 16-20 hours. Cells were fixed with fixing solution 1 (2% FA, 125 mM sucrose in 1X PBS) at room temperature (RT) for 20 minutes. After washing cells with 1X PBS, cells were fixed with fixing solution 2 (1% FA in 1X PBS) at RT for 10 minutes. After washing cells with 1X PBS, cells were either kept in 1X PBS or permeabilized with permeabilization solution (0.3% Triton, 0.05% SDS in 1X PBS) at RT for 15 minutes. The permeabilized and non-permeabilized cells were washed and incubated with blocking solution (10% FBS in 1X PBS) for at least 30 minutes at RT. Next, cells were stained with primary antibody (5% FBS in 1X PBS) at RT for 1 hour. After washing cells with 1X PBS twice, cells were further stained with secondary antibody (5% FBS in 1X PBS) at RT for 1 hour. Cells were washed with 1X PBS twice. The coverslips were mount on slides with 10 µl mowiol. Cells were kept in 1X PBS in µ-slide or Lab-Tek chambered coverglass.

3.4.2 Epi-fluorescence microscopy of fixed cells

The images of epi-fluorescence microscopy of fixed cells were acquired by Olympus IX81 inverted microscope with DAPI, GFP and mCherry filters. Either UPLSAPO 60x/1.35 oil

objective or UPLSAPO 40x/0.95 air objective was used. The images were processed and prepared with ImageJ and Adobe Illustrator, respectively.

3.4.3 Epi-fluorescence microscopy of live cells

In order to maintain cells in physiological condition while imaging, cells were kept in medium containing 20 mM Tris/HCl (pH 7.6) at 37°C, 5% CO_2. The images of epi-fluorescence microscopy of live cells were acquired by Olympus IX81 inverted microscope with UPLSAPO 60x/1.35 oil objective with GFP and mCherry filters. The images were processed and prepared with ImageJ and Adobe Illustrator, respectively.

3.4.4 Total Internal Reflection Fluorescence Microscopy (TIRF)

In order to acquire optimal TIRF images, cells were seeded in Lab-Tek chambered coverglass and kept in 1X PBS. The TIRF images were acquired by Olympus IX81 inverted microscope with PLAPO 100x/1.45 oil objective with GFP and mCherry filters. 488 nm and 561 nm lasers were used. TIRF module was adjusted with help of image facility, ZMBH. The images were processed and prepared with ImageJ and Adobe Illustrator, respectively.

3.4.5 Confocal Microscopy

The confocal microscopy images were acquired by Zeiss LSM 780 confocal microscope with 488, 561 and 633 nm lasers. Plan-APOCHROMAT 63x/1.4 oil objective was used. The images were processed and prepared with ImageJ and Adobe Illustrator, respectively.

3.4.5.1 Fluorescence resonance energy transfer (FRET)-based quantification of ER-PM contact sites

In order to quantify the amounts of ER-PM contact sites, an FRET-based assay was established as shown in fig. 12. Close proximity of ER and PM (around 10 nm) leads to generation of a FRET signal between a donor (GFP) and an acceptor (mCherry), which are anchored in one of each membranes. All ER probes were C-terminal GFP-tagged. A N-terminal mCherry tagged $PI(4,5)P_2$-binding PH domain from phospholipase C-δ1 was used as PM probe (Garcia et al, 1995) . FRET was detected by acceptor photobleaching using confocal microscopy (Bastiaens & Jovin, 1996). The acceptor (mCherry) was photobleached in defined regions of interest and scanned repeatedly with a 561-nm laser (100% power, 3-6

times repeat) until fluorescence signals were at background level. Three images of donor and acceptor were acquired before and after photobleaching. The images were processed and prepared with ImageJ and Adobe Illustrator, respectively. FRET efficiency was calculated by using quantification method as mentioned in 3.5.1.

3.5 Image Analysis

3.5.1 Quantification of ER-PM contact sites by acceptor photobleaching FRET

In order to assess acceptor photobleaching FRET locally within the cells, an ImageJ macro was developed. In short, FRET efficiencies were calculated by using two images, *i.e.* the *donor* before (I_B) bleaching image and the *donor* after (I_A) bleaching image. Both images were registered and background-subtracted. Automatic (*i.e.* default) thresholding was applied to the I_B image in order to determine regions of interest (ROIs). The FRET efficiency (E) was then calculated for each ROI as

$$E_i = \frac{\overline{I_{A,i}} - \overline{I_{B,i}}}{\overline{I_{A,i}}}$$

where I_A and I_B are the mean intensities of the ROI, *i e.* before and after photobleaching.

3.5.2 Quantification of preexisting ER-PM contact sites in live-cells imaging

In order to quantify the amounts of preexisting ER-PM contact sites, an ImageJ macro was generated. In short, time series of images were organized in a stack using ImageJ. The images were registered and background-subtracted. One image from the stack was chosen to determine the patches. A patch is an ER-PM contact site which is formed upon ER Ca^{2+} depletion. Upon automatic (i.e. default) thresholding, the resulting patch regions of interest (ROIs) were recorded and a binary mask image was generated. To separate touching patches, watershed operations were applied to the binary image where needed.

Two more channels (i.e. channels 2 and 3) were then added to the original stack. Channel 2 was filled with the binary mask image as reference. A similar procedure was applied to fill channel 3, here only considering those ROIs whose mean intensity level in channel 1 was higher than a user-defined threshold. The resulting stack with three channels could then be analyzed as a composite image.

3.6 Biochemical Techniques

3.6.1 Expression and purification of $His_{(6)}$- or $His_{(6)}$-GFP-fusion proteins

Materials

E. coli BL21 (DE3) Codon Plus

Protino® Ni-TED resin (Macherey-Nagel GmbH & Co.)

Vivaspin® 6 centrifugal concentrators (MWCO= 10 kDa, Sartorious Stedim Biotech)

Low protein binding micro tubes (Sarstedt, Germany)

Equipments

Microfludizer (EmulsiFlex-C5, Avestin)

Ultracentrifuge (Sorvall® Discovery™ 90S, Hitachi)

Ultracentrifuge rotors, 45 Ti (Beckman Coulter, Inc.)

NanoDrop® ND-1000 spectrophotometer (Thermo Scientific, Germany)

ÄKTA micro™ (GE Healthcare)

Superdex 200 5/150 GL column (GE Healthcare)

Chemicals

Ampicillin (Sigma)

Isopropyl-β-D-thiogalactopyranoside (IPTG, Applichem)

Dithiothreitol (DTT, Applichem)

Phenylmethanesulfonyl fluoride (PMSF) (Sigma)

EDTA-free protease inhibitor complex (PIC) (Roche)

HEPES (Roth)

Potassium chloride (KCl) (Applichem)

Sodium chloride (NaCl) (Sigma)

Imidazole (Merck)

Buffers

Lysis buffer	Elution buffer
50 mM Tris/HCl pH 7.5	50 mM Tris/HCl pH 7.5
250 mM NaCl	250 mM NaCl
2 mM Imidazole	300 mM Imidazole
0.5 mM EDTA	0.5 mM EDTA
2 mM DTT	2 mM DTT
1 mM PMSF	1 mM PMSF
1X PIC	1X PIC

HK buffer

25 mM HEPES/KOH pH 7.4

150 mM KCl

2 mM DTT

Recombinant $His_{(6)}$- or $His_{(6)}$-GFP-fusion proteins were expressed and purified from *E. coli* BL21 (DE3) codon plus cells using nickel affinity chromatography. For this, the cell extracts were generated as following. The overnight cultures of respective *E. coli* strains were diluted to 0.1 OD_{600} in 250 ml medium containing ampicillin (100 µg/ml). Cells were incubated at 37°C for 1.5 to 2 hours until the OD_{600} reached 0.6-0.8. Protein expression was induced by 0.25-0.4 mM IPTG at 30°C for 6 hours. *E.coli* cells were harvested (4°C, 4,000 rpm for 10 minutes) and resuspended in lysis buffer on ice. The cells were lysed using a microfluidizer at 15,000-20,000 psi (1 psi= 6.9 kPa). The lysates were ultracentrifuged by using a Ti45 rotor at 120,000 *g*, 4°C for 45 min. Supernatants were incubated with 0.5 g Protino® Ni-TED resin at 4°C for 1 hour. The protein-bound resins were washed two times with 10 ml lysis buffer and incubated with 2.5 ml elution buffer at 4°C for 30 min. The eluted proteins were concentrated to 0.5 ml by using Vivaspin® 6 centrifugal concentrators with 10 kDa cut off. Concentrated proteins were flash-frozen using liquid nitrogen and stored at -80°C.

3.6.2 SDS-PAGE and western blotting

3.6.2.1 SDS-PAGE

Materials and Equipments

Acrylamide 37.5:1 (Rotiphorese gel 30, Roth)

TEMED (Sigma)
APS (Sigma)
SDS (Roth)
ColorPlus Prestained protein ladder (NEB, P7711S)
Tween-20 (Sigma)
Chemiluminescence Blotting Substract (Roche)
Mini Protean Gel System (BioRad)
Nitrocellulose membrane (0.45 µm pore size, Protran, Whatman)
Luminescent Image Analyzer LAS-4000 (Fujifilm)

SDS-PAGE was performed according to (Laemmli, 1970). Mini gels (1 mm) were prepared as described in table 3.14.

Table 3.14 Solution mixture for polyacrylamide gel (SDS-PAGE).

	Separating gels (10ml)			Stacking gels (5 ml)
	7.5%	10%	12%	4%
dH_2O	5.3 ml	4.5 ml	3.8 ml	3 ml
2 M Tris/HCl pH 8.8	2 ml	2 ml	2 ml	-
0.5 M Tris/HCl pH 6.8	-	-	-	1.25 ml
30% acrylamide (37.5:1)	2.5 ml	3.3 ml	4 ml	670 µl
10% SDS	100 µl	100 µl	100 µl	50 µl
TEMED	5 µl	5 µl	5 µl	5 µl
10% APS	50 µl	50 µl	50 µl	50 µl

3.6.2.2 Western blotting

Table 3.15 Antibodies used in western blot

Antibody	Species	Dilution	Source/Reference
anti-HA.11 Clone:16B12	mouse	1:1000	BAbCO
anti-STIM1N	guinea pig	1:250	This study, (Ercan et al, 2012)
anti-α-tubulin Clone:DM1A	mouse	1:500	Sigma-Aldrich Fluka
anti-TRAM (86590)	rabbit	1:1000	B. Dobberstein
anti-VDAC	rabbit	1:500	Thermo Scientific

anti-GAPDH	rabbit	1:2000	Cell signaling
anti-GFP	rabbit	1:2500	Santa Cruz

Postnuclear lysates were prepared and normalized according to (Ercan et al, 2012) and (Vilardi et al, 2011), followed by western blotting. The western blotting was performed according to (Burnette, 1981). In short, the transfer was done with a three component buffer system (anode I: 300 mM Tris, 20% (v/v) methanol p.a. (Applichem); anode II: 30 mM Tris, 20% (v/v) methanol p.a.; cathode: 40 mM 6-aminohexanoic acid, 25 mM Tris, 0.01% (w/v) SDS, 20% (v/v) methanol p.a.) and with the setting of 1 mA/cm^2 for 2 hours under semi-dry condition. To visualize the successful transfer, nitrocellulose membrane was stained with Ponceau S solution (1% (v/v) acetic acid, 0.5% (w/v) Ponceau S for about 5 min at RT), followed by washing with dH_2O. After ponceau-stained scanning, membrane was blocked with blocking solution (5% dry skimmed milk dissolved in 1X PBS containing 0.05 % (w/v) Tween-20, 5% milk in PBS-T) at RT for at least 30 min. The blot was incubated with primary antibody in 5% milk in PBS-T at RT for at least 1 hour or at 4°C for overnight. After washing with PBS-T three times, blot was incubated with secondary antibody coupled to horseradish peroxidase in 5% milk in PBS-T at RT for 1 hour. Membrane was washed with PBS-T three times, followed by incubation with the Chemiluminescence Blotting Substrate. Light emission was acquired by using a LAS-4000.

3.6.3 Size-exclusion chromatography

In order to determine the assembly state of recombinant GFP-tagged proteins in solution, size-exclusion chromatography was used. 50 µl of freshly purified protein (50- 80 µM) was injected into a Superdex 200 5/150 GL column pre-equilibrated with HK buffer containing 1 mM DTT on an ÄKTA micro™ at a flow rate of 0.15 ml/min.

3.6.4 *In vitro* Microtubule (MT) Cosedimentation assay

Materials and Equipments

GTP (Roche)

AMPPNP (Roche)

2-Methyl-2-4-pentanediol (pentandiol) (Sigma)

Panlitaxel (Taxol) (T7191-5MG, Sigma-Aldrich)

Nocodazole (Sigma-Aldrich)

Glycerol (water free, Applichem)

Ultracentrifuge (Sorvall® Discovery M120SE, Hitachi)

Buffers

CSF buffer: 0.05% Triton X-100, 100 mM KCl

5X BRB80: 0.4 M PIPES, 5 mM $MaCl_2$, 5 mM EDTA, pH 6.8

The *in vitro* microtubule cosedimentation assay was established and modified according to (Barenz et al, 2013). The experimental flowchart is shown in Fig. 19A. CSF egg extracts were prepared according to (Wittmann et al, 1998). The extracts were released to interphase by addition of 0.6 mM $CaCl_2$ and 100 µg/ml cycloheximide and incubated at 18-20°C for 20-30 min. After ultracentrifugation (100,000 *g*, 4°C for 30 min), only the cytosolic fraction of the high-speed extract was collected. The cytosolic fraction was separated into two 50 µl samples, stabilized microtubule (MT) and control MT. The stabilized MTs were generated by adding 1 mM GTP, 1 mM AMPPNP, 8% pentanediol and 50 µM taxol in cytosolic fraction. In the control, MTs were depolymerized by 50 µM nocodazole in CSF buffer. Stabilized MT and control samples were incubated with recombinant proteins (4 µM) at 18-20°C for 30 min. After 30 min, both samples were diluted with 50 µl CSF buffer containing 50 µM taxol or nocodazole, respectively. 5 µl of mixture was added into 45 µl SDS-sample buffer and used as input sample. Samples were loaded on the top of the 600 µl cushion (25% glycerol in 1X BRB80) and centrifuged at 100,000 *g*, 20°C for 10 min. 5 µl supernatant was added into 45 µl SDS-sample buffer and used as MT-unbound sample. Pellets of stabilized and control MT samples were resuspended in 100 µl 1X BRB80 buffer containing 50 µM taxol or nocodazole, respectively. Dissolved pellets (100 µl) were loaded on 300 µl cushion (25% glycerol in 1X BRB80) and centrifuged at 100,000 *g*, 20°C for 10 min. Pellets were resuspended in 100 µl SDS-sample buffer and used as MT-bound samples. 15 µl samples were subjected to SDS-PAGE, followed by western blotting analysis.

4. Results

4.1 Trafficking of STIM1 to cell surface is regulated by multiple signals

In order to function in SOCE, STIM proteins require ER localization. Indeed, STIM proteins predominantly localize in the ER (Manji et al, 2000). However, a subpopulation of STIM1 travels to the cell surface in stromal and mast cells (Hewavitharana et al, 2008; Manji et al, 2000; Oritani & Kincade, 1996). In contrast, STIM2 localizes exclusively in the ER (Soboloff et al, 2006b). These observations raise the question which mechanisms on the one hand retain STIM1 and STIM2 in the ER and on the other hand allow trafficking of STIM1 to the cell surface.

4.1.1 HA-STIM1, but not HA-STIM2 travels to cell surface.

After gene duplication during chordate evolution, STIM1 and STIM2 evolved from an ancestral STIM protein (Cai, 2007). Both proteins contain K-rich domains at the end of their C termini (Fig 1A). STIM2 comprises a consensus di-lysine ER retention signal (K(X)KXX (Jackson et al, 1990) in the K-rich domain, which is most likely responsible for the retention of STIM2 in the ER. This motif does not appear in the K-rich domain of STIM1 (Fig 1A). Therefore, I was interested in the mechanism how STIM1 is retained in the ER.

To investigate this question in more detail, I analyzed the localization of STIM1 and STIM2 in HEK293T cells by flow cytometry and fluorescent microscopy. Previous studies revealed that N-terminal tagging with hexahistidine (His_6) but not GFP allows STIM1 trafficking to the cell surface (Hauser & Tsien, 2007). This finding suggests that a big tag at the N-terminus affects trafficking of STIM1 from ER to cell surface. Thus, N-terminal HA tagged constructs were used to compare the intracellular distribution of STIM1 and STIM2. If a protein can travel to the cell surface, the N-terminal HA tag can be detected under non-permeabilized condition (Fig 1B) by using an anti-HA antibody. On the contrary, the HA tag of ER-resident STIM proteins can only be detected after membrane permeabilization (Fig 1B). In order to study the surface localization of STIMs with transient transfection experiments, HA-tagged STIM proteins were coexpressed with GFP in HEK293T cells. The GFP-positive cells corresponded to transfected cells and were analyzed under non-permeabilized condition by flow cytometry. The percentage of cells expressing HA-tagged protein on the cell surface was calculated according to the ratio of HA-positive cells to total transfected cells.

Flow cytometry revealed that 5.5% of GFP-positive cells displayed HA-STIM1 on the surface (Fig 1C). In contrast, no HA-STIM2 was found on the surface of GFP-positive cells. Next, the surface localization of a STIM1 mutant, in which the K-rich domain was replaced by the K-rich domain of STIM2 (HA-STIM1ΔK-K_{STIM2}) was analyzed. Indeed, HA-STIM1ΔK-K_{STIM2} remained intracellular (Fig 1C), suggesting that the K(X)KXX located in STIM2 K-rich domain is a functional ER retention signal.

In addition to flow cytometry, the intracellular distribution of HA-STIM1 was analyzed by immunofluorescence microscopy under permeabilized or non-permeabilized conditions. Under permeabilized condition, HA-STIM1 was detected in all GFP-cotransfected HEK293T cells and showed mainly ER localization (Fig 1D, permeabilized). Under non-permeabilized condition, the GFP-cotransfected cells showed HA staining on the surface (Fig 1D, non-permeabilized). The amount of surface HA-STIM1 was different in individual cells ranging from non-detectable to very high levels (Fig 1D, non-permeabilized). Cell integrity of non-permeabilized cells was demonstrated by applying an anti-α-tubulin antibody.

These data demonstrate that STIM1 can travel to the cell surface. In addition, the surface localization of STIM1 reveals a high cell-to-cell variation. In contrast, STIM2 is retained in the ER by a functional di-lysine ER retention signal. This was further confirmed by complete ER retention of HA-STIM1ΔK-K_{STIM2}.

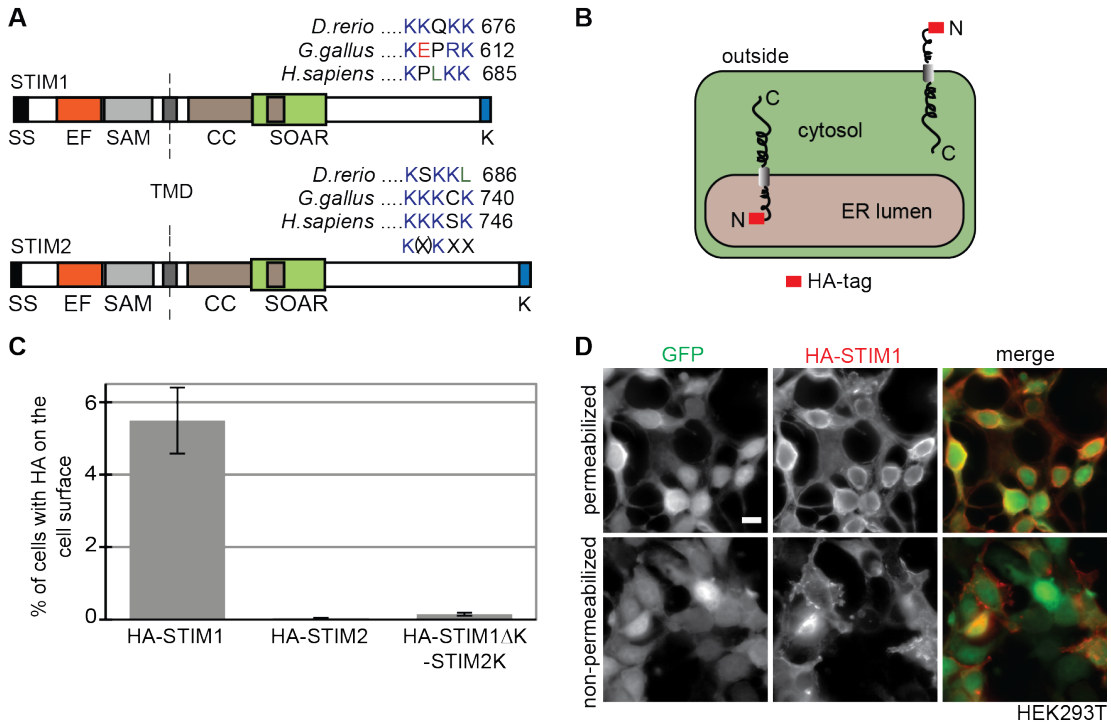

Figure 1. STIM1, but not STIM2 can travel to the surface of HEK293T cells. (A). The domain structure of STIM1 (SS, signal sequence; EF-hand domain; SAM domain; TMD, trans-membrane domain; CC, coiled-coil domain; SOAR, STIM1-Orai1 activating region; K, K-rich domain). The last five residues of STIM1 and STIM2 from *Danio rerio*, *Gallus gallus* and *Homo sapiens* and the consensus of a di-lysine ER retention signal are shown. (B). Cartoon of membrane topology and intracellular distribution of STIM1: the HA-tag at the N terminus is shown as a red box. (C). Number of GFP-positive cells (in %) with HA signal on their surface under non-permeabilized conditions determined by flow cytometry. HEK293T cells were cotransfected with GFP and human HA-STIM1, HA-STIM2 or HA-STIM1ΔK-K_{STIM2}. In HA-STIM1ΔK-K_{STIM2}, the K-rich domain of STIM1 was replaced by the K-rich domain of STIM2. (D). HEK293T cells were cotransfected with GFP (green) and HA-STIM1 (red). Cells were analyzed by fluorescence microscopy. The scale bar corresponds to 10 µm.

4.1.2 New STIM1 antibody recognizes STIM1 in the ER and at the cell surface.

For further analysis of the heterogeneous distribution of STIM1 at the cell surface, an antibody that recognizes the extracellular domain of STIM1 under non-permeabilized condition was necessary (Fig 1B). No commercial antibody was able to detect endogenous STIM1 in fluorescent microscopy and western blotting. Therefore, a polyclonal antibody against the entire N-terminal domain of STIM1 (α-STIM1N) was raised (Fig 1B). This was achieved by injecting purified $His_{(6)}$-tagged $STIM1_{23-213}$ into guinea pig applying a standard immunization procedure by Charles River, Germany. Sensitivity and specificity of the generated α-STIM1N antibody were analyzed by immunofluorescence microscopy and western blotting.

Immunofluorescence microscopy showed similar staining patterns for α-STIM1N and the HA antibodies in permeabilized and non-permeabilized HeLa (Fig 2A) and RPE-1 cells (Fig 2B) transfected with HA-STIM1. Under permeabilized conditions both antibodies were able to detect the large ER resident pool of STIM1 (Fig 2A and B, permeabilized). The staining showed reticular ER-like structures, which appeared more tubular in HeLa cells compared to RPE-1 cells (Fig 2A and B, permeabilized). Under non-permeabilized condition the antibodies recognized the PM pool of STIM1, which accumulated in distinct domains at the cell surface (Fig 2A and B, non-permeabilized).

To study the intracellular distribution of endogenous STIM1, two marker proteins calreticulin and Tom20 were used. Calreticulin, a luminal ER protein involved in folding of glycoprotein is a sheet-like ER marker (Shibata et al, 2010). Tom20 is a mitochondrial protein and a central component of the translocase of the outer mitochondrial membrane (TOM) receptor complex (Dekker et al, 1998). Cells were transfected with Tom20-GFP,

containing amino acid 1-30 of the human Tom20 (Zhan et al, 2012) and a double immunofluorescence staining with α-calreticulin or α-STIM1N was performed. Proteins recognized by α-STIM1N colocalized with calreticulin and Tom20-GFP in permeabilized HeLa and RPE-1 cells at resting state (Fig 2C and E), suggesting that α-STIM1N recognized endogenous STIM1 but also mitochondrial proteins. The distribution of STIM1 did not alter after treating HeLa cells with Thapsigargin (Tg), which blocks SERCA and inhibits pumping of Ca^{2+} from cytosol into ER lumen (Fig 2D). This treatment induces SOCE, which is characterized by a patch-like staining of STIM1 at ER-PM contacts (Jozsef et al, 2014; Liou et al, 2007; Varnai et al, 2007; Wu, 2006). This suggests that Tg-induced ER-PM junctions cannot be observed using α-STIM1N under endogenous STIM1 level.

In the next experiment, the STIM1 antibody was used in a western blot experiment against different cell components. For this experiment, isolated mitochondria and canine rough microsomes (RM) and so-called TPK-RM were used. TPK-RM were generated by removing all peripheral proteins. For this, RMs were treated with puromycin, high-salt wash and trypsin as described in (Favaloro et al, 2010). Purity of the single fractions was confirmed by applying antibodies for the ER marker TRAM and for the mitochondrial marker VDAC. The western blot exhibited that the anti-STIM1N antibody can detect recombinant $His_{(6)}$-STIM1N and endogenous STIM1 (~ 77.4 kDa) in RM (Fig 2F). This signal was not observed in TPK-RM (Fig 2F, arrowhead), instead a lower migrating band at 28 kDa was observed corresponding to STIM1 without the C-terminal domain. Compared to the detected bands in RM and TPK-RM, two bands at 55 and 35 kDa appeared only in the mitochondrial fraction. This observation suggests that STIM1N antibody recognized endogenous STIM1 but also some mitochondria localized proteins.

In conclusion α-STIM1N can detect endogenous levels of STIM1. The application of the antibody is limited since α-STIM1N cross-reacts with other proteins. However, this does not affect the analysis of endogenous STIM1 on the cell surface.

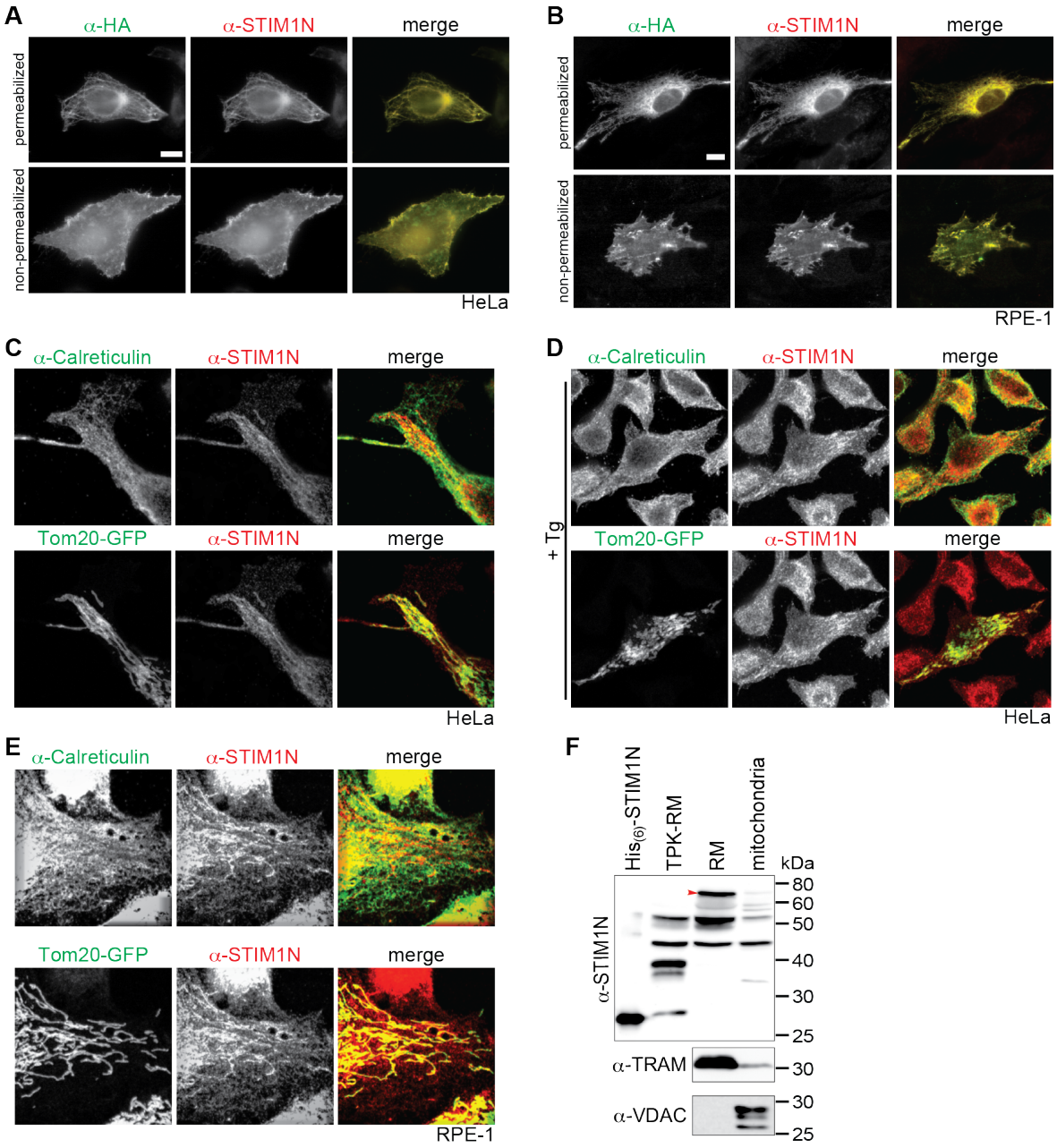

Figure 2. STIM1 antibodies recognize overexpressed HA-STIM1 and endogenous STIM1 by using fluorescence microscopy and western blotting. (A and B). HeLa (A) or RPE-1 cells (B) were transfected with HA-STIM1. Cells were fixed and incubated with HA and STIM1N specific antibodies under permeabilized and non-permeabilized conditions. (C- E). Colocalization of endogenous STIM1 (red) and Calreticulin (green) or Tom20-GFP (green). HeLa (C and D) and RPE-1 (E) cells were transfected with Tom20-GFP. Endogenous STIM1 (red) was stained by anti-STIM1N antibodies in transfected RPE-1 or HeLa cells. Calreticulin (green) was labeled by anti-Calreticulin antibody. Cells were analyzed by laser scanning confocal microscopy. (D). HeLa cells were treated with 0.5 µM Tg for 5 min before fixation. (F). Cell fractionation experiment. Anti-STIM1N was used in western blot experiment to determine the specificity of the antibody (RM: rough microsome; TPK-RM:

trypsin digested and high salt washed rough microsomes). Anti-TRAM and VDAC antibodies were used as markers for ER and mitochondria fractions, respectively. Arrowhead corresponds to endogenous STIM1 (~ 77.4 kDa).

4.1.3 Endogenous STIM1 accumulates at the cell surface of mitotic cells.

I observed that individual transfected cells have different amounts of HA-STIM1 on the cell surface. In order to study heterogeneity in surface localization of endogenous STIM1, I analyzed the distribution of endogenous STIM1 in more detail. Therefore the STIM1 specific antibodies (α-STIM1N) were applied in immunofluorescence microscopy of non-permeabilized HEK293T cells.

I was able to detect endogenous STIM1 at the cell surface of non-permeabilized HEK293T cells. Similar to the observations in cells overexpressing HA-STIM1, the amount of surface STIM1 showed a very high cell-to-cell variation (Fig 3A). A few round cells showed high concentration of endogenous STIM1 at the cell surface (Fig 3A, asterisks). These round cells were confirmed as mitotic (M) cells by co-staining of α-STIM1N and Hoechst (Fig 3A, asterisks). Next, the STIM1 surface signal was compared in interphase and M-phase cells. For quantification of cells with surface signal, images were taken and processed. Background was subtracted from all images using the background (BG) subtraction from region of interest (ROI) of ImageJ. Unspecific signals correspond to the mean pixel values of 10 randomly selected areas within cells stained without primary antibody. For the specific surface staining, mean pixel intensities from three random areas, which in interphase cells were outside of nucleus, were calculated and divided by unspecific signals. These ratios were further classified into background (ratio < 2), low signal (ratio 2-35), high signal (ratio 36-65) and strong signal (ratio > 65).

The quantification of interphase and M-phase cells with STIM1 surface signal displayed an increased surface expression during M-phase. 43% of M-phase cells had high signal (ratio 36-65) and 57% had low signal (ratio 2-35) of STIM1 on their cell surface (Fig 3B, M phase). In contrast, only 0.4% of interphase cells had high signal on the surface and 59.7% of cells had low signal. 39.9% of interphase cells had no specific STIM1 surface signal (ratio < 2).

Taken together, surface localization of endogenous STIM1 is regulated in a cell-cycle dependent manner. In M-phase, STIM1 accumulates at the cell surface, while in interphase STIM1 is efficiently retained in the ER.

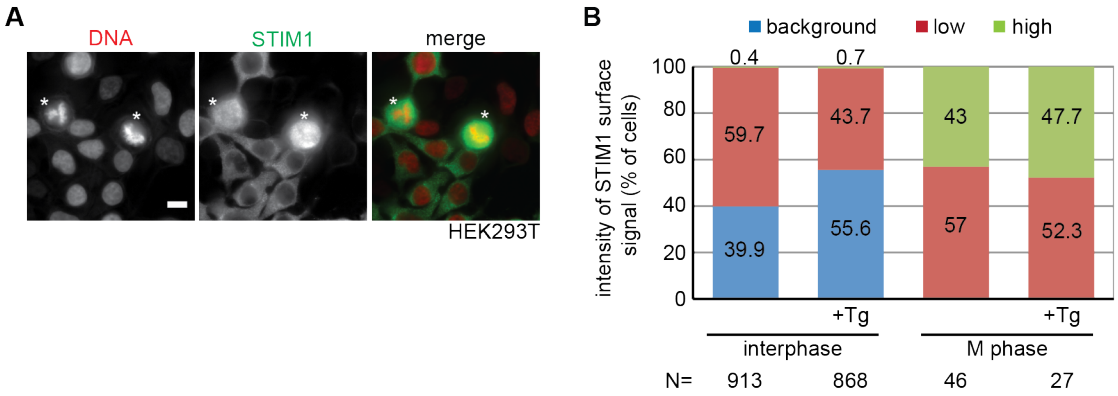

Figure 3. Cell-cycle-dependent expression of STIM1 at the surface. (A). Detection of endogenous STIM1 on the surface of non-permeabilized HEK293T cells by fluorescence microscopy. DNA was stained with Hoechst and endogenous STIM1 was detected by STIM1N-specific antibody. The scale bar corresponds to 10 µm. (B) Quantification of the STIM1 surface signal by fluorescence microscopy. Cells were grouped according to signal intensities and the number of cells (in %) in each group is shown. According to DNA staining, cells were further divided into inter- and M-phase. If indicated cells were incubated for 1 h with 0.5 µM Tg.

4.1.4 SOCE and increased $[Ca^{2+}]_c$ reduce STIM1 expression at the cell surface

Next, I asked what factors regulate surface localization of STIM1. Upon SOCE activation, STIM1 recruits ER to PM forming ER-PM contact sites (Soboloff et al, 2012). SOCE promotes interaction of STIM1 with $PI(4,5)P_2$ and Orai1, resulting in increased cytosolic Ca^{2+} concentration ($[Ca^{2+}]_c$) (Lewis, 2007; Soboloff et al, 2012; Yang et al, 2012). Therefore, I asked if SOCE and increased $[Ca^{2+}]_c$ interfere with the surface localization of STIM1. In addition, other features like physical interactions may be responsible for STIM1 retention. Two known STIM1 binding partners, Orai1 and microtubules may be involved in such a mechanism. Orai1 is recruited to STIM1-mediated ER-PM junctions and activated by STIM1 via direct physical contact (Muik et al, 2008; Park et al, 2009; Yuan et al, 2009). Besides interacting with Orai1, STIM1 is identified as a microtubule-plus-end-tracking protein (Grigoriev et al, 2008; Honnappa et al, 2009). STIM1 associates with microtubules via its EB-1 binding motif (Grigoriev et al, 2008; Honnappa et al, 2009). Apart from these factors, overexpression of STIM1 may saturate the ER retention system resulting in enhanced surface localization of STIM1.

To investigate whether overexpression of HA-STIM1 disturbs the retention signal, I compared the surface localizations in cells expressing endogenous STIM1 or overexpressing HA-STIM1. In this experiment, all cells were analyzed independently of their cell cycle state. Comparing the expression of transfected HA-STIM1 (0.5 µg/µl DNA) with the

expression of endogenous STIM1 in HEK293T cells revealed a 40- to 50-fold overexpression of HA-STIM1 (Fig 4A). Compared to endogenous STIM1, overexpression of HA-STIM1 increased the number of cells with high surface expression from 2.1 to 6.5%. Moreover, 2% of HA-STIM1 transfected cells had a strong surface signal (ratio > 65). This increased surface staining may be a consequence of overexpression. However, 36.6% of HA-STIM1 transfected cells had no STIM1 surface signal (Fig 4B). This was similar to the result observed in cells with endogenous STIM1 (37.9%) (Fig 4B), suggesting that overexpression of HA-STIM1 did not interfere with ER retention.

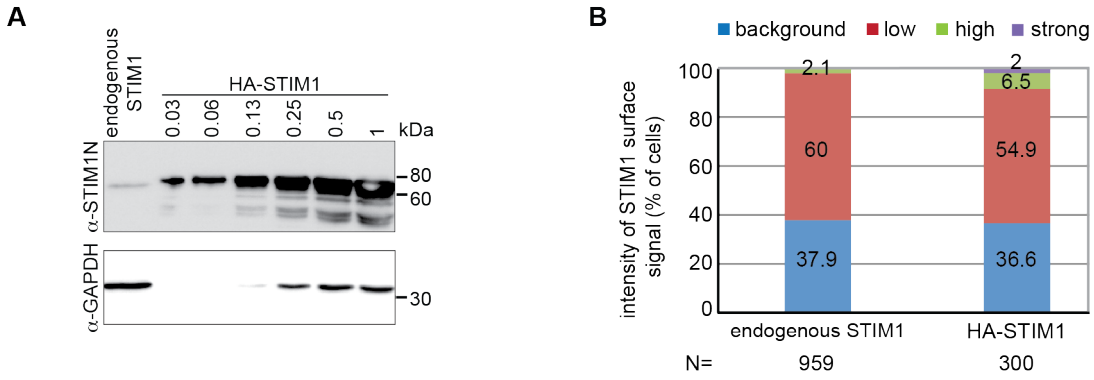

Figure 4. Overexpression of HA-STIM1 did not interfere with ER retention. (A). The overexpression levels of HA-STIM1 were analyzed by western blot using an anti-STIM1N specific antibody in cell extracts of HEK293T transfected cells. GAPDH was used as loading control. (B). Quantification of the STIM1 surface signal in untransfected and HA-STIM1 transfected cells by fluorescence microscopy. Cells were grouped according to signal intensities and the number of cells (in %) in each group is shown. All cells independently of their cell cycle stage were analyzed.

Next, the surface distribution of endogenous STIM1 in cells after activation of SOCE with increased $[Ca^{2+}]_c$ was investigated. Interphase and mitotic cells were treated with and without Tg, fixed and analyzed by immunofluorescence. Tg inhibits SERCA resulting in SOCE activation and $[Ca^{2+}]_c$ increase. In interphase, the amount of cells with no surface signal was slightly increased from 39.9 to 55.6% upon Tg treatment (Fig 3B, interphase, +Tg). On the contrary, all mitotic cells had STIM1 at the cell surface. Tg treatment did not alter the surface localization of STIM1 in M-phase cells (Fig 3B, M phase, +Tg). In addition to immunofluorescence, I used flow cytometry to analyze the effect of Tg on retention of HA-STIM1 kinetically. Cells overexpressing HA-STIM1 (0.5 µg/µl) were treated with Tg for different periods prior to flow cytometry. Tg treatment for 0.5 h did not interfere surface localization of HA-STIM1, whereas 1 h of treatment reduced the number of HA-STIM1

surface-positive cells by 42%, 2 h by 50% and 3 h by 55% (Fig 5A). This observation suggests Tg-induced STIM1 aggregation and/or increase of $[Ca^{2+}]_c$ retains STIM1 in the ER.

To investigate if interaction with Orai1 retains STIM1 in the ER, I analyzed the surface localization of HA-STIM1 in cells coexpressing Orai1. Coexpression of STIM1 and Orai1 causes STIM1-Orai1 interaction in ER-PM contact sites even under resting state conditions (Varnai et al, 2007). Cotransfection of STIM1 with Orai1 led to threefold reduction of cells with HA-STIM1 at the cell surface (Fig 5B). This increased ER retention of HA-STIM1 may be explained by ER-PM contact formation and/or Ca^{2+} influx through Orai1. To discriminate these two effects, a non-conducting mutant of Orai1 (E106A) was used (Prakriya et al, 2006). Coexpression of HA-STIM1 with Orai1 (E106A) showed similar retention of HA-STIM1 (Fig 5A), indicating that physical contact of STIM1 with Orai1 is sufficient for ER retention of STIM1. A dramatic retention of HA-STIM1 was observed upon coexpression of HA-STIM1 and Orai1 with Tg treatment (Fig 5B, +Orai1 +Tg). Furthermore, this strong reduction was not observed under same experimental set up using Orai1 (E106A) instead of Orai1 (Fig 5B, +Orai1 (E106A) +Tg). These data demonstrate that the combination of physical interaction between STIM1 and Orai1 and high $[Ca^{2+}]_c$ represses the surface expression of STIM1.

Finally, surface STIM1 was analyzed in HA-STIM1 transfected cells treated with nocodazole, a drug that depolymerizes microtubules. Microtubules were completely depolymerized with 1 µM nocodazole treatment for 20 min as analyzed by immunofluorescence ((Friedman et al, 2010); data not shown). 1 h nocodazole treatment did not enhance the number of HA-STIM1 transfected cells with surface expression (Fig 5C), suggesting that intact microtubules are not important for retention of STIM1. In contrast to this, the number of surface positive cells was decreased by 56% upon 2 h nocodazole treatment (Fig 5C), indicating that depolymerization of microtubules reduced trafficking of STIM1 to the cell surface.

In conclusion, STIM1 is retained in the ER upon SOCE activation, which promotes the interaction between STIM1 and Orai1 and results in increase of $[Ca^{2+}]_c$, whereas intact microtubules are not required for ER retention of STIM1. Intact microtubules rather play a role in trafficking of STIM1 from ER to cell surface.

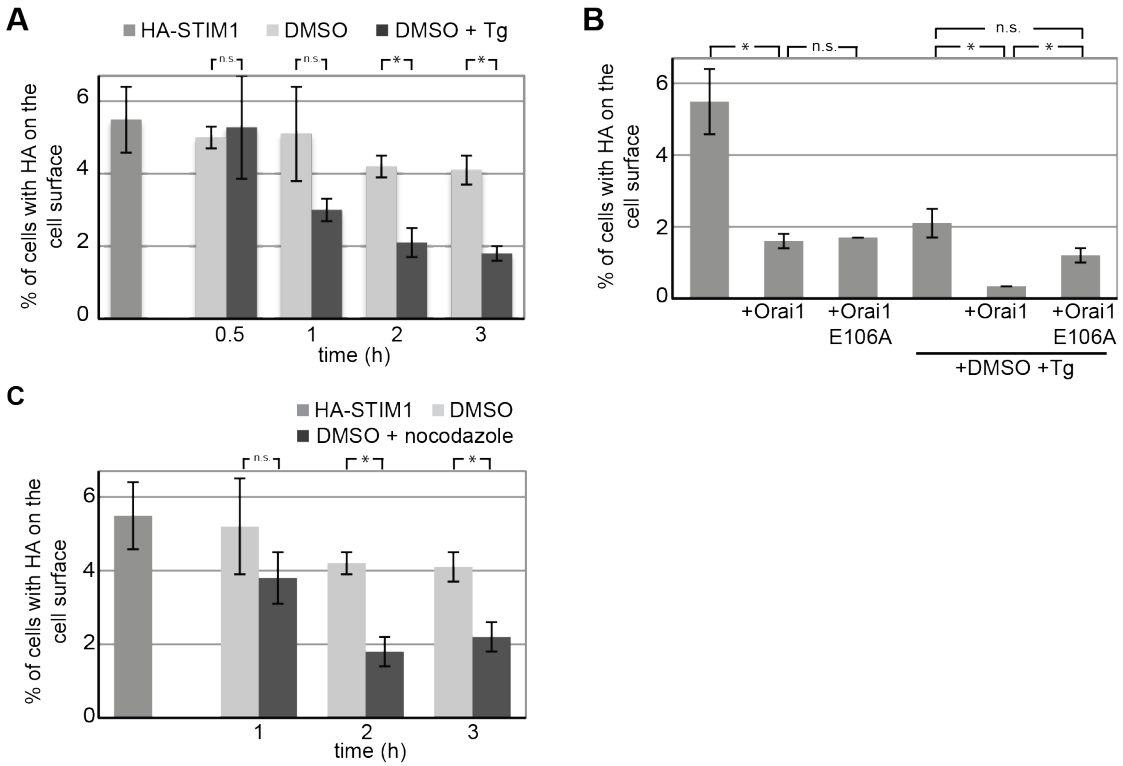

Figure 5. SOCE and increase $[Ca^{2+}]_c$ reduced STIM1 expression at the cell surface. (A- C). The number of HA-STIM1 transfected cells (in %) with HA signal on the surface under non-permeabilized conditions as determined by flow cytometry. For comparison, the first columns show the mean ± SEM of untreated cells (n = 19). All other data show the mean ± SEM (n = 3). Significant differences ($p < 0.05$) are indicated with (*) and non-significant differences with (n.s.). Cells were treated with DMSO or 1 µM Tg in DMSO (A) or with 1 µM nocodazole in DMSO (C) for the indicated times. Coexpression with GFP-Orai1 or non-conducting GFP-Orai1 (E106A) mutant and 2 h treatment with 1 µM Tg are indicated (B).

4.1.5 The K-rich domain influences the intracellular distribution of STIM1

To identify the ER retention signal in STIM1, I first focused on its lipid-binding domain, the K-rich domain. The K-rich domain can associate with Ca^{2+}/Calmodulin (Bauer et al, 2008; Bhardwaj et al, 2013) and phospholipids in the PM during the formation of ER-PM contacts (Ercan et al, 2009; Park et al, 2009; Walsh et al, 2010). Therefore, I examined whether the K-rich domain plays a role in retention of STIM1 in the ER.

To study if the K-rich domain is important for STIM1 ER retention, a mutant without K-rich domain, HA-STIM1ΔK was coexpressed with GFP in HEK293T cells. Surface localization of HA-STIM1ΔK in non-permeabilized HEK293T cells was analyzed by flow cytometry and fluorescent microscopy.

Deletion of K-rich domain led 5.2-fold increased number of HEK293T cells with HA-STIM1ΔK at the cell surface as shown by flow cytometry (Fig 6A). Consistently, an increased surface expression of HA-STIM1ΔK and a decrease in number of transfected cells with no surface signals were observed by fluorescent microscopy (Fig 6B). HA-STIM1 coexpression with Orai1 and Tg treatment led to 3.4- and 2-fold reduction of cells with surface expression, respectively (Fig 5B), however, these treatments had only a small effect on HA-STIM1ΔK with 1.2-fold reduction (Fig 6A, +Orai1 and +Tg). However, combination of Orai1 coexpression and Tg treatment led to 3.5-fold reduction of cells with HA-STIM1ΔK at the cell surface (Fig 6A, +Orai1 +Tg).

In conclusion, the K-rich domain retains STIM1 in the ER in resting cells. Coexpression with Orai1 and SOCE activation repress surface localization of HA-STIM1ΔK, suggesting that besides of the K-rich domain other signals in STIM1 contribute to ER retention of STIM1.

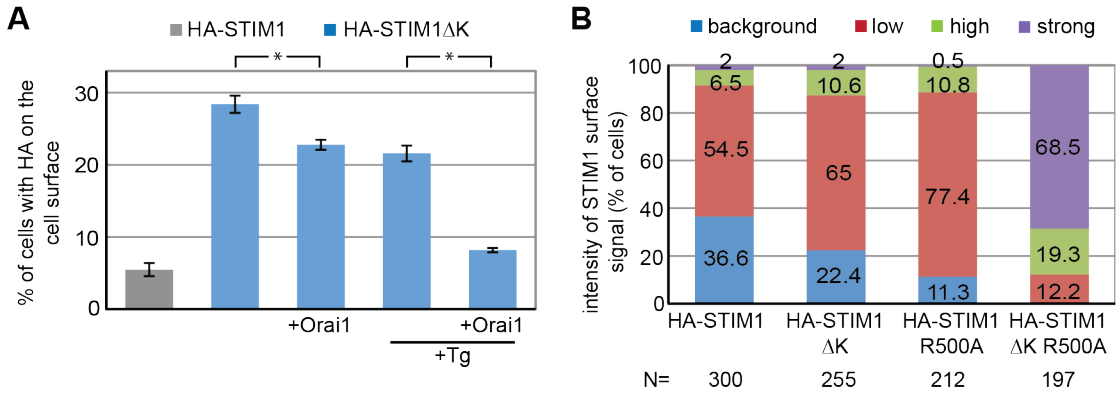

Figure 6. The K-rich domain retains STIM1 intracellular. (A) Number of HA-STIM1 and HA-STIM1ΔK transfected HEK293T cells (in %) with HA signal on the surface under non-permeabilized conditions determined by flow cytometry. If indicated Orai1 was cotransfected and the cells were treated for 2 h with 1 µM Tg. For comparison, the first column shows the mean ± SEM of untreated HA-STIM1 transfected cells (n = 19). All other data show the mean ± SEM (n = 3). Significant differences ($p < 0.05$) are indicated with (*). (B) Number of HA-STIM1, HA-STIM1ΔK, HA-STIM1 R500A and HA-STIM1ΔK R500A transfected cells (in %) with HA signal on the surface. Surface signals were detected by fluorescence microscopy of non-permeabilized cells and cells were grouped according to surface signal intensities. The non-significant differences are indicated with (n.s.). The number of analyzed cells is indicated.

4.1.6 Di-arginine signals retain STIM1 in the ER

Next, I asked what other signals in STIM1 regulate ER retention of STIM1. There are two classical ER retention signals namely the K(X)KXX and the di-arginie (RXR) (Michelsen et al, 2005; Zerangue et al, 1999). Four RXR consensus sites were found in STIM1 and STIM2 of most vertebrate and in ancestral STIMs (Rajesh, 2013) (Fig 7A). Since it was shown in a previous study (Zerangue et al, 2001) that RER is not an active retention signal, I only focused on the other three RXR signals. In human STIM1, one RXR is located in the first coiled-coil domain (RSR 311-313), and two downstream of SOAR (RQR 500-502 and RQR 530-532) (Ercan et al, 2012) (Fig 7A). I further studied if and which RXR retention signal functions in ER retention by creating STIM1 mutants in which the single RXR signals were replaced by the residues AXA. HEK293T cells coexpressing GFP and STIM1 mutants were analyzed by flow cytometry and fluorescent microscopy under non-permeabilized conditions.

Flow cytometry showed that mutation of RSR 311-313 (R311A) or RQR 530-532 (R530A) only had a small effect on the distribution of STIM1 (Fig 7B). In contrast, mutation of RQR 500-502 (R500A) revealed a strong effect on retention with 7.9-fold increase in the number of cells with surface expression of STIM1 (Fig 7B). Similar to as seen in flow cytometry, the amount of cells with HA-STIM1 R500A at cell surface was increased by 1.4-fold as and analyzed by fluorescence microscopy (Fig 6B). Compared to HA-STIM1, the amount of cells retaining HA-STIM1 R500A intracellular was decreased by 3.2-fold. Moreover, combination of mutations did not enhance surface localization of STIM1 (Fig 7C). These data suggests that RQR 500-502 functions as an ER-retention signal in STIM1.

To test if the HA-STIM1 R500A mutant still can function in SOCE, RPE-1 cells were cotransfected with GFP-Orai1 and HA-STIM1 R500A and analyzed by fluorescence microscopy under permeabilized conditions. At resting state, the majority of HA-STIM1 R500A localized in the reticular ER and GFP-Orai1 localized all over the PM (Fig 7D, -Tg). Addition of Tg caused HA-STIM1 R500A accumulation in patch-like domains (Fig 7D, +Tg) and GFP-Orai1 was recruited to these domains (Fig 7D, +Tg), indicating that mutation of RQR 500-502 does not affect STIM1 accumulation in ER-PM junctions and recruitment of Orai1.

Taken together, although three consensus RXR signals were identified in STIM1, only RQR 500-502 functions in ER retention.

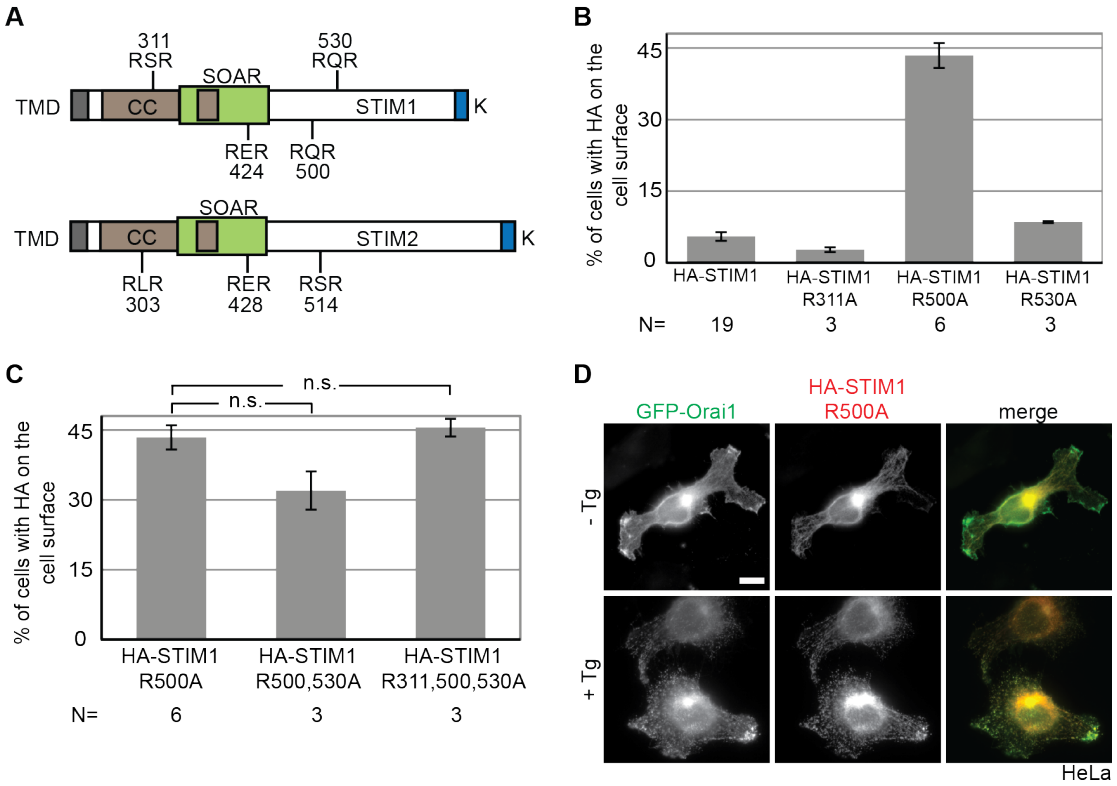

Figure 7. Di-arginine signals mediate the intracellular retention of HA-STIM1. (A). The positions of consensus sites of di-arginine signals (RXR) in the C-terminal domains of human STIM1 and STIM2 are indicated. (B). Number of GFP-positive HEK293T cells (in %) with HA signal on their surface under non- permeabilized conditions determined by flow cytometry. Cells were cotransfected with GFP and HA-STIM1, HA-STIM1 R311A, HA-STIM1 R500A or HA-STIM1 R530A. The indicated di-arginine signals were mutated (RXR to AXA). The position of the first mutated R residue is shown (R311A, R500A and R530A). (C). Quantification of the number of transfected HEK293T cells with HA-STIM1 R500A single mutant, HA-STIM1 R500, 530A double mutant and HA-STIM1 R311, 500, 530A triple mutant on the cell surface analyzed by flow cytometry. The number of experiments and the mean ± SEM of the number of transfected HEK293T cells with HA-STIM1 and RXR mutants on the surface (%) are shown. (D). Colocalization of GFP-Orai1 (green) and HA-STIM1 R500A (red) in permeabilized HeLa cells without treatment or 10 min after addition of 0.5 µM Tg. The scale bar corresponds to 10 µm.

4.1.7 Synergistic function of the K-rich domain and a di-arginine signal in the retention of STIM1

So far, I identified the K-rich domain and RQR 500-502 as STIM1 ER retention signals. To understand if there is cooperation between these two signals, the surface localization of a STIM1 mutant containing mutations in both retention signals (HA-STIM1ΔK R500A) was analyzed.

First, I tested whether HA-STIM1ΔK R500A still can mediate formation of ER-PM contacts and recruitment of Orai1. RPE-1 cells were transfected with GFP-Orai1 and HA-STIM1ΔK R500A and analyzed by fluorescence microscopy under permeabilized condition. Fluorescence microscopy showed GFP-Orai1 distributed all over the PM in resting cells. Under this condition, majority of HA-STIM1ΔK and HA-STIM1ΔK R500A remained in the reticular ER (Fig 8C and D, -Tg). In cells expressing HA-STIM1ΔK R500A, I observed additional smooth peripheral signals (Fig 8D, -Tg, arrowheads). This may correspond to surface localization of HA-STIM1ΔK R500A. Treatment with Tg led to accumulation of HA-STIM1ΔK and HA-STIM1ΔK R500A in patch-like domains representing ER-PM junctions. GFP-Orai1 was recruited to these areas (Fig 8C and D, +Tg), suggesting that HA-STIM1ΔK R500A remains its function in SOCE. However, a small amount of HA-STIM1ΔK R500A remained in smooth and peripheral structures upon Tg treatment (Fig 8D, +Tg, arrowhead), most likely corresponding to HA-STIM1ΔK R500A at the cell surface.

Next, surface distribution of the mutant (HA-STIM1ΔK R500A) was analyzed by flow cytometry and fluorescence microscopy. Fluorescence microscopy showed that all transfected cells exhibited HA-STIM1ΔK R500A surface expression (Fig 6B). Moreover, the number of cells with strong surface expression (ratio > 65) increased from 2% in cells with HA-STIM1ΔK and 0.5% in cells with HA-STIM1 R500A to 68.5% in HA-STIM1ΔK R500A (Fig 6B). Consistently, flow cytometry revealed that 79% of HEK293T cells had HA-STIM1ΔK R500A at the cell surface, which is a 14.4-fold increase in surface positive cells compared to cells with HA-STIM1 (Fig 8A). These results indicate that the K-rich domain cooperates with RQR 500-502 in ER retention of STIM1. Coexpression with Orai1 led to small but not significant decrease of cells with surface expression of HA-STIM1 R500A and HA-STIM1ΔK R500A (Fig 8A and B). Tg addition caused a 3-fold reduced number of cells with HA-STIM1 R500A at the surface (Fig 8B). In contrast, Tg treatment resulted in smaller reduction of cells with HA-STIM1ΔK R500A at the surface (1.5-fold) (Fig 8B). 51% of cells contained HA-STIM1ΔK R500A at the cell surface even when ER-PM contact formation is induced and SOCE is active (Fig 8B, HA-STIM1ΔK R500A +Orai1 and Tg). This data is consistent with the observation in fluorescence microscopy; HA-STIM1ΔK R500A remained in smooth and peripheral structures under Orai1 coexpression and Tg treatment (Fig 8D, +Tg, arrowhead). This observation is consistent with a function of HA-STIM1ΔK R500A in SOCE.

All cells expressing HA-STIM1ΔK R500A display surface localization of the protein, indicating that the K-rich domain and the di-arginine signal RQR 500-502 cooperate in a synergistic manner in the retention of STIM1.

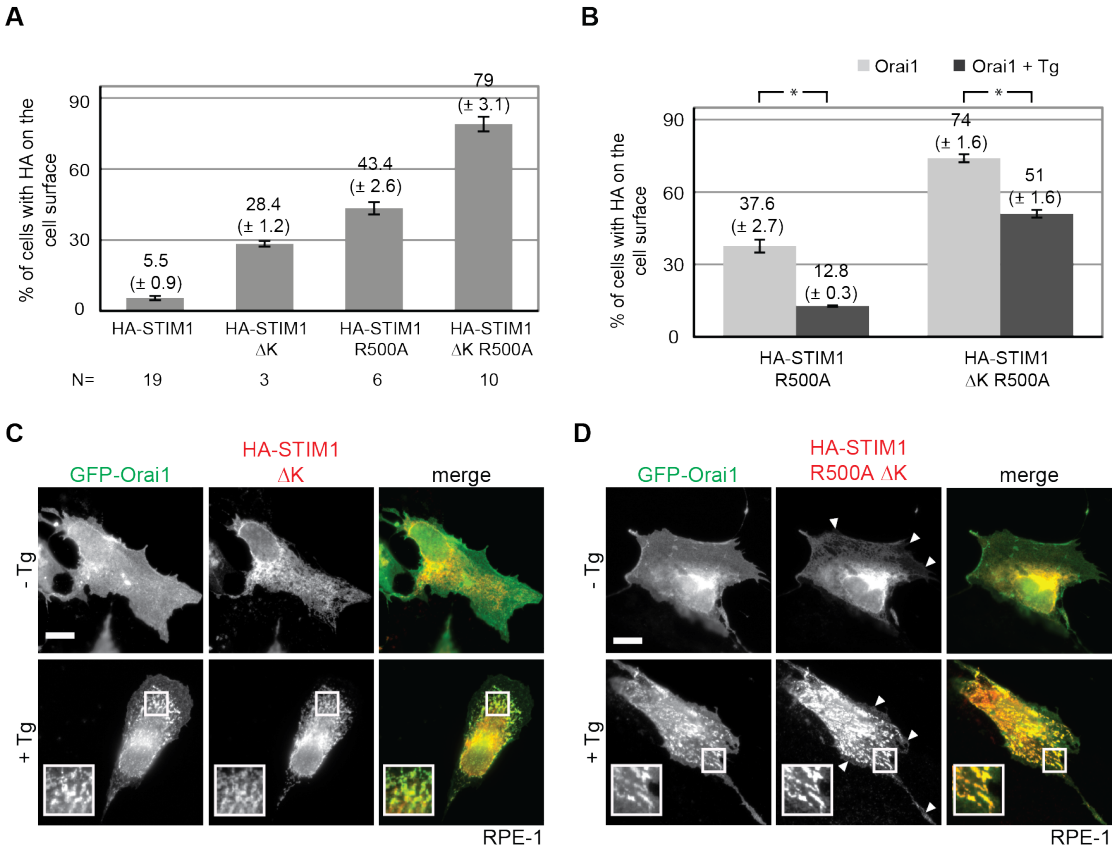

Figure 8. Di-arginine signals and K-rich domain cooperate in ER retention of STIM1. (A) Number of GFP-positive HEK293T cells (in %) with HA signal on their surface under non-permeabilized conditions determined by flow cytometry. Cells were cotransfected with GFP and HA-STIM1, HA-STIM1ΔK, HA-STIM1 R500A or HA-STIM1ΔK R500A. The number of experiments and the mean ± SEM are indicated. (B). Number of GFP-positive HEK293T cells (in %) with HA signal on their surface under non-permeabilized conditions determined by flow cytometry. Cells were cotransfected with GFP-Orai1 and HA-STIM1 R500A or HA-STIM1ΔK R500A. If indicated cells were treated for 2 h with 1 µM Tg. All data show the mean ± SEM (n = 3). Significant differences ($p < 0.05$) are indicated with (*). (C and D). Colocalization of GFP-Orai1 (green) and HA-STIM1ΔK (red) or HA-STIM1ΔK R500A (red) in permeabilized RPE-1 cells without treatment or 10 min after addition of 0.5 µM Tg. The insets show twofold magnifications of the indicated regions. Signals at the cell surface in cells expressing STIM1ΔK R500A are indicated by arrowheads. The scale bar corresponds to 10 µm.

4.1.8 HA-STIM1ΔK R500A traffics to PM in BFA-dependent manner

Next, I asked how HA-STIM1 travels from ER to PM. To inhibit protein transport from ER to Golgi apparatus, cells were treated with Brefeldin A (BFA). BFA inhibits activation of ADP-Ribosylation Factor 1 (ARF1) resulting in preventing the formation of COPI-mediated transport vesicles (Nickel et al, 2002).

After plasmid transfection for 12 h, HEK293T HA-STIM1ΔK R500A cells were treated with BFA for 6 h and analyzed by flow cytometry under non-permeabilized conditions. In a control experiment, HEK293T cells were cotransfected with the ATP-sensitive potassium channel Kir6.2-HA-GFP and its regulatory subunit Sur1. Unassembled Kir6.2 is retained in the ER by di-arginine signals. Assembling of Kir6.2 with Sur1 promotes trafficking to the surface (Zerangue et al, 1999). BFA treatment in HEK293T cells coexpressing Kir6.2-HA-GFP and Sur1 showed 2.5-fold reduction of number of cells with HA at the cell surface (Fig 9). Similarly, BFA treatment led to 2.8-fold reduction of number of cells with HA-STIM1ΔK R500A at the cell surface (Fig 9), suggesting that STIM1ΔK R500A is trafficking to the PM in a BFA-dependent manner.

In summary, STIM1 is retained in the ER by the K-rich domain and RQR 500-502 and travels to PM via the classical secretary pathway.

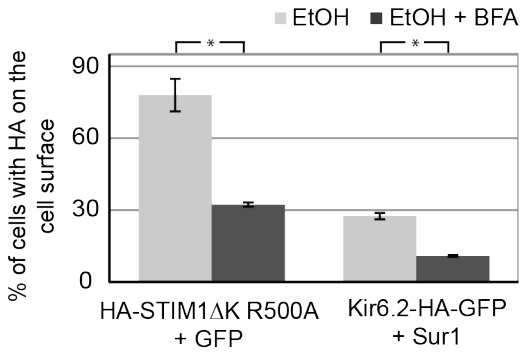

Figure 9. HA-STIM1ΔK R500A travels in a BFA-dependent manner to the cell surface. HEK293T cells coexpressing HA-STIM1ΔK R500A and GFP or Kir6.2-HA-GFP and Sur1 were treated with ethanol or with 1µg/mL BFA in ethanol for 6 h before analysis by flow cytometry. The mean ± SEM (n = 3) of the number of cells with HA on the cell surface and significant differences ($p < 0.05$; shown as *) are indicated.

4.1.9 Phosphorylation of S486 and/or S668 interferes with ER retention of STIM1

The majority of STIM1 is retained in the ER by synergistic function of a di-arginine (RXR) signal and the K-rich domain during interphase. In contrast, the surface expression of STIM1 significantly increases in M-phase. In a previous study, Smyth et al showed that SOCE is suppressed during mitosis (Smyth et al, 2009). They also identified that the residues S486 and S668 of STIM1 were phosphorylated during mitosis (Smyth et al, 2009) (Fig 10A). S486 and S668 are located closely to the retention signals, RQR 500-502 and the K-rich domain (residues 670-685), respectively (Fig 10A). Therefore, mitotic phosphorylation

of S486 and/or S668 may inactivate ER retention signals resulting in an enhanced surface expression of STIM1. In order to test this hypothesis, I asked if there is a correlation between phosphorylation of S486 and/or S668 and distribution of STIM1.

HEK293T cells were transfected with the phospho-mimicking mutants either HA-STIM1 S486D or HA-STIM1 S668D or HA-STIM1 S486D S668D and analyzed by flow cytometry and fluorescence microscopy under non-permeabilized condition. In this experiment, cells were analyzed independent of their cell cycle stage. The amount of cells expressing the phospho-mimicking mutant HA-STIM1 S668D at the surface was increased 3- fold compared to HA-STIM1 as seen by flow cytometry (Fig 10B). Cells with HA-STIM1 S486D S668D showed similar retention as cells with HA-STIM1 S668D (Fig 10B). Immunofluorescence microscopy revealed that the number of cells with no surface expression decreased from 36.6% in HA-STIM to 18.9% in HA-STIM1 S486D and 13.1% in HA-STIM1 S668D cells (Fig 10C). Overexpression of HA-STIM1 S486D S668D revealed an enhanced number of cells with strong surface expression determined by fluorescence microscopy (Fig 10C). These observations suggest that phosphorylation at residues S486 and/or S668 inactivate the di-arginine retention signal at residue 500-502 and/or the K-rich domain (residues 670-685).

Phosphorylation of STIM1 during M-phase (Smyth et al, 2009) could abolish efficient ER retention by phosphorylation of S486 and/or by phosphorylation of S668. This may explain why surface localization of STIM1 is significantly increased in M-phase.

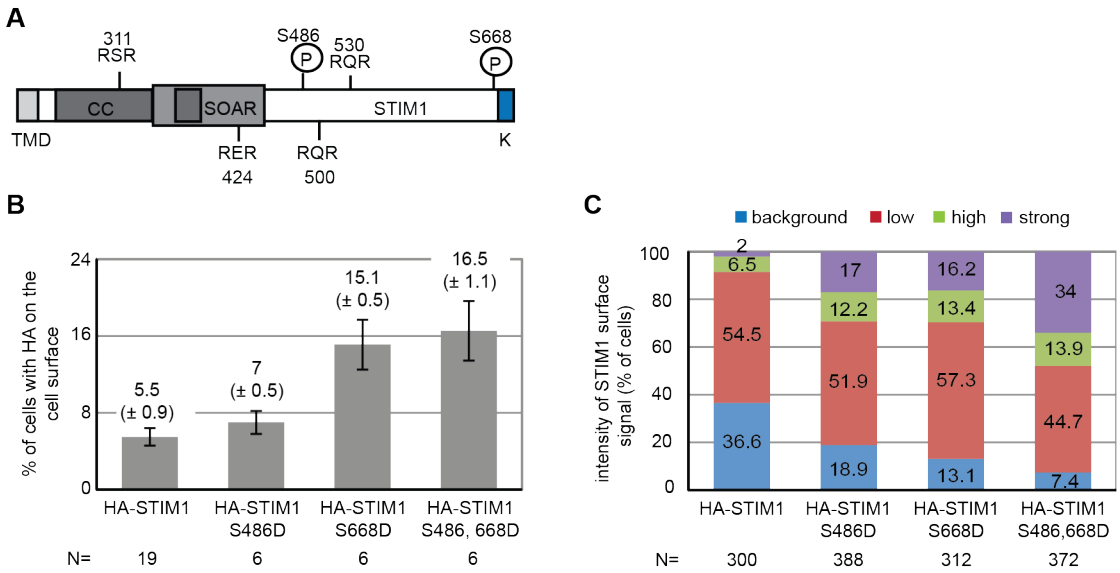

Figure 10. Phosphorylation of S486 and/or S668 interferes with ER retention of STIM1. (A). Cartoon of the C-terminal domain of STIM1 shows four conserved di- arginine signals, the K-rich

domain and two phosphorylation sites. (B). Number of HEK293T cells (in %) with HA signal on the surface under non-permeabilized conditions analyzed by flow cytometry. (C). Quantification of HA signal on the surface in HEK293T cells under non-permeabilized condition analyzed by fluorescence microscopy. Cells were grouped according to signal intensity and the number of cells (in %) in each group is shown. Cells were cotransfected with GFP and HA-STIM1, HA-STIM1 S486D, HA-STIM1 S668D and HA-STIM1 S468, 668D double mutant. The number of analyzed cells is indicated.

4.2 Localization of STIMs in specific subdomains of the ER

Although 5-10% of STIM1 localizes on the cell surface, the majority of STIM1 retains in the ER. So far, the distribution of STIM1 within subdomains of the ER is still under debate. During SOCE activation, STIM1 forms high-order oligomers and accumulates in large flattened ER sheets juxtaposed to the PM, which form punctate structures called ER-PM contact sites (Orci et al, 2009; Soboloff et al, 2012). Although the basic molecular mechanism of SOCE is understood, the molecular bases of the translocation process in SOCE remains elusive. In order to decipher the translocation process of STIM proteins in SOCE, I am especially interested in the localization of STIM1 in subdomains of the ER during resting state.

There are two different models for the activation of STIM1. The first model suggests that STIM1 distributes randomly in the entire ER. During SOCE activation, STIM1 oligomerization occurs as an essential prerequisite for STIM1 translocation. STIM1 oligomers are recruited via diffusion along ER networks to nearby ER-PM junctions where STIM1 associates with $PI(4,5)P_2$ in the PM forming *de novo* ER-PM contact sites (Liou et al, 2007). However, oligomerization of STIM1 reduces its mobility in the ER (Grigoriev et al, 2008; Liou et al, 2007). Moreover, it is unknown how STIM1 oligomers bind specifically to lipids only on the PM but not to the lipids of other organelles. This model is not in line with the fact that ER-PM contact formation is a specific and efficient process. Therefore, these arguments are suggestive of a second model.

The second model suggests that STIM1 localizes in specific subdomains of tubular ER, called preexisting ER-PM contact sites. At resting state, lower-order STIM1 oligomers form the ER-PM contacts sites (Wu, 2006). Lower-order STIM1 oligomers travel constantly from general ER to preexisting ER-PM contact sites via binding to EB-1 positive microtubule ends (Grigoriev et al, 2008). Ca^{2+} depletion causes STIM1 conformational change resulting in accumulation of higher-order STIM1 oligomers at the preexisting ER-PM contact sites (Wu, 2006). Oligomerization of STIM1 increases its lipid binding affinity significantly (Bhardwaj et

al, 2013). Thus, these preexisting ER-PM contact sites are expanded resulting in larger ER-PM contact sites formation.

The second model is further supported by the observations that the STIM1-mediated ER-PM contact sites appear repeatedly at the same location upon repetitive stimulation (Malli et al, 2008; Smyth et al, 2008), suggesting that ER-PM contact sites are pre-determined. Similarly, such constitutive ER-PM contacts can be observed in yeast (Manford et al, 2012; West et al, 2011; Wolf et al, 2012). In yeast, approximately 50% of the PM is covered by the cortical ER (West et al, 2011; Wolf et al, 2012). Unlike the situation in yeast, in mammalian cell, there is only about 2% of ER is cortical ER (Giordano et al, 2013). However, the formation of cortical ER was induced at resting state by overexpression of extended synaptotagmins (E-Syts) in HeLa cells (Giordano et al, 2013). E-Syt2 and 3 tether the ER to PM via its C2 domains binding to $PI(4,5)P_2$ in the PM (Giordano et al, 2013). Taken together, I hypothesize that STIM1 is involved in the formation of preexisting contact sites at resting state. These preexisting ER-PM contact sites are expanded in response to Ca^{2+} depletion.

4.2.1 STIMs are preferentially located in specific subdomains of tubular ER.

In order to examine if STIM1 localizes in preexisting ER-PM contact sites, I analyzed the localization of STIM1 at resting state in more detail. For this purpose, total internal reflection fluorescence (TIRF) microscopy was applied. TIRF microscopy is a technique utilized to observe fluorophores present in the plasma membrane-proximal region (distance about 100 nm from the cover slip) (Fig 11A). To study the localization of endogenous STIM1 by immunofluorescence, I first used commercial antibodies which recognize N-terminal domains of STIM1. However, the commercial antibodies failed to detect endogenous STIM1 in fluorescence microscopy and western blotting. Therefore, I raised an antibody against the entire N-terminal domain of STIM1 and analyzed the specificity by fluorescence microscopy and western blotting. The newly raised, α-STIM1N described in 4.1.2 recognized endogenous STIM1 but it also cross-reacted to mitochondrial proteins, as shown in Fig 2C-F. Therefore, it was not possible to study the localization of endogenous STIM1 using this antibody, so I overexpressed HA-STIM1-GFP or STIM1-mCherry in epithelial U2OS cells to investigate STIM1 localization in preexisting ER-PM contact sites.

In order to allow me the detection of fluorophores by TIRF microscopy under condition avoiding strong overexpression, I transfected U2OS cells with minimum amount of DNA (0.1 µg/µl). Comparing the expression of HA-STIM1-GFP after transfection (with 0.1 µg/µl DNA)

with the expression of endogenous STIM1 in U2OS cells revealed a 15- to 20-fold overexpression of HA-STIM1-GFP (Fig 11F). This overexpressed HA-STIM1-GFP localized mainly in the reticular ER and partially in dot-like domains (Fig 11B). From our previous study, it is known that 40- to 50-fold overexpression of HA-STIM1 did not interfere with ER retention (Ercan et al, 2012). Immunofluorescence microscopy revealed that overexpressed HA-STIM1 showed the same localization as overexpressed HA-STIM1-GFP (Fig 2B, permeabilized and Fig 11B), suggesting that C-terminal GFP tag does not interfere with localization of STIM1. Moreover, HA-STIM1-GFP and HA-STIM1-mCherry showed no difference in their localization as observed in a control experiment where both proteins upon coexpression displayed a complete overlap (Fig. 11D). These data suggest that introducing either GFP or mCherry after the K-rich domain did not influence the localization of overexpressed STIM1.

I compared the localization of STIM1 and STIM2 at resting state in U2OS cells using two general ER markers, an artificial luminal protein RFP-KDEL and the type I membrane protein CD3δ-GFP. RFP-KDEL is a fusion of the red fluorescent protein (RFP) and the ER retention signal KDEL. This protein reaches the ER lumen via a signal sequence and is kept in the ER by the retention signal. CD3δ is part of the T-cell receptor/CD3 complex (TCR/CD3 complex) and is involved in T-cell development and signal transduction (Gil et al, 2011).

In a colocalization experiment, I observed a partial overlap of HA-STIM1-GFP and RFP-KDEL. HA-STIM1-GFP was enriched in some areas of the reticular and tubular ER while RFP-KDEL was excluded (Fig 11B arrowheads). HA-STIM1-mcherry colocalized with CD3δ-GFP in tubular ER. This colocalization was not uniform. STIM1 accumulated in several dot-like foci, in which CD3δ-GFP was less abundant (Fig. 11C arrowheads). These data suggest that overexpressed HA-STIM1-GFP is accumulated in specific domains of the tubular ER. In contrast to STIM1, STIM2 accumulated only in dot-like domains in the tubular ER but not in reticular structures. The localization pattern of STIM2 differed significantly from that of CD3δ-GFP and RFP-KDEL (Fig. 11E arrowheads). Increased dot-like domain formation could be a result of STIM2 overexpression. However, comparing the expression of HA-STIM1-GFP with the expression of HA-STIM2-GFP in U2OS transfected cells, revealed a 5-fold higher expression level of HA-STIM1-GFP (Fig 11G).

These results suggest that at resting state STIM proteins concentrate in specific dot-like subdomains of the ER. Furthermore, STIM2 accumulates in these ER subdomains more efficiently than STIM1. These dot-like domains might correspond to preexisting ER-PM contact sites.

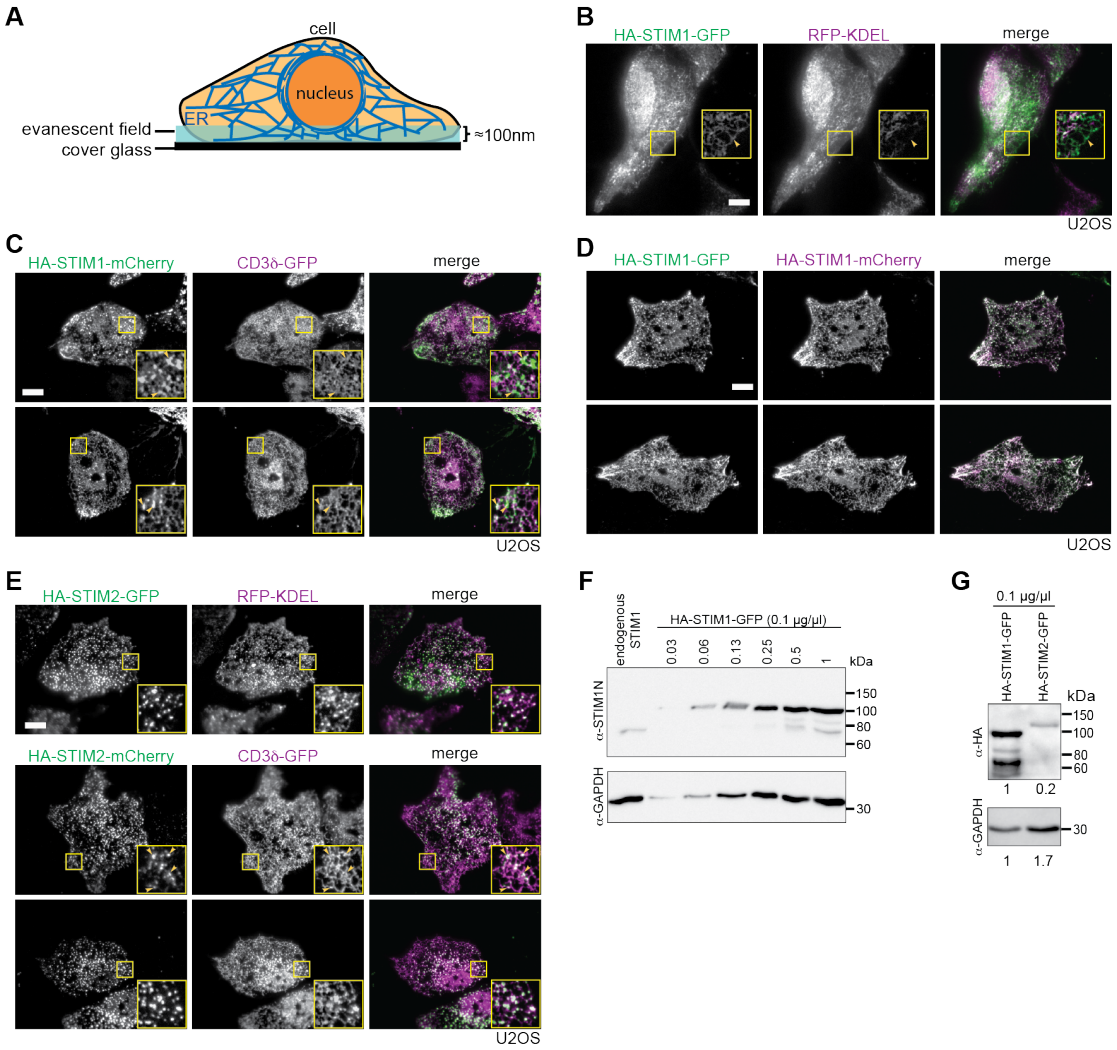

Figure 11. Overexpressed STIMs are segregated into specific subdomains of the ER. (A). Cartoon describes experimental set-up of TIRF microscopy in a tissue culture cell. The evanescent field illuminates a restricted area of the cell. ER close to cover glass (within 100 nm), can be observed under TIRF microscopy. (B- E). TIRF microscopy of U2OS cells: (B). Colocalization of HA-STIM1-GFP (green) and RFP-KDEL (purple) in U2OS cells. The insets show threefold magnification of the selected regions. (C). Colocalization of HA-STIM1-mCherry (green) and CD3δ-GFP (purple). The insets show twofold magnification of the selected regions. (D). Colocalization of HA-STIM2-GFP (green) and RFP-KDEL (purple) or HA-STIM2-mCherry (green) and CD3δ-GFP (purple). The insets show threefold magnification of the selected regions. (E). Colocalization of HA-STIM1-GFP (green) and HA-STIM1-mCherry (purple). The scale bar corresponds to 10 µm. (F). The expression levels of HA-STIM1-GFP and HA-STIM2-GFP in U2OS transfected cells were analyzed by western blot using an anti-HA specific antibody. GAPDH was used as loading control.

4.2.2 STIM1 localizes in preexisting ER-PM contact sites

At resting state, overexpressed STIM proteins localize to specific dot-like ER subdomains. These structures could correspond to preexisting ER-PM contact sites. SOCE activation leads to translocation of STIM1 to ER-PM contact sites and to a patch-like localization pattern of STIM1 (Liou et al, 2007; Wu, 2006). If the observed dot-like structures are preexisting contact sites, Tg treatment should lead to STIM1 accumulation at these domains resulting in expansion of these preexisting contact sites to larger and stable ER-PM contact sites. To elucidate if and how many ER-PM contact sites are developed from the observed dot-like domain. I followed ER-PM contact sites formation in live cell and quantified them using ImageJ-macro described in materials and methods in section 3.5.2.

Images of the same cell were taken directly after addition of 50 µM Tg (t=0) and 5, 7 and 15 min later. Pictures of all time points were overlaid with the image taken at the t=15 and HA-STIM1-mCherry localization was analyzed. At t=0, STIM1-mCherry was localized in the reticular ER and concentrated in some dot-like domains (Fig 12B, white arrowheads). Incubation with Tg for 5 min caused loss of the reticular localization of STIM1-mCherry and the proteins were clustered in patch-like domains. These patch-like domains colocalized in many cases with STIM1-mCherry concentrated areas at t=0 (compare Fig 12B white and yellow arrowheads), suggesting these sites were preexisting ER-PM contact sites. These sites were marked blue (Fig 12C).

I used this quantification method and quantified 10 selected area (21.34 X 20.24 μm^2) in different cells in three independent experiments. The majority of ER-PM contact sites (85.58% ± 6.85%) developed from preexisting ER-PM contact sites observed at resting state (Fig 12D). These findings suggest that these structures are functioning as seeds for ER-PM junctions in SOCE and support the model of preexisting ER-PM contact sites.

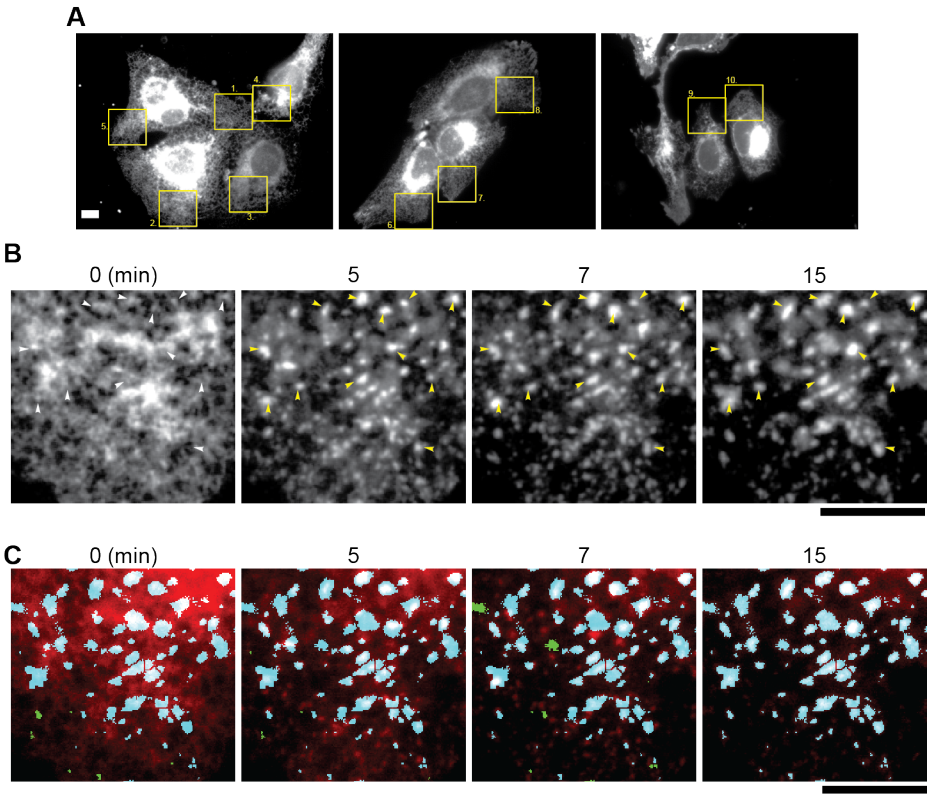

D

	pre-existing ER-PM contact sites	ER-PM contact sites after Tg treatment	percentage of pre-existing ER-PM contact sites (%)
1	56	72	77.78
2	95	113	84.07
3	75	78	96.15
4	84	102	82.35
5	70	91	75.29
6	125	136	91.91
7	91	102	89.22
8	149	182	81.87
9	93	111	83.78
10	113	121	93.39

avarage ± SD = 85.58 ± 6.85%

Figure 12. Majority of STIM1 accumulates in pre-existing ER-PM contact sites. (A). U2OS stably expressing α-tubulin-GFP (U2OS tub-GFP cells) were transfected with HA-STIM1-mCherry. The ER-PM contact sites formation after 50 nM Tg treatment were monitored in real time by using fluorescence microscope. (B). Sixfold magnification images of the crop2 from (A). Preexisting ER-PM contact sites are indicated with white arrowheads. ER-PM contact sites generated upon Ca^{2+} depletion are indicated with yellow arrowheads. (C). Quantification of pre-existing ER-PM contact sites by using ImageJ macro as described in materials and methods 3.5.2. HA-STIM1-mCherry is shown in red. Pre-existing and *de-novo* ER-PM contact sites are shown in blue and green, respectively. (D). Number of the STIM1-mediated ER-PM contact sites (in %) generated from pre-

existing ER-PM contact sites after Tg treatment in selected regions from (A). Scale bar corresponds to 10 µm.

4.2.3 STIM1 clusters localize in PI(4,5)P_2 containing ER-PM junctions

As described before, Tg treatment leads to SOCE activation and to the formation of a patch-like localization pattern of STIM1 (Liou et al, 2007; Wu, 2006). In order to confirm in more detail that these patch-like structures (Fig 12 B yellow arrowheads, 15 min) are indeed ER-PM junctions, I established an FRET-based quantification assay of ER-PM contact sites as shown in Fig 13A.

Close proximity of ER and PM (a distance of around 10 nm) generates a FRET signal between donor and acceptor. C-terminal GFP tagged STIM1 was used as ER probe and the N-terminal mCherry tagged PI(4,5)P_2 binding PH domain of phospholipase C-δ1 was used as PM probe. FRET was detected by acceptor photobleaching using confocal microscopy. In this experiment energy transfer is decreased or eliminated when the acceptor fluorophore is bleached, thereby leading to an increase in donor fluorescence (Karpova et al, 2003). STIM1-GFP and mCherry-Orai1 were used as a positive control and to examine the experimental set up. It has been shown that STIM1 associates directly with Orai1 and this association leads to a FRET signal between STIM1-YFP and CFP-Orai1 (Navarro-Borelly et al, 2008). mCherry-Orai1 was photobleached in a defined region of interest until fluorescence signals reached background level. This was achieved by scanning three times with a 561-nm laser with 100% power (Fig 13B, lower panel). FRET efficiency was calculated from fluorescence signals of pre- and post- bleach images of the donor STIM1-GFP like described in 3.5.1. By using this FRET-macro (REF), FRET was observed between STIM1-GFP and mCherry-Orai1. The maximum of FRET efficiency was around 30% in the photobleached region (Fig 13B). The overall FRET efficiency in the photobleached region was higher than that in the non-photobleached region, indicating that this FRET-based assay can be further used to quantify ER-PM contacts.

Next, I used the same experimental set up to examine FRET between mCherry-PH and CD3δ-GFP or STIM1-GFP upon ER Ca^{2+} depletion. To test if ER-PM contacts are detected under endogenous levels of STIM1, I used the ER protein CD3δ-GFP as a probe. In cells expressing endogenous levels of STIM1, the described reorganization of the ER could not be observed after Tg treatment. CD3δ-GFP localization was not altered (Fig. 13C). In addition, no FRET signal between CD3δ-GFP and mCherry-PH was observed (Fig. 13C). In COS7 cells coexpressing mCherry-PH and HA-STIM1-GFP, Tg treatment led to the

formation of patch-like domains and a FRET signal was observed (max. 25%) (Fig 13C). These data suggest that overexpressed STIM1 clustered in $PI(4,5)P_2$ containing ER-PM junctions after ER Ca^{2+} depletion and that STIM1 patch-like localization corresponds to ER-PM contact sites. However under endogenous STIM1 expression levels the used FRET setup is not sensitive enough to detect ER-PM junctions.

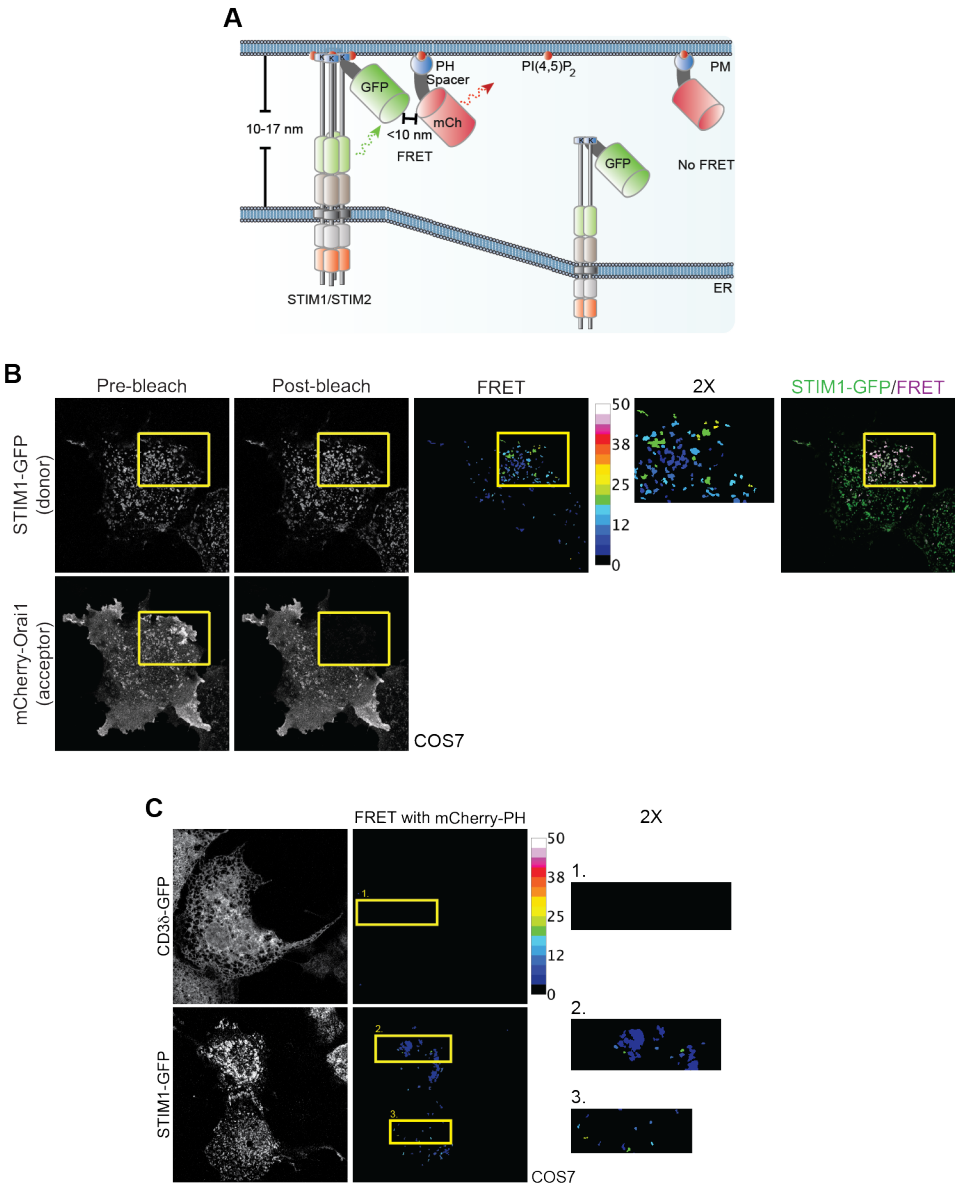

Figure 13. STIM1 clusters localize in $PI(4,5)P_2$ containing ER-PM junctions after ER Ca^{2+} depletion. (A). Cartoon of experimental set-up. Fluorescent resonance energy transfer (FRET)-based quantification of ER-PM contacts was analyzed by laser scanning confocal microscopy using acceptor photobleaching. (B). Quantification of FRET efficiency of STIM1-GFP and mCherry-Orai1 interaction. (C). FRET between PM localized mCherry-PH and GFP-tagged Cd3δ, STIM1 and STIM1ΔK in ER

Ca^{2+} depleted state. FRET efficiency is shown in imageJ 16 colors code. From left to right: TIRF images, FRET efficiency and twofold magnification images.

4.2.4 The K-rich domain is required to localize STIM1 in preexisting ER-PM contact sites

Next, I asked what signals in STIMs are involved in the accumulation of STIMs in preexisting ER-PM contact sites. ER-PM tethering is often governed by ER proteins which bind to $PI(4,5)P_2$ on the inner leaflet of the PM via their lipid-binding domains (English & Voeltz, 2013). In mammalian cells under resting condition extended synaptotagmins (E-Syt) 2 and 3 couple ER and PM via binding of their cytosolic C2 domains to $PI(4,5)P_2$ (Giordano et al, 2013). Similarly, the yeast ER membrane protein Ist2 and tricalbins tether the ER to the PM by their lipid binding domains CSS and C2 domain, respectively (Fischer et al, 2009; Manford et al, 2012). *In vitro* STIM1 and STIM2 can bind to PM-like liposomes containing 5 mol% $PI(4,5)P_2$ via their extreme C-terminal K-rich lipid-binding domains (Ercan et al, 2009). Therefore, I asked whether the K-rich domains of STIMs contribute to the formation of preexisting ER-PM contact sites. For this purpose, I compared the localization of HA-STIM1-GFP and a STIM1 mutant lacking the K-rich domain (HA-STIM1ΔK-GFP) in resting cells and in cells after induction of SOCE.

15 to 20- fold overexpression of HA-STIM1-GFP in resting U2OS cells resulted in an accumulation of STIM1-foci (Fig 11F and 14A, 0.1 µg/µl). Higher expression of HA-STIM1-GFP by transfection with increasing amount of DNA (Fig. 14C and D) led to formation of larger patches (Fig 14A arrowheads) comparable to those observed in Tg-treated cells (Fig 12B yellow arrowheads and 13C). In contrast, no patch formation was observed in cells overexpressing HA-STIM1ΔK-GFP at resting state. The protein was located in the reticular ER (Fig 14A). This difference in localization was observed despite similar expression levels of HA-STIM1-GFP and HA-STIM1ΔK-GFP (Fig 14C and E). Moreover, in cells overexpressing HA-STIM1ΔK-GFP, Tg treatment failed to induce patch formation and no FRET signal between HA-STIM1ΔK-GFP and mCherry-PH was observed (Fig 14B). These data lead to the conclusion that the K-rich domain is required to localize STIM1 in preexisting ER-PM contact sites. The lipid binding ability of STIM1 mediates the formation of preexisting ER-PM contact sites.

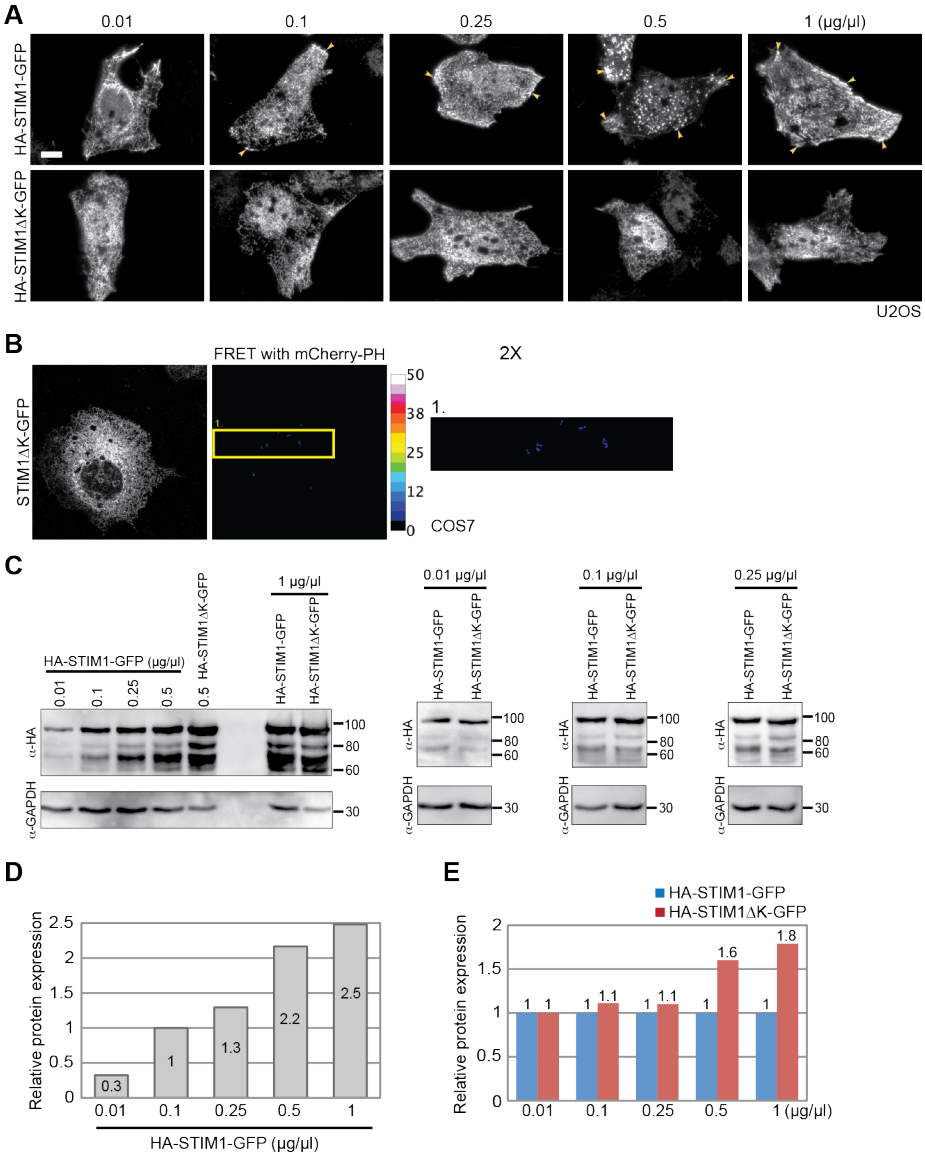

Figure 14. The lipid binding, K-rich domain contributes to the formation of ER-PM contact sites. (A). U2OS cells were transfected with HA-STIM1-mCherry or with HA-STIM1ΔK-mCherry and analyzed by TIRF microscopy. Patch-like domains are indicated with yellow arrowheads. The scale bar corresponds to 10 µm. (B). Expression levels of HA-STIM1-GFP and HA-STIM1ΔK-GFP with indicated DNA concentration used for transfection of U2OS cells as analyzed by western blot using an anti-HA specific antibody. GAPDH was used as loading control. (C and D). Quantification of (B). (C). Relative protein expression of HA-STIM1-GFP with indicated DNA concentration in transfection. (D). Relative protein expression of HA-STIM1-GFP and HA-STIM1ΔK-GFP with indicated DNA concentration in transfection.

4.2.5 STIM2 recruits ER to PM more efficient than STIM1

STIM2 K-rich domain has higher affinity to $PI(4,5)P_2$ than the K-rich domain of STIM1 (Bhardwaj et al, 2013; Ercan et al, 2009). In addition, overexpression of STIM2 in resting cells led to complete accumulation of the protein in dot-like structures (Fig. 11E), suggesting that high concentration of STIM2 induces constant ER-PM contact formation. Therefore, it seems likely that the lipid binding affinity of STIM1 and STIM2 K-rich domains correlate with the ability to form ER-PM contact sites. Thus, I asked if STIM2 tethers ER to PM more efficient than STIM1.

To answer this question, I investigated the localization of a STIM1 mutant, in which the K-rich domain was replaced by the K-rich domain of STIM2 (HA-STIM1ΔK-K_{STIM2}-GFP) (Fig 15A). If formation of preexisting ER-PM contact sites depends on the lipid-binding domain, the patch-like structures should increase in cells expressing HA-STIM1ΔK-K_{STIM2}-GFP.

As expected, I observed a significant increase in the size and the amount of patch-like domains in COS7 cells expressing HA-STIM1ΔK-K_{STIM2}-GFP (Fig 15B). Compared to the FRET signal in cells expressing PH-mCherry and HA-STIM1ΔK-K_{STIM2}-GFP in patch-like domains, the FRET signal in PH-mCherry and HA-STIM2-GFP expressing cells was in a similar range even at resting state (Fig 15D). This suggests that both HA-STIM1ΔK-K_{STIM2}-GFP and HA-STIM2-GFP containing the K-rich domain of STIM2 tether similar amount of ER to PM at resting state. Furthermore, STIM2 changed its localization from dot-like structures to reticular ER when STIM2 K-rich domain was replaced by STIM1 K-rich domain or when the K-rich domain was deleted (Fig 15B). In addition, no FRET signal was observed between mCherry-PH and HA-STIM2ΔK-GFP (Fig 15D). The protein expression levels of STIM1, STIM1ΔK and STIM1ΔK-K_{STIM2}-GFP were comparable as well as the levels of STIM2, STIM2ΔK and STIM2ΔK-K_{STIM1}-GFP (Fig 15C).

In conclusion, *in vivo* the K-rich domain of STIM2 recruits ER to PM more efficiently than the K-rich domain of STIM1. This also explains the different localization of STIM1 and STIM2 at resting state (Fig 11B, 11C and 11E). At resting state, when STIM1 most likely forms dimmer (Baba et al, 2006; Covington et al, 2010; Muik et al, 2008; Soboloff et al, 2012). Dimeric STIM1 has weaker lipid binding affinity than higher-order oligomers (Bhardwaj et al, 2013; Soboloff et al, 2012) that forms after ER Ca^{2+} depletion. Overexpression of STIM1 induces its oligomerization independently of Ca^{2+} depletion resulting in increased lipid binding ability of STIM1 (Bhardwaj et al, 2013; Luik et al, 2006; Varnai et al, 2007). I observed that even under resting condition, the K-rich domains position

overexpressed STIMs at preexisting ER-PM contact sites by interacting with $PI(4,5)P_2$ in the PM.

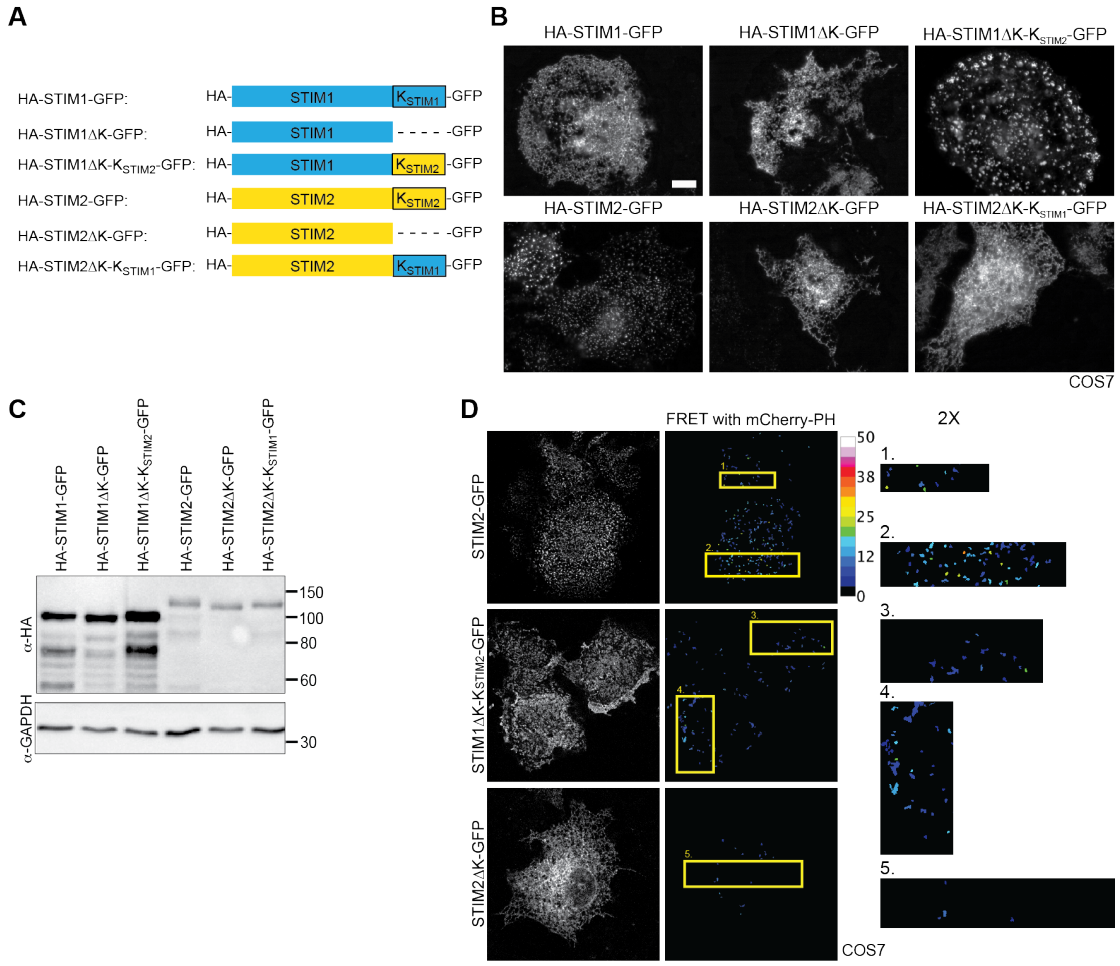

Figure 15. STIM2 K-rich domain recruits ER to PM more efficient than STIM1 K-rich domain *in vivo*. (A). Cartoon shows STIMs mutants with swapped K-rich domains. In STIM1ΔK-KSTIM2-GFP the K-rich domain of STIM1 was replaced by the K-rich domain of STIM2. In STIM2ΔK-KSTIM1-GFP the K-rich domain of STIM2 was replaced by the K-rich domain of STIM1. (B). COS7 cells were transfected with STIM1-GFP, STIM1ΔK-GFP, STIM1ΔK-KSTIM2-GFP, STIM2-GFP, STIM2ΔK-GFP and STIM2ΔK-KSTIM1-GFP and analyzed by TIRF microscopy. The scale bar corresponds to 10 µm. (C). The expression levels of STIM constructs from (A) in COS7 transfected cells were analyzed by western blot using an anti-HA specific antibody. GAPDH was used as loading control. (D). FRET between PM localized mCherry-PH and STIM2-GFP, STIM1ΔK-K_{STIM2}-GFP and STIM2ΔK-GFP at resting state. FRET was analyzed by laser scanning confocal microscopy using acceptor photobleaching. From left to right: TIRF images, FRET efficiency and twofold magnification images.

4.3 The role of microtubule in the formation of STIM1-mediated ER-PM contact sites

Next, I wanted to analyze how newly synthesized STIM1 reaches to preexisting ER-PM contact sites in the periphery of the ER network. STIM1 could diffuse in the tubular ER and get trapped in preexisting ER-PM contact sites via the binding of the K-rich domain to PM lipids. Alternatively, in additional to diffusion and trapping by the K-rich domain, other factors could assist the translocation of STIM1 from general ER to ER-PM contact sites. It has been shown that STIM1 binds to growing microtubule plus ends via interaction with the microtubule-plus-end-tracking protein EB-1. This is accomplished by an EB-1 binding motif (S/TxIP) in the C-terminus of STIM1 (Grigoriev et al, 2008). However, EB-1 depletion or inhibition of microtubule dynamics did not abolish STIM1 puncta formation and SOCE (Grigoriev et al, 2008). In contrast to this, depolymerization of microtubules impairs SOCE (Smyth et al, 2007). This observation is consistent with the fact that microtubules play an important role in ER morphology (Terasaki et al, 1986). Therefore, the roles of microtubules in the transport of STIM1 and in the formation of cortical ER are still unclear.

4.3.1 STIM1 moves along microtubules in an EB-1 independent manner

In order to decipher the role of microtubules in STIM1 localization in more detail, I analyzed the mobility and localization of STIM1 by fluorescence microscopy in the presence and the absence of the EB-1 binding motif. First I colocalized HA-tagged STIM1 with α-tubulin by immunofluorescence. HA-STIM1 aligned along microtubules in tubular ER subdomains (Fig 16A, -Tg).

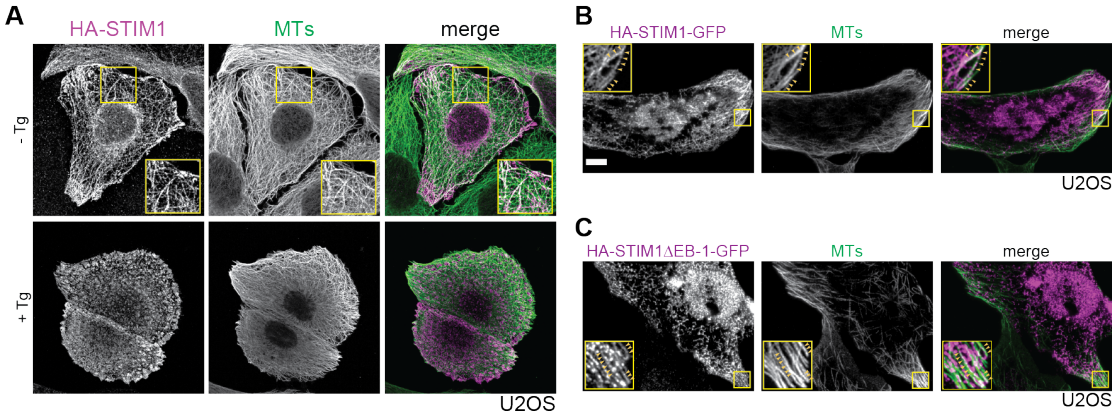

Figure 16. STIM1 aligns along microtubules in EB-1 independent manner. (A). Overexpressed HA-STIM1 (purple) was stained by anti-HA antibody in U2OS transfected cells. Microtubules (MTs, green) were labeled by an anti-α-tubulin antibody. Cells were treated with or without 0.5 µM Tg. Cells were analyzed by laser scanning confocal microscopy. The insets show 1.5-fold magnification of the

selected regions. (B). Colocalization of HA-STIM1-GFP or HA-STIM1ΔEB-1-GFP (purple) and MTs (green) in U2OS cells analyzed by TIRF microscopy. The insets show threefold magnification of the selected regions. Scale bar corresponds to 10 µm.

To track the microtubule-dependent movement of STIM1, I used U2OS cells expressing α-tubulin-GFP and performed live cell imaging. In cells overexpressing 15 to 20-fold HA-STIM1-mCherry compared to endogenous STIM1, several mobile foci were observed. These foci moved toward the plus end of microtubules. Interestingly, I found that overexpressed HA-STIM1-mCherry not just performed comet-like movement as described for EB-1-dependent mobility. HA-STIM1-mCherry was also sliding along microtubules (Fig 17A). The velocity of this sliding event was 0.33 µm/sec and is about 7.5-fold faster than microtubule tip attachment complex (TAC) dynamics (0.044 µm ± 0.018 µm/sec, (Friedman et al, 2010)). These results suggest another mechanism than TAC dynamics for the movement of STIM1.

To see whether this sliding event is independent of the EB-1 binding motif, I constructed a STIM1 mutant with a disrupted EB-1 binding motif by changing the sequence TxIP to AxNP (HA-STIM1ΔEB-1-GFP) (Honnappa et al, 2009). I performed an immunostaining of α-tubulin in U2OS cells expressing HA-STIM1-GFP or HA-STIM1ΔEB-1-GFP. Using TIRF microscopy, I observed that HA-STIM1-GFP aligned along cortical microtubules (Fig 16B arrowheads) and that HA-STIM1ΔEB-1-GFP also colocalized with cortical microtubules (Fig 16C arrowheads). Moreover, similar to HA-STIM1-mCherry, overexpressed HA-STIM1ΔEB-1-mCherry slides along microtubules with a velocity of 0.374 µm/sec.

These data suggest that STIM1 can bind to microtubules in an EB-1 independent manner and can move by other mechanism along microtubules.

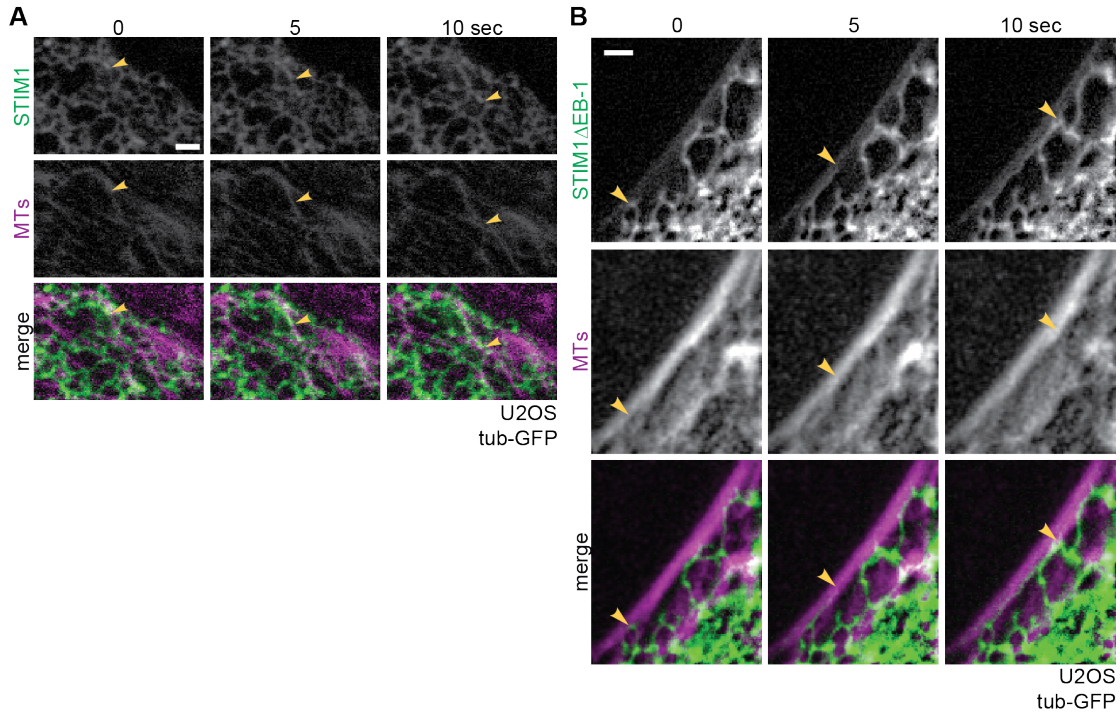

Figure 17. STIM1 slides along microtubules in an EB-1 independent manner. U2OS tub-GFP cells were transfected with HA-STIM1-mCherry (A) or HA-STIM1ΔEB-1-mCherry (B). Live cells were analyzed by using fluorescence microscopy. Movements of STIM1 and STIM1ΔEB-1 (green) along microtubules (MTs, purple) are indicated with yellow arrowheads. Scale bar corresponds to 2 µm.

4.3.2 Alignment of STIM1 with microtubules is a conserved process

Up to now, no sliding movement of STIM proteins along microtubules was described. To test whether this novel EB-1 independent interaction between STIM1 and microtubules is conserved in metazoans, I investigated an ancestral STIM from *Monosiga brevicollis*. *M. brevicollis* belongs to the species of choanoflagellates, which is placed among unicellular common ancestors of animals (Cai, 2008). Based on molecular phylogenic studies, *M. brevicollis* provides the first evidence that SOCE could operate in a unicellular organism (Cai, 2008). The C-terminus of *Monosiga* STIM (mSTIMC) consists of a conserved coiled-coil domain, which plays a role in its self-oligomerization (Soboloff et al, 2012). mSTIMC also contains a conserved STIM1-Orai1 activating region (SOAR) domain (Yuan et al, 2009), where STIM1 interacts and activates Orai1 (Soboloff et al, 2012). Besides these two domains, mSTIMC has two consensus di-arginine ER retention signals but lacks an EB-1 binding motif (Fig 18A). To analyze if mSTIM1 can bind to microtubules, I used a chimeric STIM1 protein consisting of the human STIM1 N-terminus and transmembrane domain and the *Monosiga* STIM C-terminus (HA-hSTIM1N-mSTIMC) and expressed it in U2OS cells.

Similar to HA-STIM1, HA-hSTIM1N-mSTIMC colocalized with microtubules at resting state (Fig 18B, -Tg). After treating the cells with Tg, strong microtubule binding and bundle formation was observed (Fig 18B, +Tg). In contrast, HA-STIM1 formed patch-like domains upon Tg treatment (Fig 16A, +Tg).

Like STIM1, *Monosiga* STIM (mSTIM) is able to bind to microtubules even though it lacks the EB-1 binding motif. Oligomerization of STIMs by Tg treatment usually leads to translocation of STIMs. In contrast, oligomerization of mSTIM increased microtubule binding and led to the observed bundle forming phenotype. This observation led to the hypothesis that there is a balance between lipid and microtubule binding. Oligomeric mSTIM formed bundle phenotype instead of patch-like domain may be a consequence of low affinity towards lipids in the PM. Indeed, compared to GFP-tagged STIM1 C-terminus, GFP-tagged *Monosiga* STIM C-terminus showed 10-fold lower binding to 5mol% $PI(4,5)P_2$-containing PM-like liposomes (Rajesh, 2013). However, the bundle forming phenotype was not rescued when expressing HA-hSTIM1N-mSTIMC fused to the K-rich domain of STIM2 (HA-hSTIM1N-mSTIMC-K_{STIM2}) (Fig 18C, +Tg). The inability of HA-hSTIM1N-mSTIMC-$_{KSTIM2}$ to bind to $PI(4,5)P_2$ and to form patches might be due to more complicated mechanisms regulating lipid and microtubule binding in HA-hSTIM1N-mSTIMC.

In conclusion, binding of STIM along microtubules is a conserved mechanism achieved by an EB-1 independent binding domain and regulated by oligomerization.

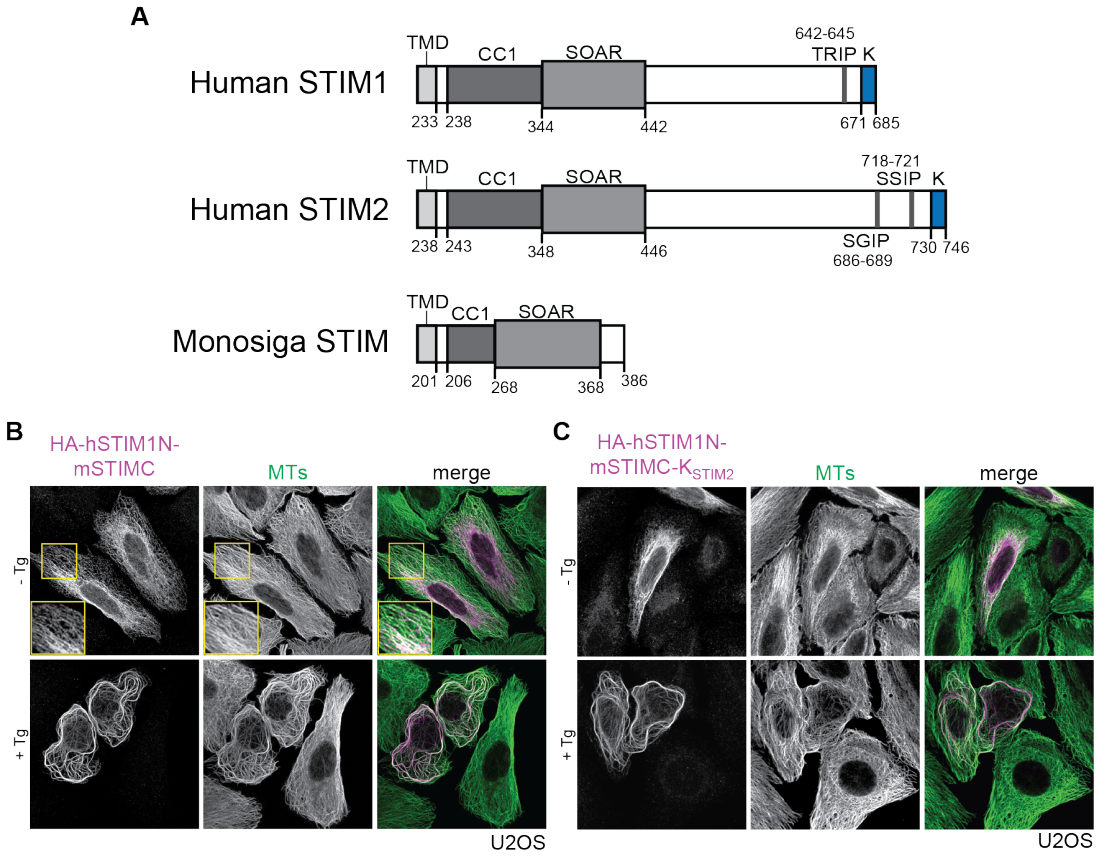

Figure 18. STIM1 binding along microtubules is a conserved mechanism. (A). Cartoon shows the C-terminal domains of human STIM1, STIM2 and *Monosiga* STIM. (B and C). Overexpressed HA-hSTIM1N-mSTIMC (purple, B) or HA-hSTIM1N-mSTIMC-K_{STIM2} (purple, C) were stained by an anti-HA antibody in U2OS transfected cells. Microtubules (MTs, green) were labeled by anti-α-tubulin antibody. Cells were treated with or without 0.5 μM Tg and analyzed by laser scanning confocal microscopy. The insets show 1.5-fold magnification of the selected regions.

4.3.3 STIM1 associates with microtubules in an EB-1 independent manner *in vitro*

STIMs colocalized with microtubules independently of the EB-1 binding motif *in vivo*. However, this colocalization did not provide a direct evidence for a true EB-1 independent microtubule binding. To examine that the observed colocalization between STIMs and microtubules is indeed a result of STIM binding to microtubules, I performed an *in vitro* microtubule cosedimentation assay(Barenz et al, 2013) (Fig 19A). In this experiment, binding of proteins to interphase microtubules from *Xenopus* egg extracts in presence of taxol or nocodazole was analyzed by western blot. The experiment was further used to map the putative EB-1 independent microtubule-binding site in STIM1. Therefore, I analyzed the interaction between microtubules and recombinant truncated STIM1 proteins.

Firstly, I tested if STIM proteins are indeed binding to microtubules. For this purpose, GFP-hSTIM1C, GFP-mSTIMC and EB-1-GFP expressed and purified from *E. coli* were incubated with microtubules as described before. All three proteins showed similar binding to taxol-stabilized microtubules (Fig 19B, E and F) whereas the negative control GFP alone did not bind (Fig 19C). The depolymerization of microtubules by nocodazole abolished the binding of GFP-hSTIM1C, GFP-mSTIMC and EB-1-GFP (Fig 19B, E and F). To analyze if this binding can be also observed in absence of the EB-1 binding motif, I performed the same experiment with GFP-hSTIM1C$_{\Delta EB-1}$. As shown in Fig 19G, GFP-hSTIM1C$_{\Delta EB-1}$ can interact with microtubules *in vitro*.

Next, in order to locate the EB-1 independent microtubule-binding site(s) of STIM1, I tested several recombinant GFP-tagged truncation mutants of hSTIM1C (Fig 19D) for their microtubule binding ability. GFP-hSTIM1C$_{233-554}$ showed similar affinity to microtubules (pellet/input = 1.91) as GFP-hSTIM1C$_{\Delta EB-1}$ (pellet/input = 2.12) (Fig 19G and H). In contrast to this, the post-SOAR segment of the protein with an EB-1 binding mutation (GFP-hSTIM1C$_{451-670, \Delta EB-1}$) did not bind to microtubules (Fig 19I). Besides GFP-hSTIM1C$_{451-670, \Delta EB-1}$, GFP-hSTIM1C$_{233-322}$ also failed to bind to microtubules (Fig 19K). Compared to GFP-hSTIM1C$_{233-554}$, GFP-hSTIM1C$_{233-390}$ had a significantly reduced binding affinity to microtubules (pellet/input = 0.31)

Taken together, the extreme C terminus of STIM1 downstream the SOAR is not required for the EB-1 independent microtubule binding (Fig 19H and I). Further truncation including the deletion of CC2 and last 22 residues of CC1 led to a much weaker binding to microtubules (pellet/input = 0.01) (Fig 19K). These results suggest the presence of multiple EB-1 independent microtubule binding sites in the coiled coil region of STIM1 (Fig 19H, J and K). One of these binding motifs could be located between residues 323 and 390 (Fig 19J and K). Beside this, further truncation in the coiled-coil domain interferes with higher oligomer formation. This might lead to weaker microtubule binding ability of GFP-hSTIM1C$_{233-322}$. Seen together, the EB-1 independent microtubule binding ability may be regulated by oligomerization.

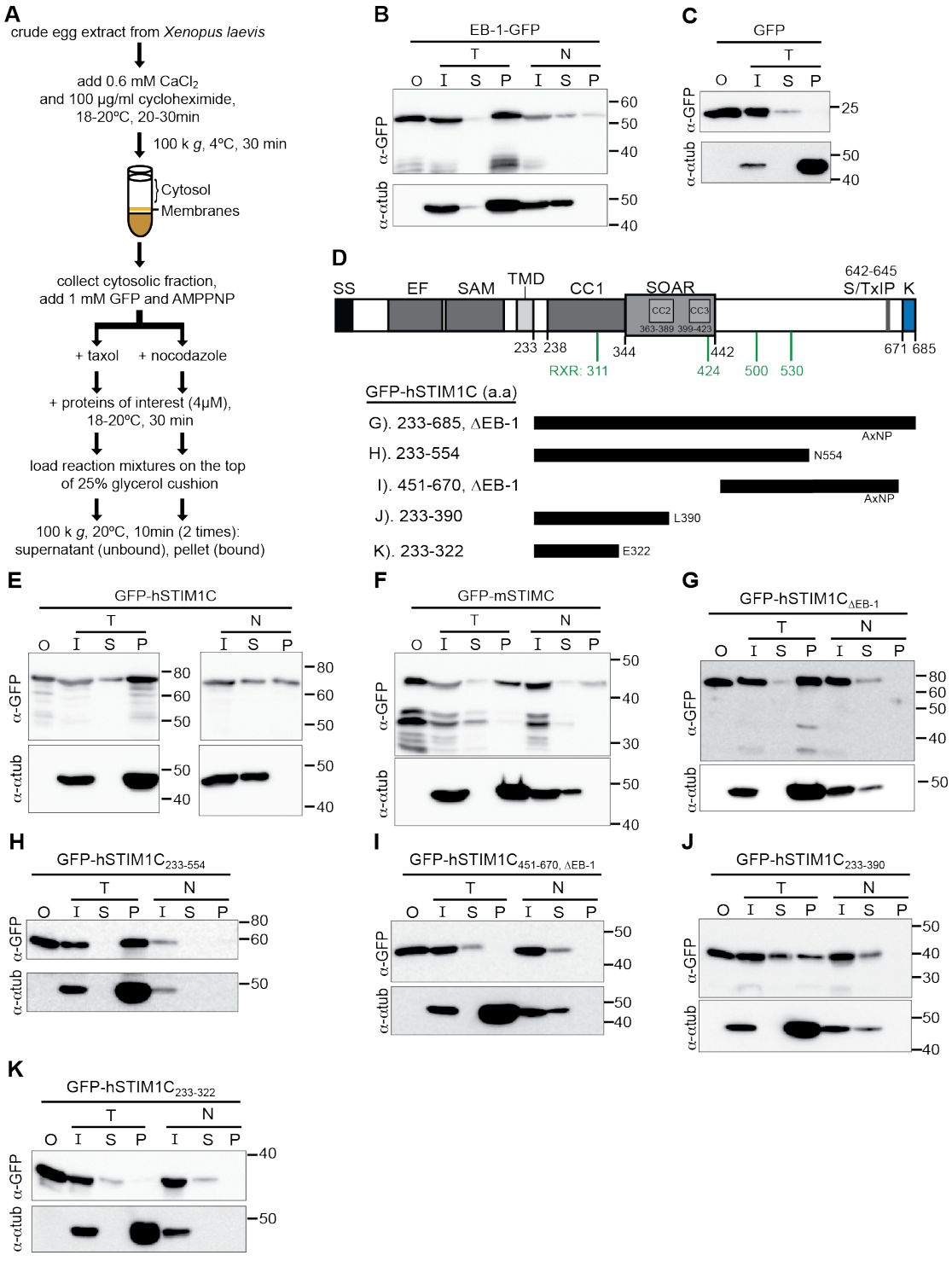

Figure 19. STIM1 associates with microtubules in an EB-1 binding motif independent manner *in vitro*. (A). Flowchart of *in vitro* microtubule cosedimentation assay. (B and C). *In vitro* microtubule cosedimentation assay with the indicated GFP-tagged EB-1 (B) and GFP (C). (D). Scheme of STIM1 subdomains and the GFP-tagged deletion mutants. (E- K). *In vitro* microtubule cosedimentation assay with the indicated GFP-tagged C-termini of human STIM1 (C, G- L) and *Monosiga* STIM (F). (L). *In*

vitro microtubule cosedimentation assay with GFP-hSTIM1$_{\Delta EB\text{-}1}$ in AMPPNP or ATP containing conditions. Taxol (T) and nocodazole (N) were added to samples as indicated. GFP-tagged proteins and microtubules were detected using GFP- and α-tubulin specific antibodies. Abbreviation: SS, signal sequence; EF, EF hand; SAM, sterile α motif domain; TMD, transmembrane domain; CC1, coiled-coil 1; SOAR, STIM1-Orai1 activating region; S/TxIP, EB-1 binding motif; K, K-rich domain; RXR, di-arginine signal; O, purified protein; I, input; S, supernatant; P, pellet.

4.3.4 Oligomerization increases the EB-1 independent microtubule-binding affinity of STIM1

In transfected U2OS cells, oligomerization of hSTIM1N-mSTIMC after Tg treatment led to strong microtubule binding (Fig 18B, +Tg). According to this result, I hypothesize that oligomerization regulates the affinity of the EB-1 independent binding domain(s) of STIM1 towards microtubules.

In order to test the correlation between assembly state and microtubule binding ability of STIM1, I performed size-exclusion chromatography followed by *in vitro* microtubule cosedimentation assay. Rajesh Bhardwaj showed that recombinant GFP-mSTIMC ran as a monomer and a dimer on a S200 gel filtration column whereas GFP-hSTIM1C ran as a tetramer (Bhardwaj et al, 2013; Rajesh, 2013). *In vitro* microtubule cosedimentation assay revealed higher microtubule binding abilities for GFP-hSTIM1C (pellet/input = 1.86) compared to GFP-mSTIMC (pellet/input = 1.05) (Fig 19E and F). In order to investigate if EB-1 independent microtubule binding of STIM1 depends on the oligomerization state of the protein, I analyzed the correlation between microtubule binding ability and the assembly states of GFP-tagged truncated hSTIM1C proteins. Gel filtration of the purified proteins showed that GFP-hSTIM1C$_{233\text{-}554}$ formed tetramers (Fig 20B), whereas GFP-hSTIM1C$_{233\text{-}390}$ and GFP-hSTIM1C$_{233\text{-}322}$ ran as monomers (Fig 20C and 21B).

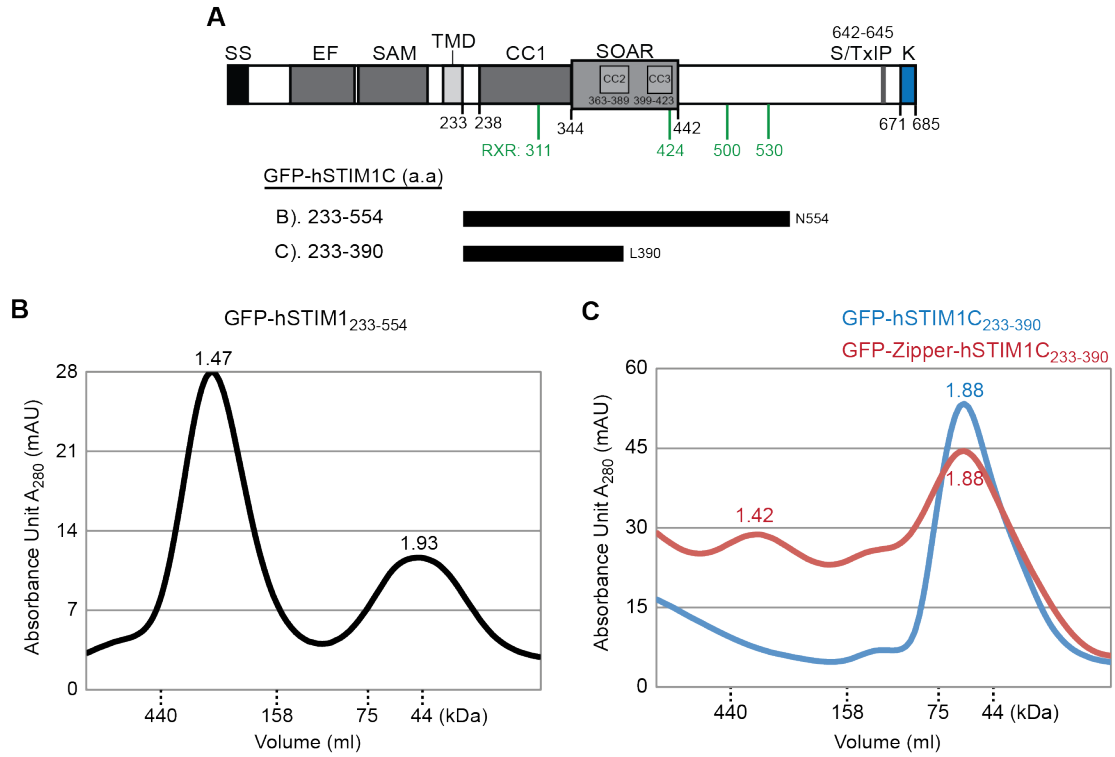

Figure 20. Deletion of the C-terminal domain affects the oligomerization of STIM1. Gel filtration chromatography of purified GFP-hSTIM1C$_{233-554}$ (A), GFP -hSTIM1C$_{233-390}$ (B, blue) and GFP-Zipper-hSTIM1C$_{233-390}$ (B, red) using a superdex 200 column. Marker (kDa) and protein elution volumes are indicated.

To see if microtubule binding abilities of GFP-hSTIM1C$_{233-390}$ and GFP-hSTIM1C$_{233-322}$ increase upon oligomerization, a leucine zipper from the yeast transcriptional factor Gcn4 was introduced between the GFP and STIM1C$_{233-322}$ or STIM1C$_{233-390}$, respectively to induce higher oligomer formation. GFP-Zipper-hSTIM1C$_{233-390}$ formed dimers (Fig 20C) but was too unstable to be used for further *in vitro* microtubule cosedimentation assays. In contrast, GFP-Zipper-hSTIM1C$_{233-322}$ formed decamers in solution (Fig 21B). The zipper-mediated oligomerization increased the binding of GFP-hSTIM1C$_{233-322}$ (pellet/input = 0.42) compared to GFP-hSTIM1C$_{233-322}$ (pellet/input = 0.01) to taxol-stabilized microtubules significantly (Fig 21C). GFP-Zipper alone did not show any binding to microtubules (Fig 21D).

In conclusion, I identified two regions within the C terminus of STIM1, residues 233-322 and 323-390, which bind microtubules. The binding affinity is regulated by the assembly state of the proteins. EB1-independent microtubule binding is increased by oligomerization of STIMs. These observations are consistent to the bundle phenotype of hSTIM1N-mSTIMC induced by Tg *in vivo*.

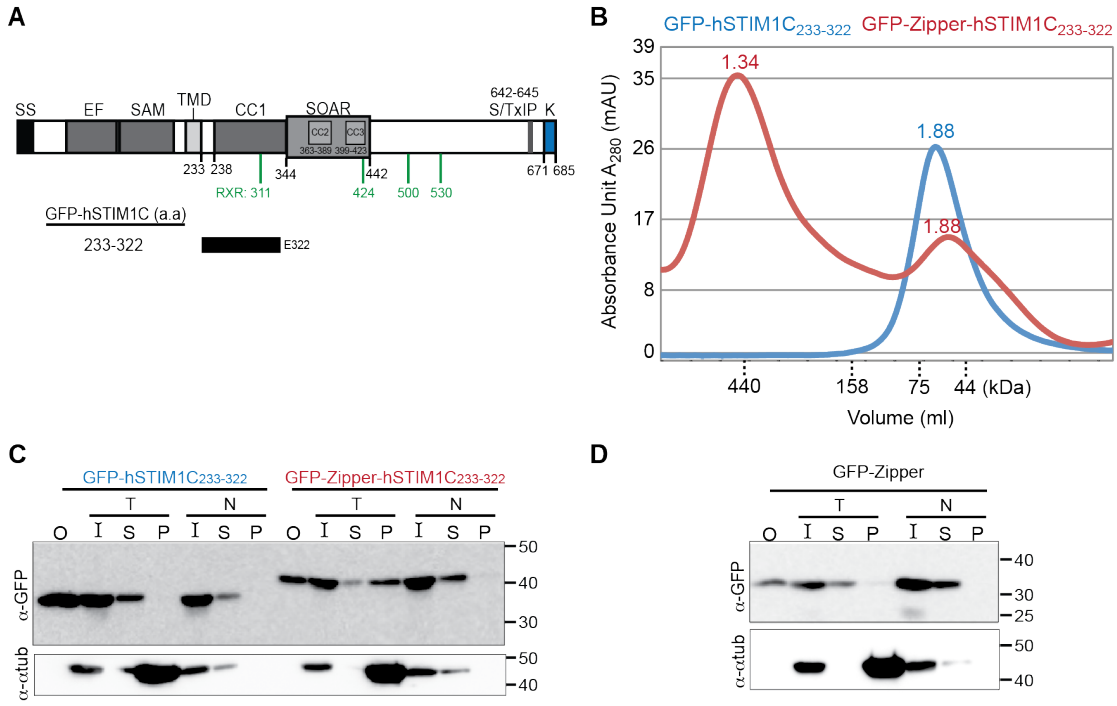

Figure 21. Oligomerization of a STIM1 domain from amino acid 233-322 mediates its microtubules association. (A). Gel filtration chromatography of purified GFP-hSTIM1C$_{233-322}$ (blue) and GFP-Zipper-hSTIM1C$_{233-322}$ (red) using superdex 200 column. Marker (kDa) and protein elution volumes are indicated. (B and C). *In vitro* microtubule cosedimentation assay with the GFP-hSTIM1C$_{233-322}$, GFP-hSTIM1C$_{233-322}$-Zipper-hSTIM1C$_{233-322}$ (B) and GFP fused with lucine-zipper (C). Taxol (T) and nocodazole (N) were added to samples as indicated. GFP-tagged proteins and microtubules were detected using GFP- and α-tubulin specific antibodies. Abbreviation: O, purified protein; I, input; S, supernatant; P, pellet.

4.3.5 Physiological function of EB-1 independent microtubule binding domains in STIM1

Next, I analyzed the physiological relevance of the EB-1 independent microtubule binding domains in STIM1. Binding to microtubules via EB-1 independent microtubule binding domains could facilitate STIM translocation from general ER to ER-PM contact sites. This might be important for the *Monosiga* STIM moving toward periphery of the cells since it has no EB-1 binding motif. Alternatively, STIM1-containing cortical ER could be stabilized and maintained in SOCE via binding to cortical microtubules. This hypothesis is further supported by several observations. Jozsef et al. suggest that STIM1 functions in SOCE mainly in tubular ER (Jozsef et al, 2014). In HeLa cells, the cortical ER is often found aligned along microtubules by electron microscopy (EM) (Orci et al, 2009). Disruption of

microtubules by nocodazole results in loss of tubular ER. This causes decrease and delay in Ca^{2+} influx during SOCE (Jozsef et al, 2014; Smyth et al, 2007). Thus, microtubules could play a role in maintaining the structure of cortical ER, where SOCE takes place.

To analyze if the EB-1 independent binding of STIM1 to microtubules is important for the translocation of the protein or rather contribute to tubular ER stabilization, I next monitored the mobility of STIM1 and STIM1ΔEB-1 in presence of Tg. Tg treatment leads to oligomerization and to fast translocation of STIM1 to ER-PM contact sites. The speed of this process makes it hard to dissect the single events. In order to prevent STIM1 interaction with the PM and to keep it associated to microtubules, I used mutants lacking the K-rich domain. In this way, it was possible to examine the events shortly before PM binding by TIRF microscopy in more detail.

First, I performed an immunostaining of α-tubulin in U2OS cells expressing HA-STIM1ΔK-GFP or HA-STIM1ΔEB-1ΔK-GFP treated with or without Tg. Interestingly, at resting state overexpressed HA-STIM1ΔEB-1ΔK-GFP aligned along microtubules in cortical regions similar as overexpressed HA-STIM1ΔK-GFP (Fig 22A and B, -Tg, arrowheads). Tg addition did not further increase the microtubule binding ability of HA-STIM1ΔK-GFP and/or HA-STIM1ΔEB-1ΔK-GFP (Fig 22A and B, +Tg, arrowheads). In contrast, in U2OS cells with CD3δ-GFP and endogenous STIM1 just a minor part of the tubular ER aligned along microtubules (Fig 22C). Moreover, the truncated STIM1 mutant with the minimum length used to investigate microtubule binding (Fig 19J and 21C) (HA-$STIM1_{390}$-GFP), colocalized with microtubules in the periphery of U2OS cells and was analyzed by confocal microscopy (Fig 22D). In a previous experiment, I showed that HA-STIM1-mCherry and HA-STIM1ΔEB-1-mCherry move along microtubules with similar velocities (Fig 17). After adding Tg, the movement of HA-STIM1ΔK-mCherry and HA-STIM1ΔEB-1ΔK-mCherry in live cell imaging, again shown similar velocities.

In summary, STIM1 can reach peripheral regions of the ER and colocalize with microtubules in cortical areas in an EB-1 independent manner. Binding to EB-1 seems not to be important for STIM1 translocation to the cell periphery, since deletion of the EB-1 binding motif had no effect on the velocity of STIM1 translocation. Furthermore the EB-1 independent microtubule binding ability of STIM1 may play a role in stabilizing cortical ER by aligning cortical microtubules.

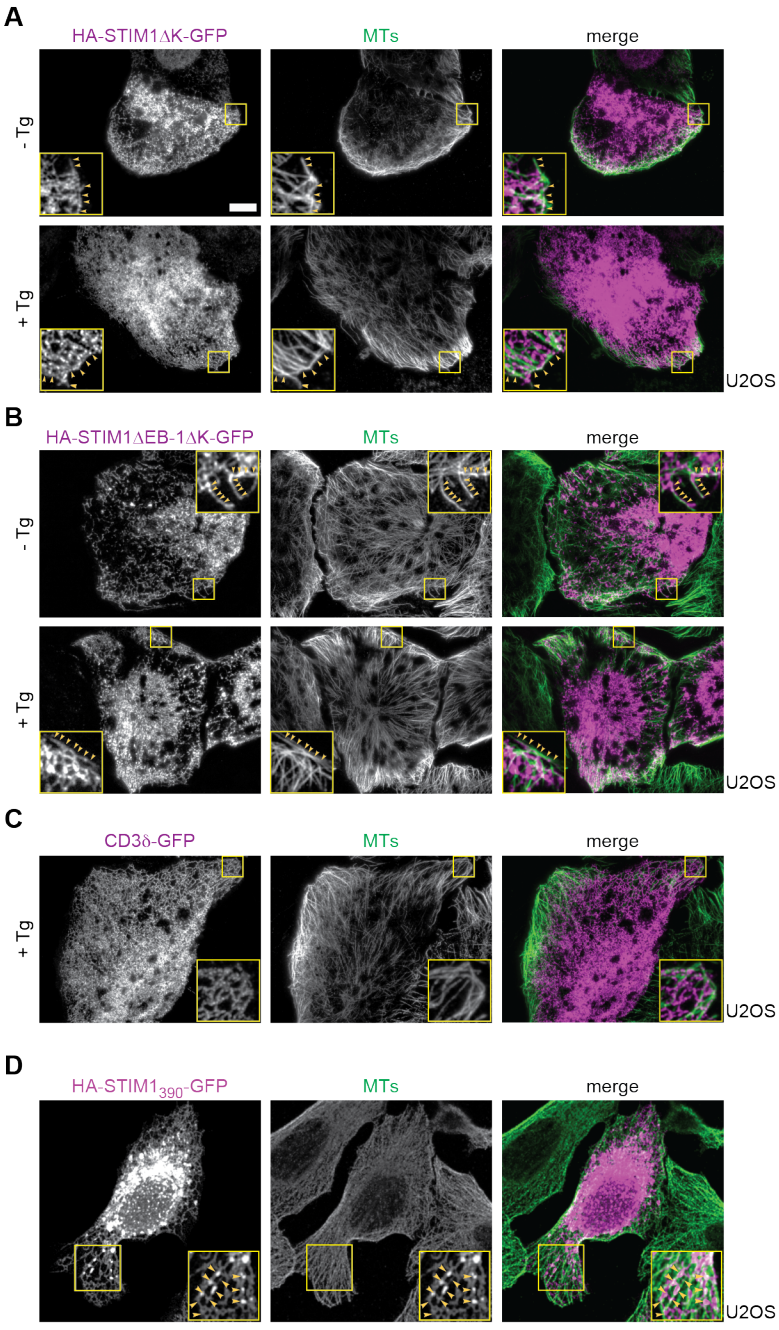

Figure 22. The ΔEB-1 mutants of STIM1 associate with cortical microtubules. (A- C). Colocalization of HA-STIM1ΔK-GFP (A) or HA-STIM1ΔEB-1ΔK-GFP (B) or CD3δ-GFP (C) (purple) and microtubules (MTs, green) in U2OS cells analyzed by TIRF microscopy. Cells were treated with or without 1 µM Tg. The insets show threefold magnification of the selected regions. The scale bar corresponds to 10 µm. (D). Colocalization of HA-STIM1$_{390}$-GFP (purple) and MTs in U2OS cells analyzed by laser scanning confocal microscopy. The insets show 1.5-fold magnification of the selected regions. MTs (green) were labeled by an anti-α-tubulin antibody.

5. Discussion

5.1 Retention of STIM1 in the ER via di-arginine retention signal is a conserved mechanism.

In order to function as ER Ca^{2+} sensor in SOCE, STIM proteins are to be retained in the ER. Two homologues of STIM proteins namely STIM1 and STIM2 exist in all vertebrates, which appeared after gene duplication in fish (Cai, 2007; Collins & Meyer, 2011; Rajesh, 2013). STIM1 primarily localizes to the ER but a small fraction of STIM1 pool has also been reported on the cell surface (Manji et al, 2000; Oritani & Kincade, 1996). STIM2 however is restricted to the ER via a conserved di-lysine (K(X)KXX) retention signal at the end of the K-rich domain. Sequence alignment analysis suggests that these di-lysine retention signals appear in STIM2 through out vertebrate evolution, whereas all vertebral STIM1 proteins lack this K(X)KXX signal (Rajesh, 2013) raising the question how STIM1 is retained in the ER. I showed that the localization of STIM1 is regulated in a cell-cycle-dependent manner and STIM1 travels to the cell surface during mitosis. However, in interphase the majority of STIM1 is retained in the ER by the synergistic function of a di-arginine (RXR) signal and the K-rich domain.

I identified four consensus di-arginine (RXR) ER retention sequences in the cytosolic C-terminal domain of STIM1 which are located in the first coiled-coil domain (RSR 311-313), in the SOAR (RER 424-426), and downstream of SOAR (RQR 500-502 and RQR 530-532) (Ercan et al, 2012). The RXR signals were also identified in STIM2 (Rajesh, 2013), in addition to the K(X)KXX ER-retention signal. The C-terminus of STIM2 harbors three conserved motifs. The first one locates in the coiled-coil domain (RLR 303-305), second in the SOAR (RER 428-430) and third one resides downstream of SOAR (RSR 514-516) (Ercan et al, 2012). These sites were found in STIM1 and STIM2 of most vertebrates and in most of the ancestral STIMs before duplication (Rajesh, 2013). Also, RXR sites are found in pre-metazoan STIMs such as RQR 347-349 and RRR 380-382 in *Monosiga brevicollis* STIM (Rajesh, 2013), suggesting that the retention of STIMs in the ER via RXR signals is a conserved mechanism.

I found that the RXR signal in STIM1 at amino acid 500-502 functions as efficient ER retention signal. The other three RXR consensus sites have only minor effect in STIM1 retention. This may be a consequence of their position within the C-terminus of STIM1. RSR 311-313 locates in the first coiled-coil domain might be embedded in the folded structure of dimeric STIM1 at resting state, based on the crystal structure of *C. elegans* STIM1

(Covington et al, 2010; Yang et al, 2012; Zhou et al, 2013). Due to a potential masking effect, RSR 311-314 might not be accessible for the COPI machinery, which mediates the retention of ER proteins (Michelsen et al, 2005; Soboloff et al, 2012). The most efficient retention signal, RQR 500-502 locates downstream of the coiled-coil domains and within a C-terminal flexible region (Soboloff et al, 2012). Therefore, conformational changes after multimerization of STIM1 via coiled-coil domains will not mask this retention signal and thus not affect interaction with the classic coat protein complex I (COPI) machinery (Soboloff et al, 2012; Zhou et al, 2013).

It has been shown that the RXR retention signal usually is impaired when surrounded by negatively charged or small, non-polar side chains (Michelsen et al, 2005). RQR 530-532 is surrounded by either acidic or non-polar amino acids, which may affect the efficiency of retention. I didn't investigate the RER 424-426 signal since RER has been reported as inactive retention signal (Zerangue et al, 2001).

It is not clear why there are four consensus RXR sites in STIM1 but only one of them functions in retention? STIM2 evolved a functional K(X)KXX ER-retention signal but maintained RXR sites arguing alternative functions of RXR signals beyond ER retention. RXR signals are known to bind to COPI (Yuan et al, 2003), and COPI has been suggested to play a role in the formation of cortical ER (Lavieu et al, 2010). Yeast Ist2 permanently localizes to the cortical ER in yeast (Ercan et al, 2009; Manford et al, 2012; Wolf et al, 2012) and contains COPI-binding KKXX signal in its K-rich domain (Lavieu et al, 2010). Expression of dimeric Ist2 in mammalian cells induces cortical ER formation triggered by its binding to COPI (Lavieu et al, 2010; Orci et al, 1994; Orci et al, 2009). Based on these findings, I suggest that RXR sites in STIM2 might associate with COPI resulting in the formation of cortical ER where ER-PM contacts and SOCE takes place (Orci et al, 2009; Shen et al, 2011).

Up to now, it is not clear why STIM2 is restricted to the ER. According to previous finding, it has been suggested that STIM2 functions as a basal regulator in Ca^{2+} homeostasis (Brandman et al, 2007). The EF-hand of STIM2 is more sensitive to Ca^{2+} drop than the one of STIM1 (Brandman et al, 2007), indicating that STIM2 is activated faster than STIM1 in SOCE. STIM2 K-rich domain has a higher lipid affinity towards PM-lipids than STIM1 K-rich domain (Bhardwaj et al, 2013; Ercan et al, 2009), indicating STIM2 can recruit ER to PM more efficient than STIM1. These observations indicate that STIM2 refills ER $Ca2^{+}$ store upon small changes rather than amplifying signals as STIM1 does (Brandman et al, 2007).

5.2 Regulation of trafficking of STIM1 from ER to PM.

STIM1 is retained in the ER by the action of the RXR retention signal at residues 500-502. In addition to this, I could show that the K-rich domain of STIM1 contributes to ER retention. Interaction of K-rich domain with phosphoinositides at the PM may explain the contribution of the K-rich domain to ER retention (Ercan et al, 2009; Liou et al, 2007; Park et al, 2009; Walsh et al, 2010). Binding of the K-rich domain to phosphoinositides may keep STIM1 in the ER-PM contact sites and avoid that STIM1 reaches the ER-exit sites. Tg treatment induces more interactions between STIM1 and $PI(4,5)P_2$, resulting in further reduction of STIM1 surface expression. This is consistent with the idea that constitutive activation of SOCE keeps STIM1 intracellular (Hewavitharana et al, 2008).

Apart from binding to $PI(4,5)P_2$ via the K-rich domain, STIM1 also interacts directly with the Ca^{2+} channel Orai1 at the PM. Co-overexpression of Orai1 kept STIM1 intracellular, suggesting that both proteins interact even under resting conditions when STIM1 is in the Ca^{2+}-bound state. This retention may be the consequence of STIM1 and Orai1 overexpression, which results in efficient ER-PM contact formation at resting state (Varnai et al, 2007). Conformational changes and oligomerization of STIM1 during SOCE activation enhances the interaction between STIM1 and Orai1 (Muik et al, 2008; Park et al, 2009; Soboloff et al, 2012) resulting in increased $[Ca^{2+}]_c$ and retention of STIM1 in the ER (Ercan et al, 2012). This is consistent with the fact that constitutively active STIM1 does not travel to cell surface (Hewavitharana et al, 2008).

Next, I asked whether the physical contact between STIM1 and Orai1 and/or increased $[Ca^{2+}]_c$ interfere with the surface localization of STIM1. Whether the $[Ca^{2+}]_c$ has a direct effect on the distribution of STIM1 remains open. Local $[Ca^{2+}]_c$ may regulate the interaction between the K-rich domain of STIM1 and lipids in the PM, which would influence the distribution of STIM1 (McLaughlin & Murray, 2005). In addition to $PI(4,5)P_2$, the K-rich domain of STIM1 can also bind to Ca^{2+}/CaM in presence of 1 mM $CaCl_2$, suggesting that fully-Ca^{2+} saturated CaM binds to K-rich domain of STIM1 at locally high $[Ca^{2+}]$ (Bauer et al, 2008; Bhardwaj et al, 2013). This binding to Ca^{2+}/CaM via its K-rich domain would allow STIM1 to sense changes in local $[Ca^{2+}]_c$ indirectly.

In addition to the K-rich domain, STIM1 contains at least two more Ca^{2+}/CaM binding sites (Ercan, 2011). Increased local $[Ca^{2+}]_c$ may trigger STIM1 binding to Ca^{2+}/CaM via its K-rich domain and/or other potential CaM-binding sites (Bauer et al, 2008; Bhardwaj et al, 2013), which may lead to conformational changes resulting in exposure of RXR retention signals or to interference with recruitment of STIM1 to ER exit sites. Other factors such as physical interaction between STIM1 and the cytosolic Ca^{2+} sensor CRACR2A, which

stabilizes CRAC channels in T cells, at ER-PM contact sites (Srikanth et al, 2010) and yet unknown components could regulate the trafficking and stability of STIM1 at the PM (Ercan et al, 2012). Surface expression of STIM1ΔK is reduced by Tg-induced SOCE and Ca^{2+} influx through Orai1, suggesting that signals outside of the K-rich domain and changes in STIM1 conformation at elevated Ca^{2+} (Korzeniowski et al, 2010; Muik et al, 2011) contribute to ER retention as well (Ercan et al, 2012).

5.3 Surface expression of STIM1 is regulated in a cell-cycle dependent manner

With a newly raised and sensitive antibody against the N-terminal domain of STIM1, I observed cell-to-cell variations of overexpressed HA-STIM1 and endogenous STIM1 surface distribution in non-synchronized cells, suggesting that the retention of STIM1 in the ER and expression at the surface are regulated processes. Besides this phenomenon, I also found that endogenous STIM1 accumulated at the cell surface in M-phase, suggesting that surface expression of STIM1 is regulated in a cell-cycle dependent manner.

Release of STIM1 from ER to PM might be one of the mechanisms to downregulate SOCE during M-phase (Preston et al, 1997; Preston et al, 1991; Smyth et al, 2009; Tani et al, 2007; Volpi & Berlin, 1988). Since endogenously generated Ca^{2+} signals are involved in the control of the cell cycle, such downregulation of SOCE during M-phase may ensure proper execution of the cell division program (Arredouani et al, 2010; Ercan et al, 2012; Whitaker, 2006). Alternatively, surface STIM1 may play an active role in Ca^{2+} homeostasis. Surface STIM1 has been reported to regulate Ca^{2+} entry via store-independent arachidonate-regulated heteromeric Orai1/Orai3 Ca^{2+} influx (ARC) channels (Mignen et al, 2007).

Phosphorylation of STIM1 during M-phase (Manji et al, 2000; Smyth et al, 2009) may inactivate the retention signals, namely RQR 500-502 and the K-rich domain, resulting in strong surface expression. It has been shown that S486 and S668 of STIM1 are phosphorylated during mitosis (Smyth et al, 2009) and these residues are located next to RQR 500-502 and the K-rich domain. Both phospho-mimicking mutants HA-STIM1 S486D and HA-STIM1 S668D showed an enhanced surface expression, suggesting that phosphorylation at residues S486 and/or S668 inactivate the RXR retention signal at residue 500-502 and/or the K-rich domain (residues 670-685). This hypothesis of phosphorylation dependent inactivation of ER retention signals is consistent with a previous model explaining NMDA receptor retention. Here the phosphorylation of nearby residues, which increase negative charge, results in the inactivation of the RXR retention signal in the NMDA receptor

subunit NR1-1 (Scott et al, 2001). However, the phosphorylation pattern of STIM1 is complex. Additional residues are phosphorylated during interphase and M-phase, whereas other residues are dephosphorylated during mitosis (Pozo-Guisado et al, 2010; Smyth et al, 2009). Therefore, the regulation of STIM1 retention by phosphorylation is still not fully understood.

In interphase, STIM1 associates with the tip of microtubules via binding to microtubule plus end binding protein 1 (EB-1) (Grigoriev et al, 2008; Honnappa et al, 2009; Smyth et al, 2012). Although STIM1-containing ER is often found to colocalize with microtubules (Orci et al, 2009), I could show that intact microtubules are not required for ER retention of STIM1 during interphase. In the experiment when microtubules are completely depolymerized by nocodazole, only small amounts of STIM1 escaped from the ER and the majority of STIM1 stayed in the ER, suggesting that the retention machinery of STIM1 are not interfered. Alternatively, transport of STIM1 from ER to the PM requires intact microtubules. Indeed, depolymerization of microtubules reduces surface expression of STIM1, suggesting that microtubules rather play a role in trafficking of STIM1 to the cell surface. Disruption of microtubules results in aberrant morphology of ER (Terasaki et al, 1986), which could affect the recruitment of STIM1 to ER exit sites where the proteins reach containers that leave the ER. Alternatively, depolymerization of microtubules may interfere with the transport of STIM1-containers along the classical secretary pathway in BFA-dependent manner to the PM. This situation changes in M-phase, where STIM1 accumulates at the surface under condition with rearranged microtubules. Thus, cell-cycle-dependent inactivation of ER retention signals allows trafficking of STIM1 to the cell surface (Ercan et al, 2012).

5.4 STIMs localize in preexisting ER-PM contact sites at resting state

So far, it was under debate whether STIM1 localizes in specific ER subdomains. In this study, I could show that at resting state STIM1 indeed localizes in ER subdomains, namely in preexisting ER-PM contact sites.

My studies mainly focus on STIM1 localization within the tubular ER networks. According to ultrastructural analysis, Orci et al. defined three structurally distinct subdomains in tubular ER namely precortical, cortical and thin cortical ER (Orci et al, 2009). Using TIRF microscopy, I could show that at resting state overexpressed STIM1 is enriched in several tubular ER domains and in some dot-like domains. Moreover, the luminal RFP-KDEL was excluded from these domains. Segregation of KDEL containing luminal protein from STIM1

in tubular ER supports the idea that STIM1 localizes in special subdomains of the tubular ER at resting state.

Due to the limited resolution of TIRF microscopy, I was not able to identify the distance between STIM1-containing tubular ER and the PM. However, using EM Orci et al. and Baba et al. showed that overexpressed YFP-STIM1 is enriched in specific subdomain of pre-cER (Baba et al, 2006; Orci et al, 2009), which is characterized by absence of luminal chaperone BiP and GFP-KDEL, which are excluded from these areas of STIM1 accumulation.

By live cell imaging, I observed that many of the observed STIM1 dot-like domains are immobile. Furthermore, upon Tg-induced SOCE activation, these foci were expanded resulting in patch-like domains that are typical for SOCE (Hogan et al, 2010; Orci et al, 2009; Shen et al, 2011). These observations suggest that STIM1-containing dot-like domains are preexisting ER-PM contact sites. Moreover, using live cell imaging I could show that 85% of ER-PM junctions induced by Tg were developed from these preexisting ER-PM contact sites. Accumulation of STIM1 at preexisting ER-PM contact sites is further supported by Chang et al (Chang et al, 2013). They found that overexpressed mCherry-STIM1 at resting state colocalized with the ER-PM junction marker MAPPER. In addition, Tg-induced ER-PM junctions mainly formed at preexisting MAPPER foci suggesting that ER-PM contact sites are formed at preexisting ER-PM contact sites and that only few ER-PM contact sites are formed *de novo* (Chang et al, 2013). This is consistent with my observation that only 15% of Tg-induced ER-PM contact sites were formed *de novo*. These findings suggest that STIM1 localizes in special structures of ER subdomains, called preexisting ER-PM contact sites. These preexisting ER-PM contact sites may be a special subcompartment of the ER specialized in Ca^{2+} homeostasis.

5.5 The K-rich domain of STIM1 is required for its clustering in PI(4,5)P_2 containing preexisting ER-PM contact sites

Binding of K-rich domains to PI(4,5)P_2 in the PM is required for accumulation of STIMs in preexisting ER-PM contact sites. Overexpressed STIM1 mutant lacking the lipid binding K-rich domain (STIM1ΔK) cannot locate in dot-like domains even upon strong overexpression, indicating that the K-rich domain is required for STIM1 localization in preexisting ER-PM contact sites. Requirement of lipid-binding domain for ER-PM contacts formation is consistent with previous reports about ER-PM junction formation in yeast and mammalian cells (Giordano et al, 2013; Manford et al, 2012). In yeast, Ist2 and tricalbin

proteins (Tcb1, Tcb2 and Tcb3) exclusively localize to cortical ER and tether ER to PM via their lipid binding domains (Fischer et al, 2009; Manford et al, 2012; Toulmay & Prinz, 2012; Wolf et al, 2012). In mammals besides STIM proteins, extended synaptotagmins (E-Syt1, E-Syt2 and E-Syt3-orthologs of tricalbin proteins) (Lee & Hong, 2006) mediate ER-PM contacts formation. E-Syt2 and E-Syt3 localize to cortical ER and tether ER to PM via multiple C2 domains (Giordano et al, 2013; Min et al, 2007). E-Syt2 and E-Syt3-mediated ER-PM contact sites are functionally distinct from those mediated by STIM1 and Orai1 (Giordano et al, 2013).

To test if STIM1 can bind to $PI(4,5)P_2$ in the PM *in vivo*, I established a FRET-based quantification assay to quantify ER-PM contacts. After Tg treatment, fluorescence energy transfer occurred between STIM1-GFP and mCherry-PH, which specifically binds to $PI(4,5)P_2$ in the PM. The result indicates that STIM1 clusters in $PI(4,5)P_2$ containing ER-PM junctions *in vivo*. In contrast, no FRET signal was detected between STIM1ΔK-GFP and mCherry-PH under the same experimental conditions, demonstrating that the K-rich domain is required for STIM1 binding to $PI(4,5)P_2$. Furthermore, E-Syts knockdown does not affect SOCE, suggesting that STIM proteins mediate ER-PM contact formation in E-Syts independent manner (Giordano et al, 2013). Taken together, I verified that STIM1 localizes to preexisting ER-PM contact sites via the K-rich domain binding to $PI(4,5)P_2$ in the PM. The localization of proteins to preexisting ER-PM contact sites via $PI(4,5)P_2$ binding is a conserved and common mechanism.

Previous *in vitro* liposome binding experiments also demonstrated that the K-rich domain of STIM2 has higher lipid binding affinity than that of STIM1 (Bhardwaj et al, 2013; Ercan et al, 2009). At resting state, STIM2 localized completely in dot-like domains. With a FRET-based quantification of ER-PM contacts at resting state, I verified that overexpressed STIM2 accumulates in ER-PM junctions. A STIM1 mutant, in which the K-rich domain was replaced by the K-rich domain of STIM2 (STIM1ΔK-K_{STIM2}) displayed a similar localization pattern as STIM2. Moreover, STIM2ΔK-K_{STIM1} showed similar reticular localization and some dot-like domains comparable to STIM1 localization. These data indicate that the localization of STIMs in preexisting ER-PM contact sites is regulated by their lipid binding affinities. In agreement with *in vitro* data (Bhardwaj et al, 2013; Ercan et al, 2009), I showed that *in vivo* STIM2 K-rich domain recruits ER to PM more efficiently than STIM1. R. Bhardwaj showed that STIM2 has coevolved an overlapping phosphoinositide and Ca^{2+}/CaM-binding site in its K-rich domain, suggesting a feedback regulation of STIM2-dependent lipid-mediated ER-PM contact formation by cytosolic Ca^{2+}/CaM (Bhardwaj et al, 2013; Rajesh, 2013). The binding of Ca^{2+}/CaM to K-rich domains at elevated cytosolic Ca^{2+} concentration downregulates the

interaction of STIMs with PM lipids (Bhardwaj et al, 2013). This data suggests that cytosolic Ca^{2+} concentration is involved in regulation of ER-PM contacts. In addition, it has been shown that E-Syt1 localizes in general ER but is recruited to cortical ER upon association with Ca^{2+} under elevated $[Ca^{2+}]_c$ (Giordano et al, 2013). Whether tethering of ER to PM by STIMs is regulated by local $[Ca^{2+}]_c$ concentration *in vivo* remains open. To test this hypothesis, an assay that can quantify ER-PM contact formation and dissociation in live cell imaging is required.

5.6 STIM1-mediated preexisting ER-PM contact sites transform to large ER-PM contacts during SOCE

During SOCE activation, STIM1 forms high-order oligomers and these oligomers accumulate at ER-PM junctions, where they activate Orai1 ((Muik et al, 2008; Park et al, 2009; Soboloff et al, 2012; Xu et al, 2006; Yuan et al, 2009); refer Fig 1-11). The mechanism by which STIM1 translocates to ER-PM contact sites is still under debate. One model suggests that STIM1 localizes in the general ER, where it forms higher order oligomers in response to ER Ca^{2+} depletion. STIM1-oligomers diffuse along ER and bind to $PI(4,5)P_2$ in the PM forming *de novo* ER-PM contact sites. However, I showed that only 15% of all Tg-induced ER-PM contact sites were formed *de novo*. Moreover, oligomerization of STIM1 reduces its mobility in the ER (Grigoriev et al, 2008; Liou et al, 2007), which would delay ER-PM contacts formation and SOCE. In addition, high-order STIM1 oligomers have higher affinity towards PM lipids than low-order oligomers (Bhardwaj et al, 2013). If oligomerization of STIM1 occurs in general ER, how could high-order STIM1 oligomers bind specifically to PM lipids? Taken together, this model does not fit to the fact that STIM1-mediated ER-PM contact formation is a specific and efficient process upon SOCE activation. Therefore, these arguments together with the data from this study suggest a second model.

At resting state, STIM1 forms low-order oligomers such as dimers which localize in preexisting ER-PM contact sites (Baba et al, 2006; Covington et al, 2010; Soboloff et al, 2012). Dimeric STIM1, which has low lipid-binding affinity and specificity (Bhardwaj et al, 2013), travels constantly from general ER to preexisting ER-PM contact sites via binding to EB-1 positive microtubule ends (Grigoriev et al, 2008). Ca^{2+} depletion causes conformational change in STIM1 resulting in accumulation of high-order STIM1 oligomers at the preexisting ER-PM contact sites (Wu, 2006). These high-order STIM1 oligomers have higher lipid binding affinities than low-order oligomers (Bhardwaj et al, 2013). Thus, these preexisting ER-PM contact sites are expanded resulting in larger ER-PM contact sites formation, where

Orai1 is recruited and activated ((Muik et al, 2008; Park et al, 2009; Soboloff et al, 2012; Xu et al, 2006; Yuan et al, 2009); refer Fig 1-11). The second model is further supported by the observation that the STIM1-mediated ER-PM contact formed repeatedly at the same location upon repetitive stimulation (Malli et al, 2008; Smyth et al, 2008), suggesting that ER-PM contact sites are pre-determined. Localization of preexisting ER-PM contact sites allows STIM1 to mediate efficient, specific and local ER-PM contact formation during SOCE activation.

5.7 The role of microtubules in ER-PM contact site formation

ER structure and mobility in animal cells depend mainly on microtubules (Bola & Allan, 2009; Terasaki et al, 1986). The diffusion of STIM1 in the ER is relatively slow compared to other ER proteins, which may be linked to the large size of the cytosolic domain or to the association with other cytosolic proteins like microtubules (Covington et al, 2010; Liou et al, 2007; Lippincott-Schwartz et al, 2000). In addition, STIM1 often appears to localize not only to the ER but also to microtubule-like structures (Ercan et al, 2012; Liou et al, 2007; Smyth et al, 2007). Therefore, I asked whether microtubules contribute to the formation of STIM1-mediated ER-PM contact sites. I focused on how newly synthesized STIM1 reaches preexisting ER-PM contact sites in the periphery of the ER network. Low-order STIM1 oligomers could diffuse in the tubular ER and get trapped in preexisting ER-PM contact sites via binding of K-rich domains to PM lipids.

Alternatively, in addition to diffusion and trapping mechanisms, transport along microtubules could assist the translocation of STIM1 from general ER to ER-PM contact sites. Up to now, only EB-1 dependent movement of STIM1 has been reported. EB-1 is a microtubule-plus-end-tracking protein, which binds to growing (plus) ends of microtubules (Akhmanova & Steinmetz, 2008; Kumar & Wittmann, 2012). STIM1 associates with EB-1 via its EB-1 binding motif (S/TxIP) resulting in comet-like movement towards the cell periphery (Grigoriev et al, 2008; Honnappa et al, 2009). However, EB-1 depletion and disruption of microtubule dynamics had no impact on ER-PM contacts formation and SOCE (Grigoriev et al, 2008), indicating that EB-1-dependent movement of STIM1 is not required for SOCE activation. However, depolymerization of microtubules impairs SOCE activation (Smyth et al, 2007), suggesting that intact microtubules and ER morphology are important for SOCE.

In addition to accumulation of STIM1 at microtubule plus ends, I observed that STIM1 aligned along microtubules. This alignment of STIM1 with microtubules was in EB-1 independent manner. By live cell imaging, I discovered that STIM1 performed EB-1-

dependent (comet-like) and EB-1-independent (sliding) movement. Friedman et al. showed that ER proteins can slide along acetylated microtubules (Friedman et al, 2010), where the majority of mitochondria localize. These observations support the idea that ER sliding on acetylated microtubules may establish and/or maintain the integrity of ER-mitochondria contacts (Friedman et al, 2010). It was not investigated whether STIM1 slides along acetylated microtubules. Therefore, it remains open whether this sliding movement is important for STIM1-mediated ER-PM contact formation.

The deletion of the EB-1 binding motif did not affect the velocity of STIM movement. The velocities of STIM1 and STIM1ΔEB-1 sliding movement are 0.33 µm/sec and 0.374 µm/sec respectively, which are much faster than microtubule tip attachment complex (TAC) dynamics (0.044 µm ± 0.018 µm/sec, (Friedman et al, 2010)). The measured velocities led to the assumption that STIM1 moves along microtubules in an alternative motor-dependent process. However, if a motor and/or which motor are involved in sliding movement of STIM1 still needs further investigation.

I established an *in vitro* microtubule cosedimentation assay based on (Barenz et al, 2013). Using this assay, I verified that the C-terminal domain of STIM1 and STIM1ΔEB-1 cosediment with microtubules, indicating that STIM1 associates with microtubules in an EB-1 independent manner *in vitro*. Furthermore, I identified two EB-1-independent microtubule-binding domains located within the C-terminus of STIM1 at residues 233-322 and 233-390. This finding is consistent with the idea that coiled-coil domain residues 247-344 may associate with microtubules resulting in slow diffusion of STIM1 within the ER (Covington et al, 2010). Moreover, I also demonstrated that oligomerization increases EB-1 independent microtubule-binding affinity of STIM1 *in vitro*, suggesting an avidity mechanism for STIM1 binding to microtubules. Compared to low order-oligomers of STIM1, high order-oligomers of STIM1 have a more extended structure (Soboloff et al, 2012), which may result in more exposure of EB-1 independent microtubule-binding domains thereby increase microtubule binding.

Upon SOCE activation, STIM1 forms high-order oligomers, which have enhanced microtubule and lipid-binding capacities (Bhardwaj et al, 2013), suggesting that there is a balance between these two binding activities. Ancestral *Monosiga* STIM (mSTIM) lacks the EB-1 binding motif and the K-rich domain but contains a conserved coiled-coil domain and SOAR (Cai, 2008; Rajesh, 2013). A chimeric STIM1 protein (HA-hSTIM1N-mSTIMC) showed increased microtubule binding ability when oligomerization of the protein was induced and led to strong association with microtubules and a bundle forming phenotype. This observation indicates that EB-1 independent microtubule binding of STIM1 is a

conserved mechanism. Such a phenotype has been described in COS7 cells expressing CLIMP63 mutant (CLIMP-$63_{S3A,S17A,S19A}$), which exhibits enhanced static interactions with microtubules (Vedrenne et al, 2005). mSTIM may be trapped to microtubules due to its weak lipid binding ability. However, the bundle forming phenotype was not rescued when expressing the lipid-binding domain of STIM2 fused to mSTIMC (HA-hSTIM1N-mSTIMC-$_{KSTIM2}$). The inability of HA-hSTIM1N-mSTIMC-$_{KSTIM2}$ to bind to PI(4,5)P_2 and to form patches might be due to more complicated mechanisms regulating lipid and microtubule binding in HA-hSTIM1N-mSTIMC.

Last, I analyzed the physiological function of EB-1 independent microtubule binding domains in STIM1. In muscle cells, a STIM1 isoform, STIM1L colocalizes with Orai1 and cortical actin to form permanent clusters allowing fast repetitive SOCE activation (Darbellay et al, 2011). Therefore, STIM1-containing cortical ER could be stabilized and maintained in SOCE via binding to microtubules at cortical region, called cortical microtubules (Orci et al, 2009). This hypothesis is further supported by several observations. Jozsef et al. suggest that STIM1 functions in SOCE mainly in tubular ER (Jozsef et al, 2014). In HeLa cells, the cortical ER is often found aligned along cortical microtubules by electron microscopy (EM) (Orci et al, 2009). Disruption of microtubules by nocodazole results in loss of tubular ER. This causes decrease and delay in Ca^{2+} influx during SOCE (Jozsef et al, 2014; Smyth et al, 2007). Thus, microtubules could play a role in maintaining the structure of cortical ER, where SOCE takes place. I demonstrated that a STIM1 mutant (STIM1ΔKΔEB-1) and a truncated STIM1 ($STIM1_{390}$) containing EB-1 independent microtubule binding domains colocalize with cortical microtubules. Whether these cortical microtubules are distinct microtubule populations to establish and/or maintain ER-PM contacts remains unclear and has to be addressed by further experiments. Oligomerization of STIM1 increases its microtubule binding but reduced microtubule-dependent movement (Grigoriev et al, 2008; Liou et al, 2007), suggesting that STIM1-containing cortical ER is stabilized via interaction with cortical microtubules upon SOCE activation.

5.8 Proposed model of STIM1-mediated ER-PM contact formation

At resting state, low-order oligomers of STIM1 localize in preexisting ER-PM contact sites via binding of the K-rich domain to PM lipids (Fig 23A). Dimeric STIM1 travels to preexisting ER-PM contacts by TAC dynamic via binding to EB-1 (Fig 23A). In addition, STIM1 slides along microtubules via an unknown motor (Fig 23A). During SOCE activation, STIM1 undergoes conformational changes and oligomerization in proximity of preexisting ER-PM contact sites, resulting in increased lipid-binding ability of STIM1 (Fig 23B). Preexisting ER-PM contacts are expanded and form large ER-PM junctions where Orai1 is recruited and activated (Fig 23B). Interaction between high-order STIM1 oligomers and cortical microtubules may stabilize cortical ER, where SOCE takes place (Fig 23B).

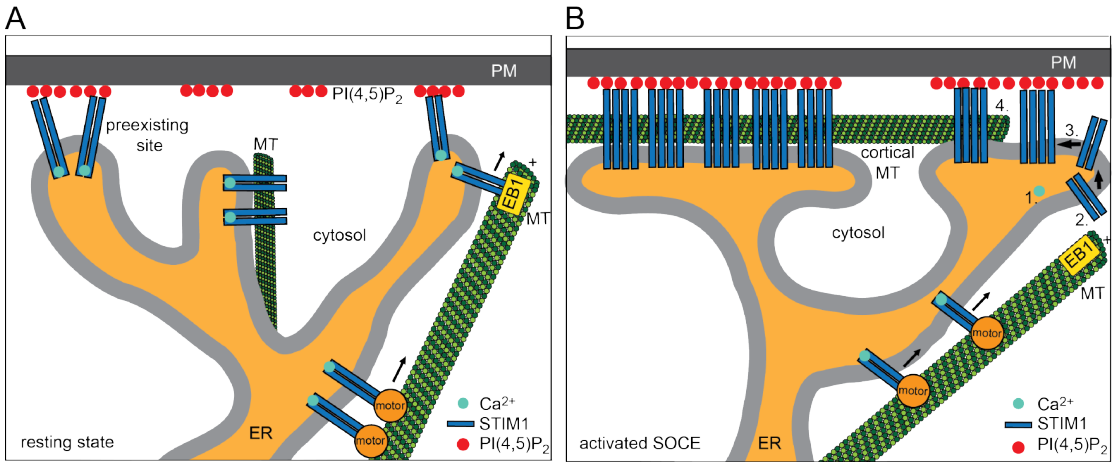

Figure 23. Proposed model of STIM1-mediated ER-PM contact formation (A) at resting state and (B) upon SOCE activation.

6. References

Akhmanova A, Steinmetz MO (2008) Tracking the ends: a dynamic protein network controls the fate of microtubule tips. *Nat Rev Mol Cell Biol* **9:** 309-322

Anderson DJ, Hetzer MW (2007) Nuclear envelope formation by chromatin-mediated reorganization of the endoplasmic reticulum. *Nat Cell Biol* **9:** 1160-1166

Anderson DJ, Hetzer MW (2008) Reshaping of the endoplasmic reticulum limits the rate for nuclear envelope formation. *J Cell Biol* **182:** 911-924

Arredouani A, Yu F, Sun L, Machaca K (2010) Regulation of store-operated Ca2+ entry during the cell cycle. *J Cell Sci* **123:** 2155-2162

Baba Y, Hayashi K, Fujii Y, Mizushima A, Watarai H, Wakamori M, Numaga T, Mori Y, Iino M, Hikida M, Kurosaki T (2006) Coupling of STIM1 to store-operated Ca2+ entry through its constitutive and inducible movement in the endoplasmic reticulum. *Proc Natl Acad Sci U S A* **103:** 16704-16709

Barenz F, Inoue D, Yokoyama H, Tegha-Dunghu J, Freiss S, Draeger S, Mayilo D, Cado I, Merker S, Klinger M, Hoeckendorf B, Pilz S, Hupfeld K, Steinbeisser H, Lorenz H, Ruppert T, Wittbrodt J, Gruss OJ (2013) The centriolar satellite protein SSX2IP promotes centrosome maturation. *J Cell Biol* **202:** 81-95

Barlowe C, Orci L, Yeung T, Hosobuchi M, Hamamoto S, Salama N, Rexach MF, Ravazzola M, Amherdt M, Schekman R (1994) COPII: a membrane coat formed by Sec proteins that drive vesicle budding from the endoplasmic reticulum. *Cell* **77:** 895-907

Bastiaens PI, Jovin TM (1996) Microspectroscopic imaging tracks the intracellular processing of a signal transduction protein: fluorescent-labeled protein kinase C beta I. *Proc Natl Acad Sci U S A* **93:** 8407-8412

Bauer MC, O'Connell D, Cahill DJ, Linse S (2008) Calmodulin binding to the polybasic C-termini of STIM proteins involved in store-operated calcium entry. *Biochemistry* **47:** 6089-6091

Baumann NA, Sullivan DP, Ohvo-Rekila H, Simonot C, Pottekat A, Klaassen Z, Beh CT, Menon AK (2005) Transport of newly synthesized sterol to the sterol-enriched plasma membrane occurs via nonvesicular equilibration. *Biochemistry* **44:** 5816-5826

Beh CT, McMaster CR, Kozminski KG, Menon AK (2012) A detour for yeast oxysterol binding proteins. *J Biol Chem* **287:** 11481-11488

Berridge MJ, Bootman MD, Roderick HL (2003) Calcium: Calcium signalling: dynamics, homeostasis and remodelling. *Nature Reviews Molecular Cell Biology* **4:** 517-529

Berridge MJ, Lipp P, Bootman MD (2000) The versatility and universality of calcium signalling. *Nat Rev Mol Cell Biol* **1:** 11-21

Bhardwaj R, Muller HM, Nickel W, Seedorf M (2013) Oligomerization and Ca2+/calmodulin control binding of the ER Ca2+-sensors STIM1 and STIM2 to plasma membrane lipids. *Biosci Rep* **33**

Bola B, Allan V (2009) How and why does the endoplasmic reticulum move? *Biochemical Society Transactions* **37:** 961

Brandman O, Liou J, Park WS, Meyer T (2007) STIM2 is a feedback regulator that stabilizes basal cytosolic and endoplasmic reticulum Ca2+ levels. *Cell* **131:** 1327-1339

Breslow DK, Weissman JS (2010) Membranes in balance: mechanisms of sphingolipid homeostasis. *Mol Cell* **40:** 267-279

Burnette WN (1981) "Western blotting": electrophoretic transfer of proteins from sodium dodecyl sulfate--polyacrylamide gels to unmodified nitrocellulose and radiographic detection with antibody and radioiodinated protein A. *Anal Biochem* **112:** 195-203

Cai X (2007) Molecular evolution and functional divergence of the Ca(2+) sensor protein in store-operated Ca(2+) entry: stromal interaction molecule. *PLoS One* **2:** e609

Cai X (2008) Unicellular Ca2+ signaling 'toolkit' at the origin of metazoa. *Mol Biol Evol* **25:** 1357-1361

Calloway N, Holowka D, Baird B (2010) A basic sequence in STIM1 promotes Ca2+ influx by interacting with the C-terminal acidic coiled coil of Orai1. *Biochemistry* **49:** 1067-1071

Carrasco S, Meyer T (2011) STIM proteins and the endoplasmic reticulum-plasma membrane junctions. *Annu Rev Biochem* **80:** 973-1000

Chang CL, Hsieh TS, Yang TT, Rothberg KG, Azizoglu DB, Volk E, Liao JC, Liou J (2013) Feedback regulation of receptor-induced Ca2+ signaling mediated by E-Syt1 and Nir2 at endoplasmic reticulum-plasma membrane junctions. *Cell Rep* **5:** 813-825

Chen S, Novick P, Ferro-Novick S (2013) ER structure and function. *Curr Opin Cell Biol* **25:** 428-433

Clapham DE (2007) Calcium Signaling. *Cell* **131:** 1047-1058

Collins SR, Meyer T (2011) Evolutionary origins of STIM1 and STIM2 within ancient Ca2+ signaling systems. *Trends Cell Biol* **21:** 202-211

Covington ED, Wu MM, Lewis RS (2010) Essential role for the CRAC activation domain in store-dependent oligomerization of STIM1. *Mol Biol Cell* **21:** 1897-1907

Csordas G, Varnai P, Golenar T, Roy S, Purkins G, Schneider TG, Balla T, Hajnoczky G (2010) Imaging interorganelle contacts and local calcium dynamics at the ER-mitochondrial interface. *Mol Cell* **39:** 121-132

D'Angelo G, Vicinanza M, De Matteis MA (2008) Lipid-transfer proteins in biosynthetic pathways. *Curr Opin Cell Biol* **20:** 360-370

Darbellay B, Arnaudeau S, Bader CR, Konig S, Bernheim L (2011) STIM1L is a new actin-binding splice variant involved in fast repetitive Ca2+ release. *J Cell Biol* **194:** 335-346

de Brito OM, Scorrano L (2008) Mitofusin 2 tethers endoplasmic reticulum to mitochondria. *Nature* **456:** 605-610

de Saint-Jean M, Delfosse V, Douguet D, Chicanne G, Payrastre B, Bourguet W, Antonny B, Drin G (2011) Osh4p exchanges sterols for phosphatidylinositol 4-phosphate between lipid bilayers. *J Cell Biol* **195:** 965-978

De Vos KJ, Morotz GM, Stoica R, Tudor EL, Lau KF, Ackerley S, Warley A, Shaw CE, Miller CC (2012) VAPB interacts with the mitochondrial protein PTPIP51 to regulate calcium homeostasis. *Hum Mol Genet* **21:** 1299-1311

Dekker PJ, Ryan MT, Brix J, Muller H, Honlinger A, Pfanner N (1998) Preprotein translocase of the outer mitochondrial membrane: molecular dissection and assembly of the general import pore complex. *Mol Cell Biol* **18:** 6515-6524

Demuro A, Penna A, Safrina O, Yeromin AV, Amcheslavsky A, Cahalan MD, Parker I (2011) Subunit stoichiometry of human Orai1 and Orai3 channels in closed and open states. *Proc Natl Acad Sci U S A* **108:** 17832-17837

Derler I, Fahrner M, Muik M, Lackner B, Schindl R, Groschner K, Romanin C (2009) A Ca2(+)release-activated Ca2(+) (CRAC) modulatory domain (CMD) within STIM1 mediates fast Ca2(+)-dependent inactivation of ORAI1 channels. *J Biol Chem* **284:** 24933-24938

Elbaz Y, Schuldiner M (2011) Staying in touch: the molecular era of organelle contact sites. *Trends Biochem Sci* **36:** 616-623

Endo M (2009) Calcium-induced calcium release in skeletal muscle. *Physiol Rev* **89:** 1153-1176

English AR, Voeltz GK (2013) Endoplasmic reticulum structure and interconnections with other organelles. *Cold Spring Harb Perspect Biol* **5:** a013227

English AR, Zurek N, Voeltz GK (2009) Peripheral ER structure and function. *Curr Opin Cell Biol* **21:** 596-602

Ercan E (2011) The formation of endoplasmic reticulum-plasma membrane contact sites in mammalian cells. *University of Heidelberg*

Ercan E, Chung SH, Bhardwaj R, Seedorf M (2012) Di-arginine signals and the K-rich domain retain the Ca(2)(+) sensor STIM1 in the endoplasmic reticulum. *Traffic* **13:** 992-1003

Ercan E, Momburg F, Engel U, Temmerman K, Nickel W, Seedorf M (2009) A Conserved, Lipid-Mediated Sorting Mechanism of Yeast Ist2 and Mammalian STIM Proteins to the Peripheral ER. *Traffic* **10:** 1802-1818

Favaloro V, Vilardi F, Schlecht R, Mayer MP, Dobberstein B (2010) Asna1/TRC40-mediated membrane insertion of tail-anchored proteins. *J Cell Sci* **123:** 1522-1530

Feske S, Gwack Y, Prakriya M, Srikanth S, Puppel SH, Tanasa B, Hogan PG, Lewis RS, Daly M, Rao A (2006) A mutation in Orai1 causes immune deficiency by abrogating CRAC channel function. *Nature* **441:** 179-185

Fischer MA, Temmerman K, Ercan E, Nickel W, Seedorf M (2009) Binding of plasma membrane lipids recruits the yeast integral membrane protein Ist2 to the cortical ER. *Traffic* **10:** 1084-1097

Friedman JR, Voeltz GK (2011) The ER in 3D: a multifunctional dynamic membrane network. *Trends Cell Biol* **21:** 709-717

Friedman JR, Webster BM, Mastronarde DN, Verhey KJ, Voeltz GK (2010) ER sliding dynamics and ER-mitochondrial contacts occur on acetylated microtubules. *J Cell Biol* **190:** 363-375

Garbino A, van Oort RJ, Dixit SS, Landstrom AP, Ackerman MJ, Wehrens XH (2009) Molecular evolution of the junctophilin gene family. *Physiol Genomics* **37:** 175-186

Garbino A, Wehrens XH (2010) Emerging role of junctophilin-2 as a regulator of calcium handling in the heart. *Acta Pharmacol Sin* **31:** 1019-1021

Garcia P, Gupta R, Shah S, Morris AJ, Rudge SA, Scarlata S, Petrova V, McLaughlin S, Rebecchi MJ (1995) The pleckstrin homology domain of phospholipase C-delta 1 binds with high affinity to phosphatidylinositol 4,5-bisphosphate in bilayer membranes. *Biochemistry* **34:** 16228-16234

Gerhardt P, Murray RGE, Wood WA, Krieg NR (1994) Methods for general and molecular bacteriology. *Am Soc Microbiol, Washington, DC*

Gil J, Busto EM, Garcillan B, Chean C, Garcia-Rodriguez MC, Diaz-Alderete A, Navarro J, Reine J, Mencia A, Gurbindo D, Belendez C, Gordillo I, Duchniewicz M, Hohne K, Garcia-Sanchez F, Fernandez-Cruz E, Lopez-Granados E, Schamel WW, Moreno-Pelayo MA, Recio MJ, Regueiro JR (2011) A leaky mutation in CD3D differentially affects alphabeta and gammadelta T cells and leads to a Talphabeta-Tgammadelta+B+NK+ human SCID. *J Clin Invest* **121:** 3872-3876

Giordano F, Saheki Y, Idevall-Hagren O, Colombo SF, Pirruccello M, Milosevic I, Gracheva EO, Bagriantsev SN, Borgese N, De Camilli P (2013) PI(4,5)P(2)-dependent and Ca(2+)-regulated ER-PM interactions mediated by the extended synaptotagmins. *Cell* **153:** 1494-1509

Glick BS, Nakano A (2009) Membrane traffic within the Golgi apparatus. *Annu Rev Cell Dev Biol* **25:** 113-132

Graham SJ, Dziadek MA, Johnstone LS (2011) A cytosolic STIM2 preprotein created by signal peptide inefficiency activates ORAI1 in a store-independent manner. *J Biol Chem* **286:** 16174-16185

Grigoriev I, Gouveia SM, van der Vaart B, Demmers J, Smyth JT, Honnappa S, Splinter D, Steinmetz MO, Putney JW, Jr., Hoogenraad CC, Akhmanova A (2008) STIM1 is a MT-plus-end-tracking protein involved in remodeling of the ER. *Curr Biol* **18:** 177-182

Haj FG, Sabet O, Kinkhabwala A, Wimmer-Kleikamp S, Roukos V, Han HM, Grabenbauer M, Bierbaum M, Antony C, Neel BG, Bastiaens PI (2012) Regulation of signaling at regions of cell-cell contact by endoplasmic reticulum-bound protein-tyrosine phosphatase 1B. *PLoS One* **7:** e36633

Hammond GR, Fischer MJ, Anderson KE, Holdich J, Koteci A, Balla T, Irvine RF (2012) PI4P and PI(4,5)P2 are essential but independent lipid determinants of membrane identity. *Science* **337:** 727-730

Hanada K (2010) Intracellular trafficking of ceramide by ceramide transfer protein. *Proc Jpn Acad Ser B Phys Biol Sci* **86:** 426-437

Hanada K, Kumagai K, Tomishige N, Yamaji T (2009) CERT-mediated trafficking of ceramide. *Biochim Biophys Acta* **1791:** 684-691

Hauser CT, Tsien RY (2007) A hexahistidine-Zn2+-dye label reveals STIM1 surface exposure. *Proc Natl Acad Sci U S A* **104:** 3693-3697

Helle SC, Kanfer G, Kolar K, Lang A, Michel AH, Kornmann B (2013) Organization and function of membrane contact sites. *Biochim Biophys Acta* **1833:** 2526-2541

Hewavitharana T, Deng X, Wang Y, Ritchie MF, Girish GV, Soboloff J, Gill DL (2008) Location and function of STIM1 in the activation of Ca2+ entry signals. *J Biol Chem* **283:** 26252-26262

Hogan PG, Lewis RS, Rao A (2010) Molecular Basis of Calcium Signaling in Lymphocytes: STIM and ORAI. *Annual Review of Immunology* **28:** 491-533

Honnappa S, Gouveia SM, Weisbrich A, Damberger FF, Bhavesh NS, Jawhari H, Grigoriev I, van Rijssel FJA, Buey RM, Lawera A (2009) An EB1-Binding Motif Acts as a Microtubule Tip Localization Signal. *Cell* **138:** 366-376

Inoue H, Nojima H, Okayama H (1990) High efficiency transformation of Escherichia coli with plasmids. *Gene* **96:** 23-28

Iwasawa R, Mahul-Mellier AL, Datler C, Pazarentzos E, Grimm S (2011) Fis1 and Bap31 bridge the mitochondria-ER interface to establish a platform for apoptosis induction. *EMBO J* **30:** 556-568

Jackson MR, Nilsson T, Peterson PA (1990) Identification of a consensus motif for retention of transmembrane proteins in the endoplasmic reticulum. *EMBO J* **9:** 3153-3162

Jansen M, Ohsaki Y, Rita Rega L, Bittman R, Olkkonen VM, Ikonen E (2011) Role of ORPs in sterol transport from plasma membrane to ER and lipid droplets in mammalian cells. *Traffic* **12:** 218-231

Jozsef L, Tashiro K, Kuo A, Park EJ, Skoura A, Albinsson S, Rivera-Molina F, Harrison KD, Iwakiri Y, Toomre D, Sessa WC (2014) Reticulon 4 is necessary for endoplasmic reticulum tubulation, STIM1-Orai1 coupling, and store-operated calcium entry. *J Biol Chem* **289:** 9380-9395

Karpova TS, Baumann CT, He L, Wu X, Grammer A, Lipsky P, Hager GL, McNally JG (2003) Fluorescence resonance energy transfer from cyan to yellow fluorescent protein detected by acceptor photobleaching using confocal microscopy and a single laser. *J Microsc* **209:** 56-70

Kawano M, Kumagai K, Nishijima M, Hanada K (2006) Efficient trafficking of ceramide from the endoplasmic reticulum to the Golgi apparatus requires a VAMP-associated protein-interacting FFAT motif of CERT. *J Biol Chem* **281:** 30279-30288

Kim JY, Muallem S (2011) Unlocking SOAR releases STIM. *EMBO J* **30:** 1673-1675

Kincade PW, Oritani K, Zheng Z, Borghesi L, Smithson G, Yamashita Y (1998) Cell interaction molecules utilized in bone marrow. *Cell Adhes Commun* **6:** 211-215

Klopfenstein DR, Kappeler F, Hauri HP (1998) A novel direct interaction of endoplasmic reticulum with microtubules. *EMBO J* **17:** 6168-6177

Koch GL (1990) The endoplasmic reticulum and calcium storage. *Bioessays* **12:** 527-531

Kornmann B, Currie E, Collins SR, Schuldiner M, Nunnari J, Weissman JS, Walter P (2009) An ER-mitochondria tethering complex revealed by a synthetic biology screen. *Science* **325:** 477-481

Kornmann B, Walter P (2010) ERMES-mediated ER-mitochondria contacts: molecular hubs for the regulation of mitochondrial biology. *J Cell Sci* **123:** 1389-1393

Korzeniowski MK, Manjarres IM, Varnai P, Balla T (2010) Activation of STIM1-Orai1 involves an intramolecular switching mechanism. *Sci Signal* **3:** ra82

Krapivinsky G, Krapivinsky L, Stotz SC, Manasian Y, Clapham DE (2011) POST, partner of stromal interaction molecule 1 (STIM1), targets STIM1 to multiple transporters. *Proc Natl Acad Sci U S A* **108:** 19234-19239

Kumar P, Wittmann T (2012) +TIPs: SxIPping along microtubule ends. *Trends Cell Biol* **22:** 418-428

Kutay U, Hetzer MW (2008) Reorganization of the nuclear envelope during open mitosis. *Curr Opin Cell Biol* **20:** 669-677

Ladinsky MS, Mastronarde DN, McIntosh JR, Howell KE, Staehelin LA (1999) Golgi structure in three dimensions: functional insights from the normal rat kidney cell. *J Cell Biol* **144:** 1135-1149

Laemmli UK (1970) Cleavage of structural proteins during the assembly of the head of bacteriophage T4. *Nature* **227:** 680-685

Landstrom AP, Weisleder N, Batalden KB, Bos JM, Tester DJ, Ommen SR, Wehrens XH, Claycomb WC, Ko JK, Hwang M, Pan Z, Ma J, Ackerman MJ (2007) Mutations in JPH2-encoded junctophilin-2 associated with hypertrophic cardiomyopathy in humans. *J Mol Cell Cardiol* **42:** 1026-1035

Lavieu G, Orci L, Shi L, Geiling M, Ravazzola M, Wieland F, Cosson P, Rothman JE (2010) Induction of cortical endoplasmic reticulum by dimerization of a coatomer-binding peptide anchored to endoplasmic reticulum membranes. *Proceedings of the National Academy of Sciences* **107:** 6876-6881

Lebiedzinska M, Szabadkai G, Jones AW, Duszynski J, Wieckowski MR (2009) Interactions between the endoplasmic reticulum, mitochondria, plasma membrane and other subcellular organelles. *Int J Biochem Cell Biol* **41:** 1805-1816

Lee I, Hong W (2006) Diverse membrane-associated proteins contain a novel SMP domain. *FASEB J* **20:** 202-206

Lee KP, Yuan JP, Zeng W, So I, Worley PF, Muallem S (2009) Molecular determinants of fast Ca2+-dependent inactivation and gating of the Orai channels. *Proc Natl Acad Sci U S A* **106:** 14687-14692

Lehto M, Hynynen R, Karjalainen K, Kuismanen E, Hyvarinen K, Olkkonen VM (2005) Targeting of OSBP-related protein 3 (ORP3) to endoplasmic reticulum and plasma membrane is controlled by multiple determinants. *Exp Cell Res* **310:** 445-462

Lev S (2010) Non-vesicular lipid transport by lipid-transfer proteins and beyond. *Nat Rev Mol Cell Biol* **11:** 739-750

Lev S (2012) Nonvesicular lipid transfer from the endoplasmic reticulum. *Cold Spring Harb Perspect Biol* **4**

Levine T, Loewen C (2006) Inter-organelle membrane contact sites: through a glass, darkly. *Curr Opin Cell Biol* **18:** 371-378

Lewis RS (2001) Calcium signaling mechanisms in T lymphocytes. *Annu Rev Immunol* **19:** 497-521

Lewis RS (2007) The molecular choreography of a store-operated calcium channel. *Nature* **446:** 284-287

Li Y, Prinz WA (2004) ATP-binding cassette (ABC) transporters mediate nonvesicular, raft-modulated sterol movement from the plasma membrane to the endoplasmic reticulum. *J Biol Chem* **279:** 45226-45234

Li Z, Liu L, Deng Y, Ji W, Du W, Xu P, Chen L, Xu T (2011) Graded activation of CRAC channel by binding of different numbers of STIM1 to Orai1 subunits. *Cell Res* **21:** 305-315

Li Z, Lu J, Xu P, Xie X, Chen L, Xu T (2007) Mapping the interacting domains of STIM1 and Orai1 in Ca2+ release-activated Ca2+ channel activation. *J Biol Chem* **282:** 29448-29456

Liou J, Fivaz M, Inoue T, Meyer T (2007) Live-cell imaging reveals sequential oligomerization and local plasma membrane targeting of stromal interaction molecule 1 after Ca2+ store depletion. *Proceedings of the National Academy of Sciences* **104:** 9301-9306

Liou J, Kim M, Doheo W, Jones J, Myers J, Ferrelljr J, Meyer T (2005) STIM Is a Ca Sensor Essential for Ca-Store-Depletion-Triggered Ca Influx. *Current Biology* **15:** 1235-1241

Lippincott-Schwartz J, Roberts TH, Hirschberg K (2000) Secretory protein trafficking and organelle dynamics in living cells. *Annu Rev Cell Dev Biol* **16:** 557-589

Loewen CJ, Levine TP (2005) A highly conserved binding site in vesicle-associated membrane protein-associated protein (VAP) for the FFAT motif of lipid-binding proteins. *J Biol Chem* **280:** 14097-14104

Loewen CJ, Young BP, Tavassoli S, Levine TP (2007) Inheritance of cortical ER in yeast is required for normal septin organization. *J Cell Biol* **179:** 467-483

Luik RM, Wu MM, Buchanan J, Lewis RS (2006) The elementary unit of store-operated Ca2+ entry: local activation of CRAC channels by STIM1 at ER-plasma membrane junctions. *J Cell Biol* **174:** 815-825

Lur G, Haynes LP, Prior IA, Gerasimenko OV, Feske S, Petersen OH, Burgoyne RD, Tepikin AV (2009) Ribosome-free terminals of rough ER allow formation of STIM1 puncta and segregation of STIM1 from IP(3) receptors. *Curr Biol* **19:** 1648-1653

Malhotra V, Serafini T, Orci L, Shepherd JC, Rothman JE (1989) Purification of a novel class of coated vesicles mediating biosynthetic protein transport through the Golgi stack. *Cell* **58:** 329-336

Malli R, Naghdi S, Romanin C, Graier WF (2008) Cytosolic Ca2+ prevents the subplasmalemmal clustering of STIM1: an intrinsic mechanism to avoid Ca2+ overload. *J Cell Sci* **121:** 3133-3139

Manford AG, Stefan CJ, Yuan HL, Macgurn JA, Emr SD (2012) ER-to-plasma membrane tethering proteins regulate cell signaling and ER morphology. *Dev Cell* **23:** 1129-1140

Manji SS, Parker NJ, Williams RT, van Stekelenburg L, Pearson RB, Dziadek M, Smith PJ (2000) STIM1: a novel phosphoprotein located at the cell surface. *Biochim Biophys Acta* **1481:** 147-155

McLaughlin S, Murray D (2005) Plasma membrane phosphoinositide organization by protein electrostatics. *Nature* **438:** 605-611

Meisinger C, Pfannschmidt S, Rissler M, Milenkovic D, Becker T, Stojanovski D, Youngman MJ, Jensen RE, Chacinska A, Guiard B, Pfanner N, Wiedemann N (2007) The morphology proteins Mdm12/Mmm1 function in the major beta-barrel assembly pathway of mitochondria. *EMBO J* **26:** 2229-2239

Michelsen K, Yuan H, Schwappach B (2005) Hide and run. Arginine-based endoplasmic-reticulum-sorting motifs in the assembly of heteromultimeric membrane proteins. *EMBO Rep* **6:** 717-722

Mignen O, Thompson JL, Shuttleworth TJ (2007) STIM1 regulates Ca2+ entry via arachidonate-regulated Ca2+-selective (ARC) channels without store depletion or translocation to the plasma membrane. *J Physiol* **579:** 703-715

Min SW, Chang WP, Sudhof TC (2007) E-Syts, a family of membranous Ca2+-sensor proteins with multiple C2 domains. *Proc Natl Acad Sci U S A* **104:** 3823-3828

Minogue S, Waugh MG (2012) The Phosphatidylinositol 4-Kinases: Don't Call it a Comeback. *Subcell Biochem* **58:** 1-24

Monteleone MC, Gonzalez Wusener AE, Burdisso JE, Conde C, Caceres A, Arregui CO (2012) ER-bound protein tyrosine phosphatase PTP1B interacts with Src at the plasma membrane/substrate interface. *PLoS One* **7:** e38948

Muik M, Fahrner M, Derler I, Schindl R, Bergsmann J, Frischauf I, Groschner K, Romanin C (2008) A Cytosolic Homomerization and a Modulatory Domain within STIM1 C Terminus Determine Coupling to ORAI1 Channels. *Journal of Biological Chemistry* **284:** 8421-8426

Muik M, Fahrner M, Schindl R, Stathopulos P, Frischauf I, Derler I, Plenk P, Lackner B, Groschner K, Ikura M, Romanin C (2011) STIM1 couples to ORAI1 via an intramolecular transition into an extended conformation. *EMBO J* **30:** 1678-1689

Navarro-Borelly L, Somasundaram A, Yamashita M, Ren D, Miller RJ, Prakriya M (2008) STIM1-Orai1 interactions and Orai1 conformational changes revealed by live-cell FRET microscopy. *J Physiol* **586:** 5383-5401

Nickel W, Brugger B, Wieland FT (2002) Vesicular transport: the core machinery of COPI recruitment and budding. *J Cell Sci* **115:** 3235-3240

Orci L, Perrelet A, Ravazzola M, Amherdt M, Rothman JE, Schekman R (1994) Coatomer-rich endoplasmic reticulum. *Proc Natl Acad Sci U S A* **91:** 11924-11928

Orci L, Ravazzola M, Le Coadic M, Shen WW, Demaurex N, Cosson P (2009) From the Cover: STIM1-induced precortical and cortical subdomains of the endoplasmic reticulum. *Proc Natl Acad Sci U S A* **106:** 19358-19362

Oritani K, Kincade PW (1996) Identification of stromal cell products that interact with pre-B cells. *J Cell Biol* **134:** 771-782

Osman C, Haag M, Potting C, Rodenfels J, Dip PV, Wieland FT, Brugger B, Westermann B, Langer T (2009) The genetic interactome of prohibitins: coordinated control of cardiolipin and phosphatidylethanolamine by conserved regulators in mitochondria. *J Cell Biol* **184:** 583-596

Parekh AB, Putney JW, Jr. (2005) Store-operated calcium channels. *Physiol Rev* **85:** 757-810

Park CY, Hoover PJ, Mullins FM, Bachhawat P, Covington ED, Raunser S, Walz T, Garcia KC, Dolmetsch RE, Lewis RS (2009) STIM1 Clusters and Activates CRAC Channels via Direct Binding of a Cytosolic Domain to Orai1. *Cell* **136:** 876-890

Penna A, Demuro A, Yeromin AV, Zhang SL, Safrina O, Parker I, Cahalan MD (2008) The CRAC channel consists of a tetramer formed by Stim-induced dimerization of Orai dimers. *Nature* **456:** 116-120

Peretti D, Dahan N, Shimoni E, Hirschberg K, Lev S (2008) Coordinated lipid transfer between the endoplasmic reticulum and the Golgi complex requires the VAP proteins and is essential for Golgi-mediated transport. *Mol Biol Cell* **19:** 3871-3884

Pichler H, Gaigg B, Hrastnik C, Achleitner G, Kohlwein SD, Zellnig G, Perktold A, Daum G (2001) A subfraction of the yeast endoplasmic reticulum associates with the plasma membrane and has a high capacity to synthesize lipids. *Eur J Biochem* **268:** 2351-2361

Pizzo P, Pozzan T (2007) Mitochondria-endoplasmic reticulum choreography: structure and signaling dynamics. *Trends Cell Biol* **17:** 511-517

Porter KR, Palade GE (1957) Studies on the endoplasmic reticulum. III. Its form and distribution in striated muscle cells. *J Biophys Biochem Cytol* **3:** 269-300

Pozo-Guisado E, Campbell DG, Deak M, Alvarez-Barrientos A, Morrice NA, Alvarez IS, Alessi DR, Martin-Romero FJ (2010) Phosphorylation of STIM1 at ERK1/2 target sites modulates store-operated calcium entry. *J Cell Sci* **123:** 3084-3093

Prakriya M, Feske S, Gwack Y, Srikanth S, Rao A, Hogan PG (2006) Orai1 is an essential pore subunit of the CRAC channel. *Nature* **443:** 230-233

Prescott AR, Farmaki T, Thomson C, James J, Paccaud JP, Tang BL, Hong W, Quinn M, Ponnambalam S, Lucocq J (2001) Evidence for prebudding arrest of ER export in animal cell mitosis and its role in generating Golgi partitioning intermediates. *Traffic* **2:** 321-335

Preston GA, Barrett JC, Biermann JA, Murphy E (1997) Effects of alterations in calcium homeostasis on apoptosis during neoplastic progression. *Cancer Res* **57:** 537-542

Preston SF, Sha'afi RI, Berlin RD (1991) Regulation of Ca2+ influx during mitosis: Ca2+ influx and depletion of intracellular Ca2+ stores are coupled in interphase but not mitosis. *Cell Regul* **2:** 915-925

Puhka M, Vihinen H, Joensuu M, Jokitalo E (2007) Endoplasmic reticulum remains continuous and undergoes sheet-to-tubule transformation during cell division in mammalian cells. *J Cell Biol* **179:** 895-909

Rajesh (2013) Endoplasmic reticulum-plasma membrane contact formation by STIM proteins and regulation of their lipid-binding activity by oligomerization and cytosolic Ca2+/Calmodulin. *University of Heidelberg, Germany*

Rizzuto R, Pinton P, Carrington W, Fay FS, Fogarty KE, Lifshitz LM, Tuft RA, Pozzan T (1998) Close contacts with the endoplasmic reticulum as determinants of mitochondrial Ca2+ responses. *Science* **280:** 1763-1766

Roos J, DiGregorio PJ, Yeromin AV, Ohlsen K, Lioudyno M, Zhang S, Safrina O, Kozak JA, Wagner SL, Cahalan MD, Velicelebi G, Stauderman KA (2005) STIM1, an essential and conserved component of store-operated Ca2+ channel function. *J Cell Biol* **169:** 435-445

Roy A, Levine TP (2004) Multiple pools of phosphatidylinositol 4-phosphate detected using the pleckstrin homology domain of Osh2p. *J Biol Chem* **279:** 44683-44689

Saitoh N, Oritani K, Saito K, Yokota T, Ichii M, Sudo T, Fujita N, Nakajima K, Okada M, Kanakura Y (2011) Identification of functional domains and novel binding partners of STIM proteins. *J Cell Biochem* **112:** 147-156

Sambrook JaR, D. W. (2001) Molecular cloning: A laboratory manual, 3rd ed. *Cold Spring Harbor Laboratory Press, Cold Spring Harbor, New York, USA***:** pp.1.51-51.54

Schulz TA, Choi MG, Raychaudhuri S, Mears JA, Ghirlando R, Hinshaw JE, Prinz WA (2009) Lipid-regulated sterol transfer between closely apposed membranes by oxysterol-binding protein homologues. *J Cell Biol* **187:** 889-903

Scott DB, Blanpied TA, Swanson GT, Zhang C, Ehlers MD (2001) An NMDA receptor ER retention signal regulated by phosphorylation and alternative splicing. *J Neurosci* **21:** 3063-3072

Shen WW, Frieden M, Demaurex N (2011) Remodelling of the endoplasmic reticulum during store-operated calcium entry. *Biol Cell* **103:** 365-380

Shibata Y, Hu J, Kozlov MM, Rapoport TA (2009) Mechanisms shaping the membranes of cellular organelles. *Annu Rev Cell Dev Biol* **25:** 329-354

Shibata Y, Shemesh T, Prinz WA, Palazzo AF, Kozlov MM, Rapoport TA (2010) Mechanisms determining the morphology of the peripheral ER. *Cell* **143:** 774-788

Shibata Y, Voeltz GK, Rapoport TA (2006) Rough sheets and smooth tubules. *Cell* **126:** 435-439

Shibata Y, Voss C, Rist JM, Hu J, Rapoport TA, Prinz WA, Voeltz GK (2008) The reticulon and DP1/Yop1p proteins form immobile oligomers in the tubular endoplasmic reticulum. *J Biol Chem* **283:** 18892-18904

Smyth JT, Beg AM, Wu S, Putney JW, Jr., Rusan NM (2012) Phosphoregulation of STIM1 leads to exclusion of the endoplasmic reticulum from the mitotic spindle. *Curr Biol* **22:** 1487-1493

Smyth JT, DeHaven WI, Bird GS, Putney JW, Jr. (2007) Role of the microtubule cytoskeleton in the function of the store-operated Ca2+ channel activator STIM1. *J Cell Sci* **120:** 3762-3771

Smyth JT, Dehaven WI, Bird GS, Putney JW, Jr. (2008) Ca2+-store-dependent and -independent reversal of Stim1 localization and function. *J Cell Sci* **121:** 762-772

Smyth JT, Petranka JG, Boyles RR, DeHaven WI, Fukushima M, Johnson KL, Williams JG, Putney JW, Jr. (2009) Phosphorylation of STIM1 underlies suppression of store-operated calcium entry during mitosis. *Nat Cell Biol* **11:** 1465-1472

Soboloff J, Rothberg BS, Madesh M, Gill DL (2012) STIM proteins: dynamic calcium signal transducers. *Nat Rev Mol Cell Biol* **13:** 549-565

Soboloff J, Spassova MA, Dziadek MA, Gill DL (2006a) Calcium signals mediated by STIM and Orai proteins--a new paradigm in inter-organelle communication. *Biochim Biophys Acta* **1763:** 1161-1168

Soboloff J, Spassova MA, Hewavitharana T, He LP, Xu W, Johnstone LS, Dziadek MA, Gill DL (2006b) STIM2 is an inhibitor of STIM1-mediated store-operated Ca2+ Entry. *Curr Biol* **16:** 1465-1470

Srikanth S, Jung HJ, Kim KD, Souda P, Whitelegge J, Gwack Y (2010) A novel EF-hand protein, CRACR2A, is a cytosolic Ca2+ sensor that stabilizes CRAC channels in T cells. *Nat Cell Biol* **12:** 436-446

Stathopulos PB, Li GY, Plevin MJ, Ames JB, Ikura M (2006) Stored Ca2+ depletion-induced oligomerization of stromal interaction molecule 1 (STIM1) via the EF-SAM region: An initiation mechanism for capacitive Ca2+ entry. *J Biol Chem* **281:** 35855-35862

Stathopulos PB, Zheng L, Ikura M (2009) Stromal interaction molecule (STIM) 1 and STIM2 calcium sensing regions exhibit distinct unfolding and oligomerization kinetics. *J Biol Chem* **284:** 728-732

Stathopulos PB, Zheng L, Li GY, Plevin MJ, Ikura M (2008) Structural and mechanistic insights into STIM1-mediated initiation of store-operated calcium entry. *Cell* **135:** 110-122

Stefan CJ, Manford AG, Baird D, Yamada-Hanff J, Mao Y, Emr SD (2011) Osh proteins regulate phosphoinositide metabolism at ER-plasma membrane contact sites. *Cell* **144:** 389-401

Stefan CJ, Manford AG, Emr SD (2013) ER-PM connections: sites of information transfer and inter-organelle communication. *Curr Opin Cell Biol* **25:** 434-442

Szabadkai G, Bianchi K, Varnai P, De Stefani D, Wieckowski MR, Cavagna D, Nagy AI, Balla T, Rizzuto R (2006) Chaperone-mediated coupling of endoplasmic reticulum and mitochondrial Ca2+ channels. *J Cell Biol* **175:** 901-911

Takeshima H, Komazaki S, Nishi M, Iino M, Kangawa K (2000) Junctophilins: a novel family of junctional membrane complex proteins. *Mol Cell* **6:** 11-22

Tani D, Monteilh-Zoller MK, Fleig A, Penner R (2007) Cell cycle-dependent regulation of store-operated I(CRAC) and Mg2+-nucleotide-regulated MagNuM (TRPM7) currents. *Cell Calcium* **41:** 249-260

Terasaki M, Chen LB, Fujiwara K (1986) Microtubules and the endoplasmic reticulum are highly interdependent structures. *J Cell Biol* **103:** 1557-1568

Tian Y, Schreiber R, Kunzelmann K (2012) Anoctamins are a family of Ca2+-activated Cl- channels. *J Cell Sci* **125:** 4991-4998

Toulmay A, Prinz WA (2011) Lipid transfer and signaling at organelle contact sites: the tip of the iceberg. *Curr Opin Cell Biol* **23:** 458-463

Toulmay A, Prinz WA (2012) A conserved membrane-binding domain targets proteins to organelle contact sites. *J Cell Sci* **125:** 49-58

Vance JE (1990) Phospholipid synthesis in a membrane fraction associated with mitochondria. *J Biol Chem* **265:** 7248-7256

Varnai P, Toth B, Toth DJ, Hunyady L, Balla T (2007) Visualization and manipulation of plasma membrane-endoplasmic reticulum contact sites indicates the presence of additional molecular components within the STIM1-Orai1 Complex. *J Biol Chem* **282:** 29678-29690

Vedrenne C, Hauri HP (2006) Morphogenesis of the endoplasmic reticulum: beyond active membrane expansion. *Traffic* **7:** 639-646

Vedrenne C, Klopfenstein DR, Hauri HP (2005) Phosphorylation controls CLIMP-63-mediated anchoring of the endoplasmic reticulum to microtubules. *Mol Biol Cell* **16:** 1928-1937

Vilardi F, Lorenz H, Dobberstein B (2011) WRB is the receptor for TRC40/Asna1-mediated insertion of tail-anchored proteins into the ER membrane. *J Cell Sci* **124:** 1301-1307

Voeltz GK, Prinz WA, Shibata Y, Rist JM, Rapoport TA (2006) A class of membrane proteins shaping the tubular endoplasmic reticulum. *Cell* **124:** 573-586

Voeltz GK, Rolls MM, Rapoport TA (2002) Structural organization of the endoplasmic reticulum. *EMBO Rep* **3:** 944-950

Volpi M, Berlin RD (1988) Intracellular elevations of free calcium induced by activation of histamine H1 receptors in interphase and mitotic HeLa cells: hormone signal transduction is altered during mitosis. *J Cell Biol* **107:** 2533-2539

Walsh Ciara M, Chvanov M, Haynes Lee P, Petersen Ole H, Tepikin Alexei V, Burgoyne Robert D (2010) Role of phosphoinositides in STIM1 dynamics and store-operated calcium entry. *Biochemical Journal* **425:** 159-168

Wang PY, Weng J, Anderson RG (2005) OSBP is a cholesterol-regulated scaffolding protein in control of ERK 1/2 activation. *Science* **307:** 1472-1476

Wang X, Schwarz TL (2009) The mechanism of Ca2+ -dependent regulation of kinesin-mediated mitochondrial motility. *Cell* **136:** 163-174

Waterman-Storer CM, Salmon ED (1998) Endoplasmic reticulum membrane tubules are distributed by microtubules in living cells using three distinct mechanisms. *Curr Biol* **8:** 798-806

Wei D, Jacobs S, Modla S, Zhang S, Young CL, Cirino R, Caplan J, Czymmek K (2012) High-resolution three-dimensional reconstruction of a whole yeast cell using focused-ion beam scanning electron microscopy. *Biotechniques* **53:** 41-48

West M, Zurek N, Hoenger A, Voeltz GK (2011) A 3D analysis of yeast ER structure reveals how ER domains are organized by membrane curvature. *J Cell Biol* **193:** 333-346

Whitaker M (2006) Calcium microdomains and cell cycle control. *Cell Calcium* **40:** 585-592

Wiedemann C, Cockcroft S (1998) The Role of Phosphatidylinositol Transfer Proteins (PITPs) in Intracellular Signalling. *Trends Endocrinol Metab* **9:** 324-328

Williams RT, Manji SS, Parker NJ, Hancock MS, Van Stekelenburg L, Eid JP, Senior PV, Kazenwadel JS, Shandala T, Saint R, Smith PJ, Dziadek MA (2001) Identification and characterization of the STIM (stromal interaction molecule) gene family: coding for a novel class of transmembrane proteins. *Biochem J* **357:** 673-685

Williams RT, Senior PV, Van Stekelenburg L, Layton JE, Smith PJ, Dziadek MA (2002) Stromal interaction molecule 1 (STIM1), a transmembrane protein with growth suppressor activity, contains an extracellular SAM domain modified by N-linked glycosylation. *Biochim Biophys Acta* **1596:** 131-137

Wittmann T, Boleti H, Antony C, Karsenti E, Vernos I (1998) Localization of the kinesin-like protein Xklp2 to spindle poles requires a leucine zipper, a microtubule-associated protein, and dynein. *J Cell Biol* **143:** 673-685

Wolf W, Kilic A, Schrul B, Lorenz H, Schwappach B, Seedorf M (2012) Yeast Ist2 recruits the endoplasmic reticulum to the plasma membrane and creates a ribosome-free membrane microcompartment. *PLoS One* **7:** e39703

Wozniak MJ, Bola B, Brownhill K, Yang YC, Levakova V, Allan VJ (2009) Role of kinesin-1 and cytoplasmic dynein in endoplasmic reticulum movement in VERO cells. *J Cell Sci* **122:** 1979-1989

Wu MM (2006) Ca2+ store depletion causes STIM1 to accumulate in ER regions closely associated with the plasma membrane. *The Journal of Cell Biology* **174:** 803-813

Xu P, Lu J, Li Z, Yu X, Chen L, Xu T (2006) Aggregation of STIM1 underneath the plasma membrane induces clustering of Orai1☆. *Biochemical and Biophysical Research Communications* **350:** 969-976

Yang L, Guan T, Gerace L (1997) Integral membrane proteins of the nuclear envelope are dispersed throughout the endoplasmic reticulum during mitosis. *J Cell Biol* **137:** 1199-1210

Yang X, Jin H, Cai X, Li S, Shen Y (2012) Structural and mechanistic insights into the activation of Stromal interaction molecule 1 (STIM1). *Proc Natl Acad Sci U S A* **109:** 5657-5662

Yuan H, Michelsen K, Schwappach B (2003) 14-3-3 Dimers Probe the Assembly Status of Multimeric Membrane Proteins. *Current Biology* **13:** 638-646

Yuan JP, Zeng W, Dorwart MR, Choi Y-J, Worley PF, Muallem S (2009) SOAR and the polybasic STIM1 domains gate and regulate Orai channels. *Nature Cell Biology* **11:** 337-343

Zerangue N, Malan MJ, Fried SR, Dazin PF, Jan YN, Jan LY, Schwappach B (2001) Analysis of endoplasmic reticulum trafficking signals by combinatorial screening in mammalian cells. *Proc Natl Acad Sci U S A* **98:** 2431-2436

Zerangue N, Schwappach B, Jan YN, Jan LY (1999) A new ER trafficking signal regulates the subunit stoichiometry of plasma membrane K(ATP) channels. *Neuron* **22:** 537-548

Zhan T, Poppelreuther M, Ehehalt R, Fullekrug J (2012) Overexpressed FATP1, ACSVL4/FATP4 and ACSL1 increase the cellular fatty acid uptake of 3T3-L1 adipocytes but are localized on intracellular membranes. *PLoS One* **7:** e45087

Zhang SL, Yu Y, Roos J, Kozak JA, Deerinck TJ, Ellisman MH, Stauderman KA, Cahalan MD (2005) STIM1 is a Ca2+ sensor that activates CRAC channels and migrates from the Ca2+ store to the plasma membrane. *Nature* **437:** 902-905

Zheng L, Stathopulos PB, Li GY, Ikura M (2008) Biophysical characterization of the EF-hand and SAM domain containing Ca2+ sensory region of STIM1 and STIM2. *Biochem Biophys Res Commun* **369:** 240-246

Zheng L, Stathopulos PB, Schindl R, Li GY, Romanin C, Ikura M (2011) Auto-inhibitory role of the EF-SAM domain of STIM proteins in store-operated calcium entry. *Proc Natl Acad Sci U S A* **108:** 1337-1342

Zheng Y, Tsai MY (2006) The mitotic spindle matrix: a fibro-membranous lamin connection. *Cell Cycle* **5:** 2345-2347

Zhou Y, Srinivasan P, Razavi S, Seymour S, Meraner P, Gudlur A, Stathopulos PB, Ikura M, Rao A, Hogan PG (2013) Initial activation of STIM1, the regulator of store-operated calcium entry. *Nat Struct Mol Biol* **20:** 973-981